12-2015

Development and Validation of a Novel In Vitro Model for the Assessment of Heterocellular Interactions Mediated by Connexin43

Emily Ongstad
Clemson University, nemily@gmail.com

DEVELOPMENT AND VALIDATION OF A NOVEL IN VITRO MODEL FOR THE ASSESSMENT OF HETEROCELLULAR INTERACTIONS MEDIATED BY CONNEXIN43

A Dissertation
Presented to
the Graduate School of
Clemson University

In Partial Fulfillment
of the Requirements for the Degree
Doctor of Philosophy
Bioengineering

---

by
Emily Lynn Ongstad
December 2015

Accepted by:
Martine LaBerge, PhD, Committee Chair
Robert Gourdie, PhD, Research Advisor
Michael Yost, PhD
Ann Foley, PhD

ABSTRACT

The injury border zone (IBZ), a region of transitional tissue between intact myocardium and the ischemic area, is often the site of lethal reentrant arrhythmia generation in post-myocardial infarction (MI) patients. Disruption to normal connexin43 (Cx43) localization at the intercalated disc (ID), separation of myocytes by activated fibroblasts and deposited scar tissue are thought to be factors that render the IBZ a pro-arrhythmic substrate, though there is a current need to better understand these changes so directed therapies can be developed. There are no clinically available therapies focused on the mechanistic changes in the IBZ. Additionally, generation of new compounds is challenged by the inefficiencies of the drug development pipeline, including the use of *in vitro* testing platforms that are of little relevance to human disease. In order to address the need for directed therapies and improved testing platforms, we developed a 3D *in vitro* aggregate model of the IBZ that was validated against a murine cryo-injury model of infarction. This model was used to examine the changes in heterocellular myocyte-fibroblast interactions via Cx43 and cell organization patterns in response to αCT1 – a Cx43 carboxyl-terminal mimetic peptide which was previously shown to alter cell organization in the IBZ of a murine cryo-injury model. Imaging results indicated that αCT1 increased fibroblast migration, as well as myocyte cohesion, as evidenced by increased cell clustering in aggregates at 72 hours. This was likely an effect of Cx43 adhesion properties. Optical mapping studies indicated that αCT1 could protect cryo-injured hearts against conduction delay through the IBZ

in conditions of altered extracellular ion concentration. Subsequent analyses from a gap junction (GJ) intercellular communication (GJIC) assay indicated that this may be a result of altered communication, as αCT1 was found to decrease GJIC in myocyte-fibroblast connections and in fibroblast-fibroblast connections. This decrease in GJIC was correlated with an increase in Cx43 phosphorylated at serine 368 (pS368) in myocyte-fibroblast interactions *in vitro* an *in vivo*, which is known to decrease GJ channel conductance. Super-resolution imaging of GJ plaques revealed a novel sub-domain organization with respect to non-phosphorylated Cx43 and Cx43 pS368. Together, the data provided in this dissertation describe the development of a novel *in vitro* model of the IBZ of relevance to drug response and disease mechanism that can be used as a high-throughput testing platform for candidate compounds. These studies, furthermore, suggest the importance of Cx43 heterocellular interactions as a therapeutic target for reducing cardiac arrhythmias.

ACKNOWLEDGEMENTS

Before I can acknowledge the support of those who have contributed to the completion of this dissertation, I must thank two influential teachers from my secondary education. Dr. Johnny Bland, my junior high school science teacher, whose unconventional, but passionate, engaging, and humorous ways of teaching inspired a love of science in me at an early age. And Mr. Karimi, my high school physics teacher, who encouraged me to pursue an engineering degree because of its versatility.

The years I have spent studying for my PhD have been both professionally and personally rewarding, and have provided more surprises and challenges than I could have imagined. I am indebted to many individuals for their support and encouragement in this process, though these pages will not suffice to recognize them all.

First, my research advisor, Dr. Robert Gourdie, has taught me what it means to be a scientist. Your mentorship and guidance have challenged me to think deeply and carefully about scientific problems and how to convey their importance to any audience. You encouraged me to follow my interests, as well as pursue opportunities outside of lab.

I would like to thank my committee: Dr. Martine LaBerge, Dr. Michael Yost, and Dr. Ann Foley. Thank you for your insightful and challenging questions and for the

guidance you have provided to make me think like an engineer. My committee chair, Dr. LaBerge, has supported my participation in the Clemson Bioengineering Department from day 1, even through all of the changes in course of my PhD tenure. To my committee member and collaborator Dr. Michael Yost, thank you for your knowledge, guidance, and technical support on my skeletal muscle project. Dr. Ann Foley, thank you for agreeing to step in near the end of my PhD tenure and for your inspiring curiosity.

I thank our lab manager, Jane Jourdan, for countless hours of training and discussion. Her extensive experience and careful thought into experimental design and project management have provided me with the knowledge and skills to develop into a technically skilled scientist.

Thank you to members of the Gourdie Lab, especially Sai, Katie, and Jade, for your insightful discussion and technical assistance. Thank you to past lab member Matt Rhett for teaching me how to be a wizard on the confocal and for excellent scientific discussion.

In the Clemson Bioengineering Department, Dr. Richard Swaja, former CU-MUSC Bioengineering Program Director, deserves a special thank you for being our program's biggest advocate. You truly listened to the needs of the students. Thank you, also, for your years of service on my dissertation committee. A huge thank you to Maria Torres, Graduate Student Coordinator, for being a friendly voice on the Clemson end of the phone to solve whatever problems the distance students

were creating. You have made the hassles of department forms, college requirements, and fellowship applications/administration seem insignificant.

Thank you to my scientific collaborators: Sharon George, Dr. Steven Poelzing, Dr. Graça Almeida-Porada, and Dr. Terence Partidge.

The success of my education is greatly dependent upon my family. My parents, Ricky Ongstad and Mary Dittrich, have supported me every step of the way and never once complained or made me feel guilty for spending the last 11 years of my life away from home studying. My sisters, Amanda and Kristine, who remain my best friends, despite the fact that I have been so far from home for so long. Thank you for the gentle reminders to come home more often.

My dearest and closest friends – Christi Perich, Vrushali Chavan, Michelle Dittrich, Kristina Ravenel, Wenjun He, and Erin Sproul – carried me through the tough times and always found something wild to take my mind off the slog of PhD candidacy. My partner, John, has provided endless support and encouragement, especially during the writing of this dissertation. Your lighthearted and goofy personality reminds me to step back and see the big picture. The students in the Clemson-MUSC Bioengineering Program, who are all scattered now, have become enduring friends. And to my friends outside of lab who have made my time in Charleston and Roanoke so memorable: Thanks for taking me in and being my family away from home.

TABLE OF CONTENTS

Page

Table of Contents (Continued)

Page

LIST OF TABLES

Table **Page**

LIST OF FIGURES

Figure **Page**

List of Figures (Continued)

Figure **Page**

CHAPTER 1: INTRODUCTION

1.1 Myocardial infarction and the injury border zone – clinical problem and significance

Heart disease is the number one killer of people worldwide, causing an estimated 17.5 million deaths in 2012 (Fig. 1-1A) [1]. Ischemic heart disease – the cause of myocardial infarction – is responsible for over 7.2 million deaths each year (Fig. 1.1B) [2]. In the western world, cardiovascular disease (CVD) is a major health and economic burden, responsible for three quarters of a million deaths in the United States alone [3], with indirect costs totaling over $200 billion [3]. However, over three quarters of deaths from cardiovascular disease (CVD) occur in low- and middle-income countries, because of the lack of access to primary care and early detection programs in contrast to those that are available in high-income countries (Fig. 1.1). These health issues create a heavy economic burden on these low- and middle-income countries. For example, the annual direct costs of CVD in China comprise 4% of their gross national income, estimated at more than $40 billion [4]. Projections from the World Heart Federation suggest that the burden of CVD in developing countries will rise to match that seen in industrialized countries because of increased urbanization and the associated lifestyle changes [4,5].

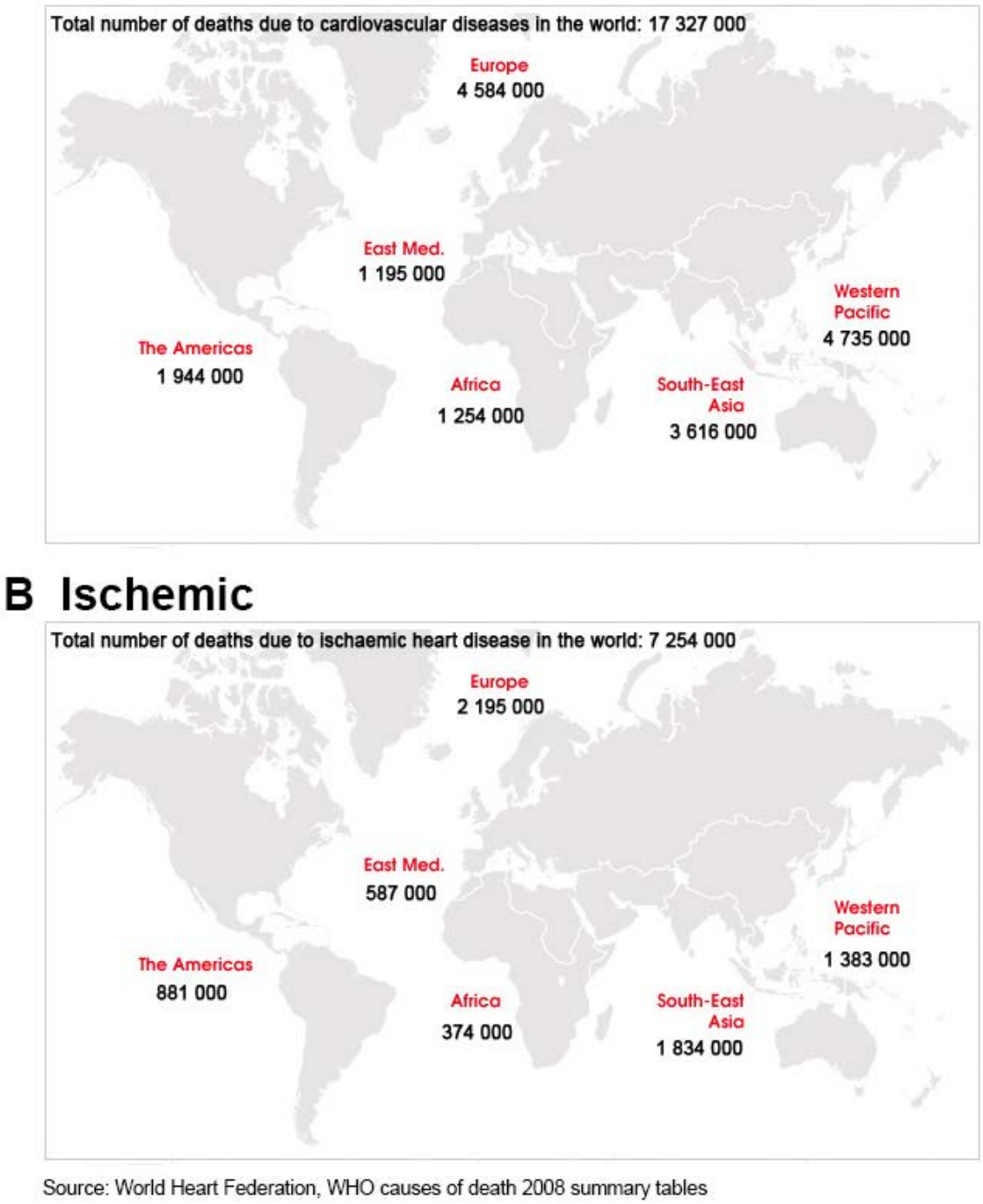

Figure 1-1. Prevalence of cardiovascular disease worldwide. A) Total number of deaths from CVD by region in 2008. B) Total number of deaths from ischemic heart disease (which encompasses MI) by region in 2008. Reproduced from [1].

Commonly known as heart attack, myocardial infarction (MI) is the death of cardiac tissue caused by prolonged ischemia [6]. It is most often caused by rupture of an atherosclerotic plaque with thrombus formation in a coronary vessel, blocking the blood supply to a portion of the myocardium (Fig. 1-2A). After the onset of ischemia, cell death occurs in minutes to hours. The extent of damage can be determined by factors such as location of the thrombus in the coronary vascular tree, the extent of collateral circulation to the ischemic zone, preconditioning, and reperfusion. A fully-healed infarct, as seen in Figure 1-2B, may not differentiate until 5 to 6 weeks after the MI [6]. Infarct size in a major predictor of outcome in MI patients [7]. Large infarcts result in extensive cardiac remodeling, including changes in gross morphology, histology, and molecular function/interactions [8]. Part of the remodeling process after MI includes excessive collagen deposition in the injured area of the myocardium, which prevents wall rupture, but generates a new non-contractile tissue that can no longer actively longer contribute to the mechanical pump function of the heart. Replacement fibrosis occurs in the area of injured myocardium, where collagen is deposited by activated fibroblasts (aka myofibroblasts). MI often results in reduced systolic and diastolic function and can predispose patients to arrhythmias because of the extensive remodeling that occurs [9]. Though an infarct may be healed by 5-6 weeks, the remodeling process is often ongoing; with continued dilation, heart function deteriorates over time, leading to heart failure and the eventual death of the patient [10].

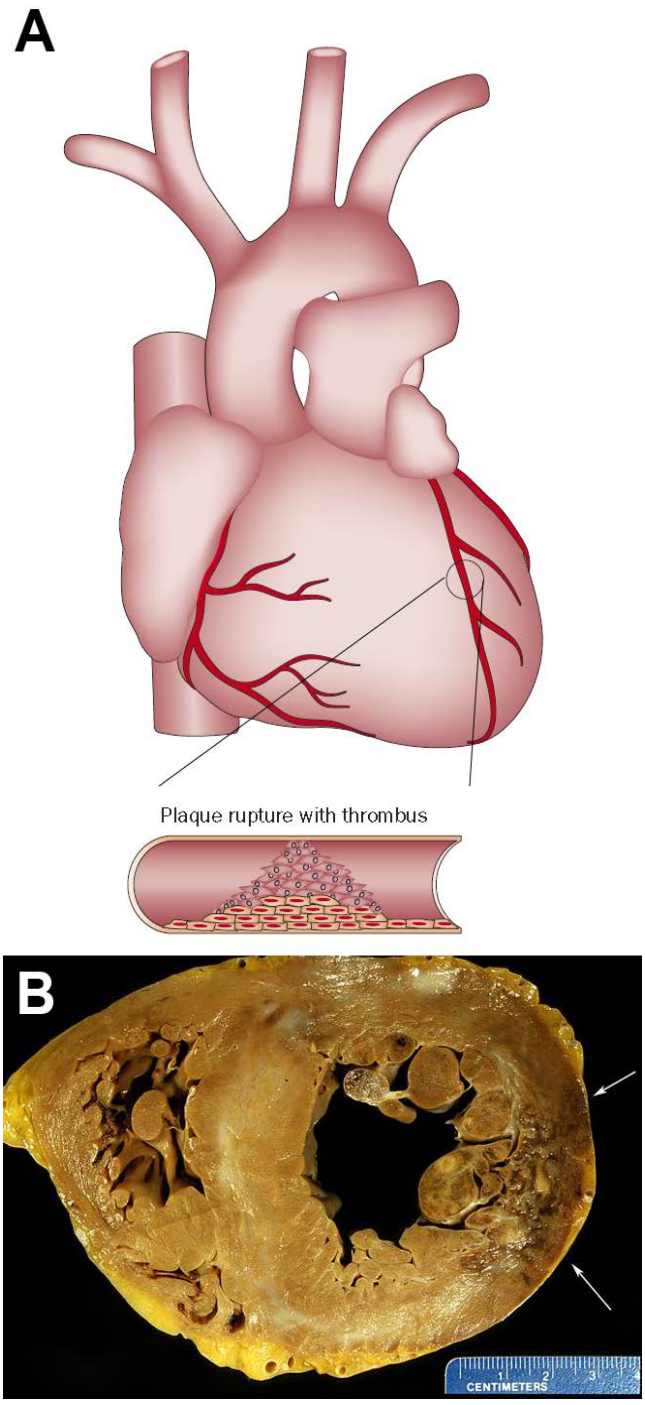

Figure 1-2. Myocardial infarction. A) A plaque rupture and thrombus blocking blood flow to a portion of the myocardium is the most common cause of acute MI. B) An infarcted human heart with a healing infarcted area indicated by arrows. Reproduced from [6] and [328].

Bordering the infarct area is the injury border zone (IBZ), which is a few cell layer-thick area of transition between the scar and the viable myocardium. The changes in tissue electrophysiological properties, cell organization, collagen deposition, and inefficient removal of toxic biochemical products, among other factors, can contribute to the generation of lethal arrhythmias in the IBZ [11–13]. The structural and biophysical changes that occur in the IBZ will be discussed in depth below.

Standard of care for acute MI is focused on restoring blood flow to the ischemic tissue. Early treatment for MI may include oxygen therapy, aspirin and nitroglycerin to improve blood flow, as well as treatment for pain. Thrombolytics may be administered to dissolve the clot causing the MI, though this treatment is most effective within a few hours of the clot forming. Coronary angioplasty may be used acutely to open the blocked artery and a stent may be placed to maintain patency of the blood vessel. Pharmacological treatments such as beta blockers, angiotensin converting enzyme (ACE) inhibitors, and anti-coagulants may also be given [14]. More patients in the developing world are surviving MI due to improved clinical interventions, though the frequency of re-hospitalization is high [3]. While clinical interventions for acute MI are focused on dissolving the clot and reestablishing blood flow, there are few therapies focused on supporting healing of the heart, let alone regeneration of lost tissue and cells.

1.2 Structure and biophysical properties of connexins and gap junctions

The connexin proteins that form gap junctions (GJs) are thought to be responsible for spread of electrical signals and subsequent coordinated contraction of the heart. GJs are present in nearly all mammalian tissues, and they serve an important function in direct intercellular communication, coordinating events in tissues and between cells. The connexin proteins that comprise GJs are tightly clustered together in the cell membrane, directly connecting the cytoplasm of two cells. This cytoplasmic continuity is the property that confers a functional syncytium. Work from Engleman in 1870 first described a functional syncytium when he reported a wave of contraction that traveled down a ureter after application of an electrical stimulus [15], a property later attributed to smooth muscle cells. Later work in the heart showed the ventricles could still contract rhythmically after being severed from innervation [16,17]. It was initially thought that a syncytium involved fusion of a portion of the membranes of adjacent cells, though later electron microscopy studies in mouse heart and liver showed that an electron dense tracer added during tissue processing filled the small “gap” between the membranes of two adjacent cells (Fig. 1-3A) [18] and in *en face* GJs between two cells, the tracer outlined the hexagonal array of the GJ plaque structure (Fig. 1-3B). It was Dewey and Barr that first suggested that these structures were sites of electrical coupling between cells [19,20].

GJs are comprised of connexin proteins. Six connexin proteins oligomerize to form a connexon, or hemichannel, in the membrane of a cell. Two hemichannels from adjacent cells dock to form a GJ channel. Tens to thousands of GJ channels aggregate into a GJ plaque (Fig. 1-3 and Fig. 1-4A) [19,21,22]. In mammals, there are 22 known members of the connexin family of proteins, which can combine to form homotypic or heterotypic GJ channels (Fig. 1-4B) [23,24]. Connexins are a membrane tetraspan protein with intracellular amino- (N-) and carboxyl-terminal (C-terminal) domains. Within the four transmembrane domains are two extracellular loops and one cytoplasmic loop (Fig. 1-4C). The various connexin isoforms are named for their molecular mass, ranging in size from 25 to 60 kDa [25,26]. Much of the four transmembrane domains are conserved, with variability between the isoforms coming from differences in the C-terminus [25]. In the extracellular loop domains, disulfide bonds between cysteine residues are thought to be involved in docking of connexons between adjacent cells (Fig. 1-4C) [26], potentially playing a role in cell adhesion. Sequence similarity between different isoforms of the molecule allows connexins to form heterotypic channels, where the GJ channel is comprised of a connexon of different protein isoforms contributed by each cell (Fig. 1-4B) [27]. Sequence similarity in the transmembrane regions of the protein allows formation of heteromeric channels, where each connexon is made up of different isoforms of connexins (Fig. 1-4B) [28].

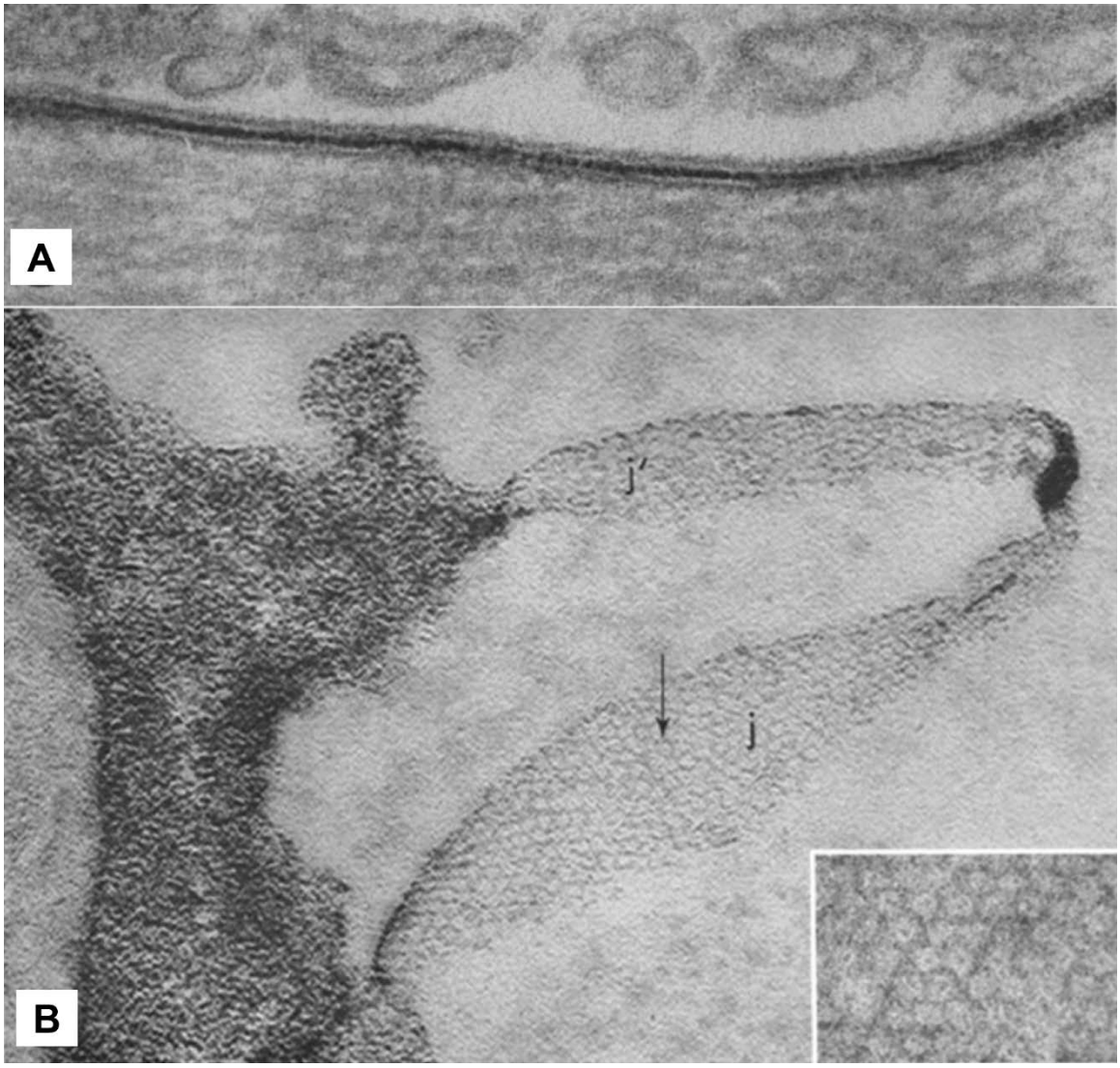

Figure 1-3. Electron microscopy of GJs. A) Work by Revel and Karnovsky used lanthanum, an electron dense tracer, that revealed the 'gap' between the two membranes that gap junctions would come to be named for. B) The lanthanum tracer revealed a hexagonal array structure ('j' and higher magnification in inset), when used on tangential sections through the gap junction plaque. Reproduced from [18].

Molecules of less than 1 kD in size can passively diffuse through a GJ channel, including water, metabolites, second messengers, nucleotides, and ions mediating the spread of electrical signals [29–31]. Hemichannels, or connexon channels that are located in the cell membrane, can also function in intracellular-extracellular

exchange of these same molecules. While all connexins act as nonselective channels, passage of solutes through the channel may differ between compounds of similar chemical composition [32]. Selectivity, conductance, and gating of GJ channels can vary slightly between isoforms of connexins, and these properties are sensitive to voltage, chemical changes, and pH [32,33]. Other factors affecting the permselectivity of channels include phosphorylation and formation of heterotypic and heteromeric channels. The C-terminus and intracellular loop are thought to be largely responsible for differences in function between different isoforms of connexins. The C-terminus interacts with numerous proteins and contains many phosphorylation sites that can play roles in altering intercellular communication through direct changes in protein trafficking, distribution, degradation, and post translational modification [26,34,35].

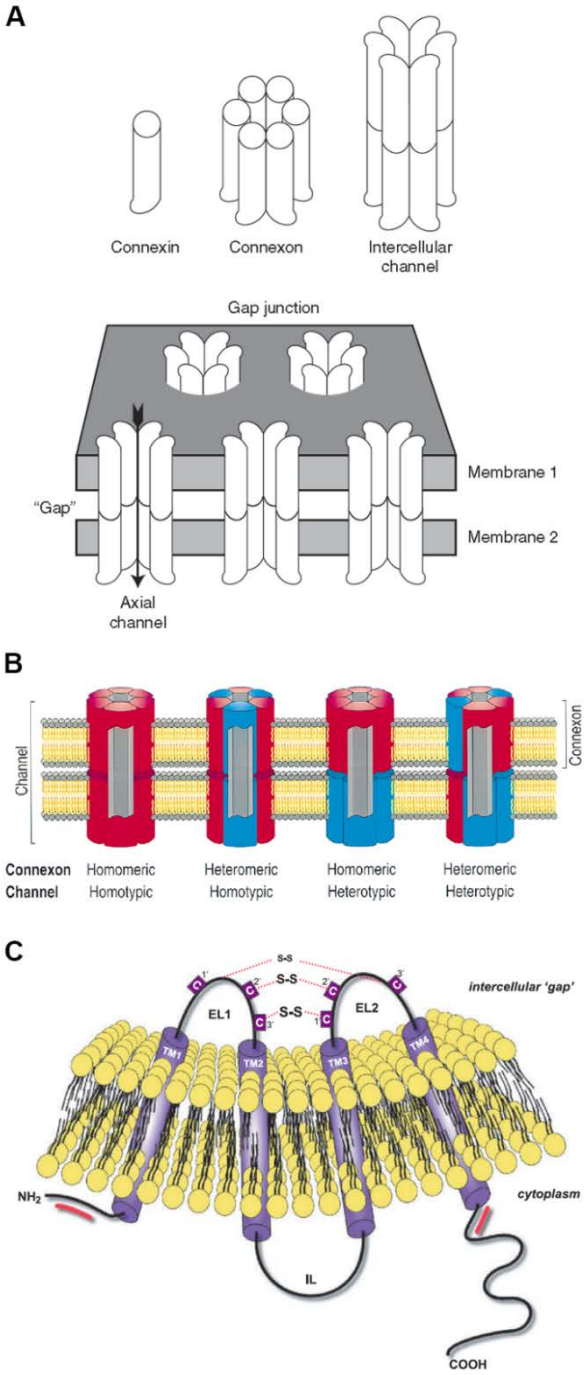

Figure 1-4. Molecular structure of the GJ. A) Connexin proteins assemble into connexons. Connexons from adjacent cells dock to form an intercellular GJ channel in the membranes of adjacent cells. B) GJs may form heterotypic or heteromeric channels, which can affect their permselectivity. C) Connexins have four transmembrane domains, a C-terminus that interacts extensively with other proteins, and extracellular loops with disulfide bonds that may play a role in adhesion. Reproduced from [26,30].

Though there are no reports discussing adhesive properties of connexins in the heart, several studies in the nervous system detail the function of connexins in intercellular adhesion. Cellular adhesion of a glioma cell line increased when transfected with Cx43, and this occurred independently of GJ channel function [36]. When antibodies directed against the extracellular loops of connexin were added, aggregation of Cx43-expressing cells was reduced. Connexin-mediated adhesion is also known to be required for radial migration of cells in the developing cortex [37]. In C6 glioma cells and HeLa cells (cells which do not normally interact), transfection of both cell types with Cx43 enabled adhesion to occur between the cells types in a short-term suspension aggregation assay [38]. Aggregation did not occur in untransfected cells.

In 1970, Steinberg postulated that cells could sort due to differences in intercellular adhesion strengths [39]. In theory, cells with higher intercellular adhesion forces would sort to the center of co-culture aggregates, leaving the cells with lower adhesion forces on the outside. Foty and Steinberg later showed that expression of different levels of cadherins in cells provided evidence in favor of this hypothesis, as cells expressing higher levels of cadherins sorted to the inside of co-culture aggregates [40]. If connexins are involved in adhesion, then different levels of connexins between cells may also account for some level of sorting. More recent work demonstrated that this is, indeed, the case, as altering Cx43 in multiple cell lines led to changes in cell aggregate formation [41]. Sterically inhibiting Cx43 docking with an antibody directed against the second extracellular loop of Cx43

slowed aggregation of cells, while enzymatic digestion of cellular adhesion molecules and N-cadherin neutralizing antibody decreased cell aggregation a comparable amount to inhibiting connexins. Interestingly, treating cells with Gap26 – a Cx43 mimetic peptide that blocks gap junction intercellular communication (GJIC) but does not inhibit docking – accelerated cellular adhesion [41]. These data provide evidence that Cx43 does indeed have adhesive properties, and it may be that altered levels of Cx43 in the heart post-MI change patterns of cell migration and cohesion.

1.3 Regulation of gap junction intercellular communication

Several factors influence GJIC, including plaque size, phosphorylation, and formation of heterotypic and heteromeric channels. Additionally, there are several known compounds and peptides that can alter GJIC.

From production through degradation of connexin proteins, the half-life of connexin proteins is measured at 1-5 hours [42,43], though in neonatal rat ventricular myocytes (NRVMs), it is reported to be 1-2 hours [44–46]. Regulation of GJ formation and degradation is likely important in control of GJIC. After transcription into mRNA, connexins are co-translated into the membrane of the endoplasmic reticulum (ER), where protein folding occurs [47,48], disulfide bonds are formed [49–51], and connexons are formed when individual connexin proteins oligomerize

[52]. Oligomerization may also occur in the *trans*-golgi compartment [53,54]. Phosphorylation of connexins, which will be discussed in detail below, and other post-translational modifications occur in the golgi compartment [44]. Additionally, Cx43 is known to be trafficked to the membrane via a microtubule-dependent mechanism [26,55].

Connexin proteins are then inserted throughout the membrane, diffuse laterally, and are incorporated into GJ plaques [26,52,56]. In the non-junctional region surrounding the plaque, called the 'perinexus,' connexon incorporation into the GJ plaque is constrained by interaction with Zonula Occludens-1 (ZO-1; discussed below) [57]. Single channel recordings of human Cx43 GJs expressed in a human liver cell line showed two unitary conductance states: one at 60-70 pS and one at 90-100 pS. The decreased conductance state was correlated with Cx43 phosphorylation [58]. Formation of heterotypic and heteromeric channels leads to complex changes in channel conductance [59–64]. For example, heterotypic Cx43/45 channels had a conductance that was the sum of each of the hemichannel conductances [65], while conductance of homotypic and heterotypic channels comprised of two connexin subtypes are dissimilar [61,63,64].

Communication between adjacent cells can also be regulated by increasing the number of channels in a GJ plaque [66]. Work from our lab showed that in Cx43-expressing HeLa cells, an increase in GJIC due to increased plaque size happened at the expense of hemichannel communication [57]. While connexons

are likely added to the plaque by lateral diffusion in the membrane, they are removed from the center of the plaque [67,68] as annular junctions – sections of GJs that span both cell membranes [69,70]. GJs are then degraded by proteasomal and lysosomal pathways [42,43,52].

Connexins are known to interact with many other proteins that affect their trafficking, lifecycle, function, and organization. The C-terminal binding partners of Cx43 have been shown to affect its secondary structure. Extensive reviews on the subject can be found here: [71,72]. Figure 1-5 illustrates the binding partners of Cx43. Work from the Gourdie lab and others suggests that accretion and stability of GJ channels can be regulated by Cx43-interacting proteins like Src and ZO-1 [73–79]. For the purpose of relevant background for this project, we will focus on ZO-1 interactions with the Cx43 C-terminus, as well as other interactions that can regulate GJIC.

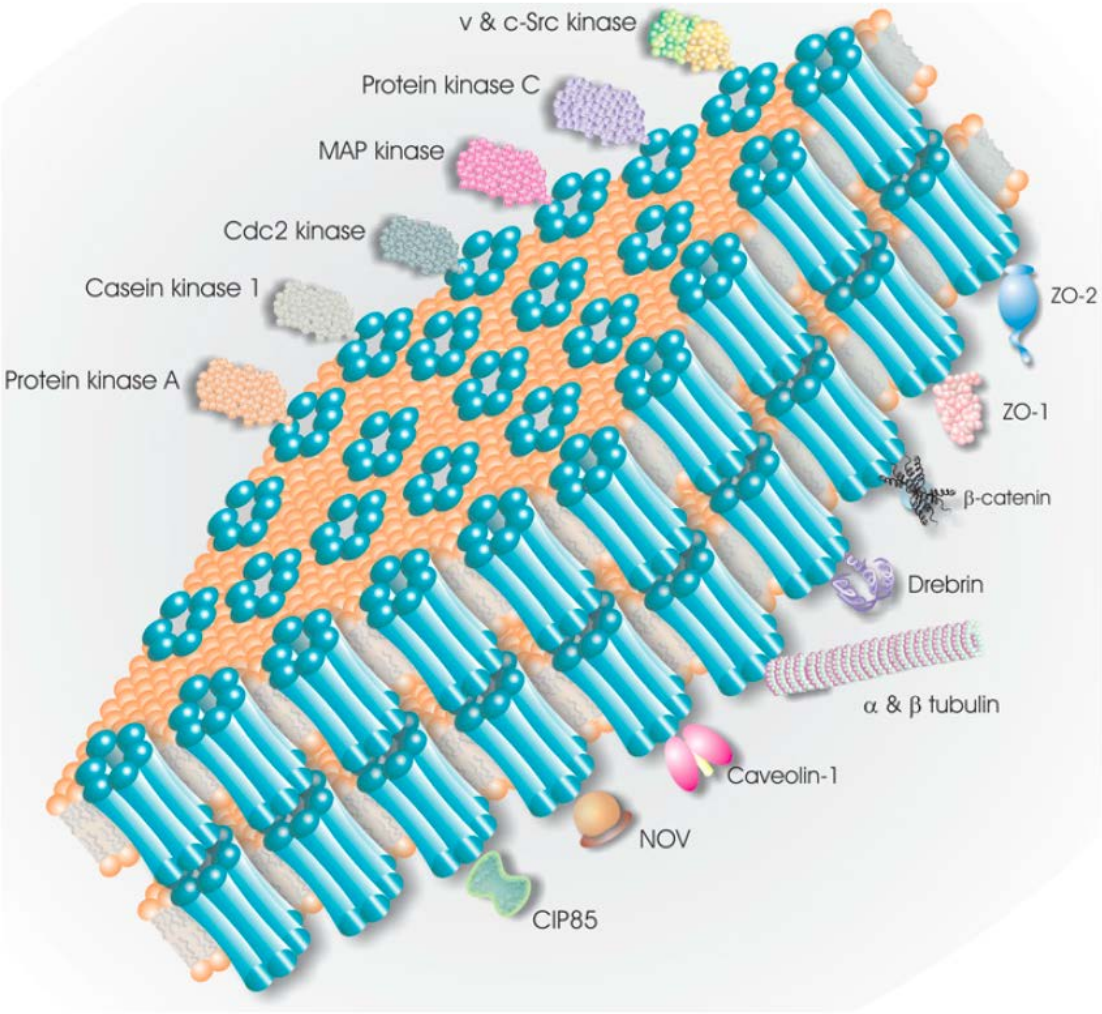

Figure 1-5. Cx43 interacting proteins. Connexins interact with many proteins (bottom half of membrane) and are phosphorylated by many kinases (top half of membrane). Reproduced from [52].

Cx43-ZO-1 interaction plays a key role in regulating GJ organization and remodeling and, as such, has been studied extensively [57,73–77,80–85]. Work from our lab suggested a role for ZO-1 in the control of GJ plaque size, as ZO-1 was found primarily localized to the edges of GJ plaques in immunolabeling studies [86]. A tool developed in our lab to investigate the interaction between Cx43 and

ZO-1 was a peptide mimetic of the Cx43 C-terminus [77]. This peptide – αCT1 – contains an amino (N)-terminal biotin tag, an antennapedia internalization sequence, and the nine most extreme C-terminal amino acids – a known PDZ binding ligand mediating interaction with the ZO-1 PDZ2 domain (Fig. 1-6). A control peptide of the same C-terminal amino acids, but in reverse order was used in further experiments. In these experiments, it was found that treatment of neonatal rat cardiomyocytes with αCT1 decreased co-localization of ZO-1 at the edge of GJs and increased plaque size [77]. This reduced interaction between Cx43 and ZO-1 did not alter total Cx43 levels in cells, but did result in a shift in the pools of Cx43 so that more Cx43 was located at the interface between two cells and less was located in intracellular pools. Together, these data suggest that Cx43-ZO-1 interaction at the GJ plaque periphery may regulate GJ size by controlling the rate at which hemichannels transition into the GJ plaque.

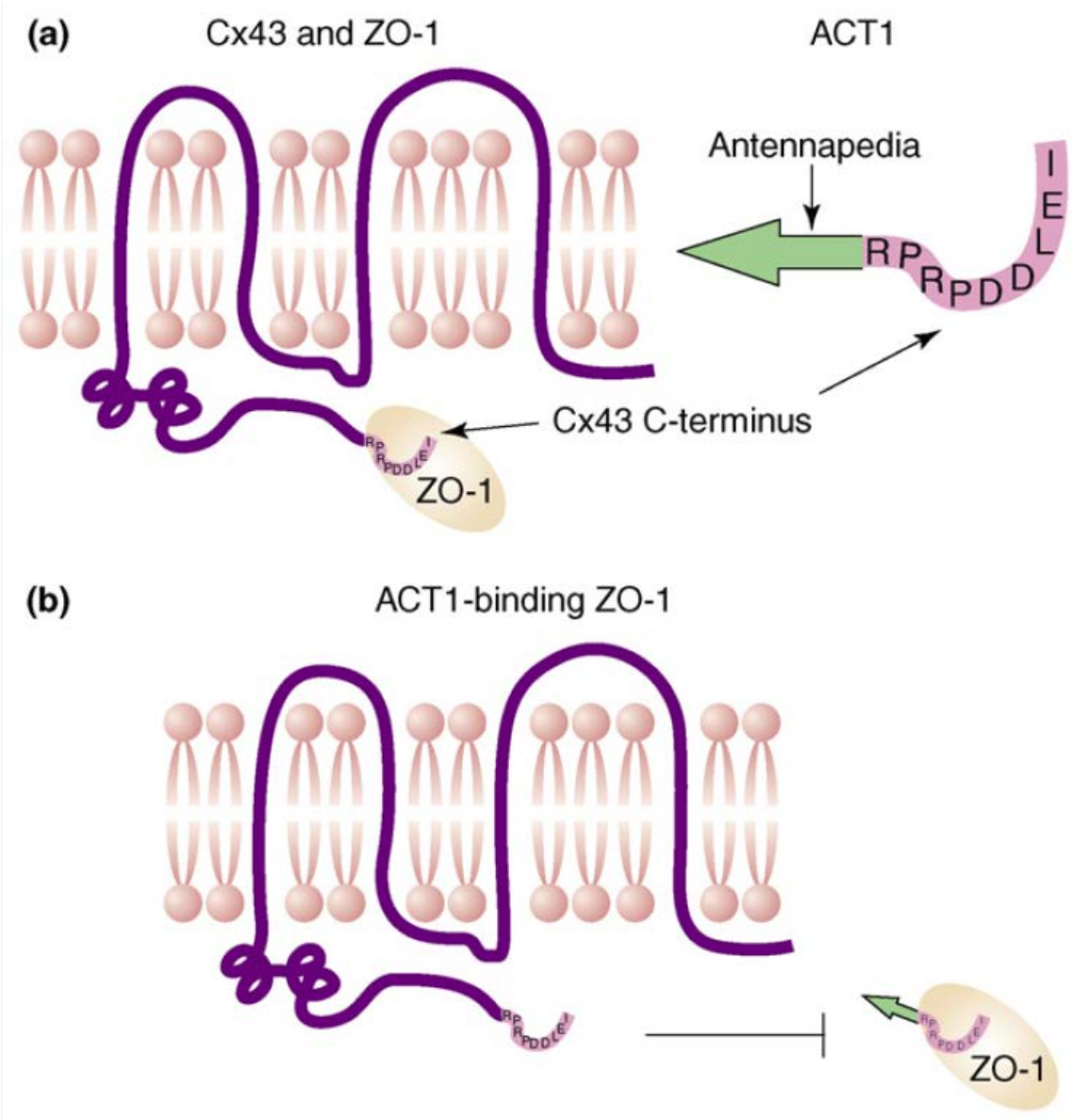

Figure 1-6. αCT1 interrupts binding of ZO-1 to the Cx43 C-terminus. A) ZO-1 normally binds the Cx43 C-terminus. αCT1 was developed to investigate this interaction. αCT1 is a peptide mimetic of the Cx43 C-terminus attached to an antennapedia cell-internalization sequence. B)When added to cells, αCT1 crosses the cell membrane and bind to ZO-1, inhibiting the interaction of Cx43 and ZO-1. Reproduced from [329].

Further studies in our lab showed that this Cx43-ZO-1 interaction occurred at the ‘perinexus’ – a specialized domain around the GJ plaque. In this domain, it was proposed that the function of Cx43-ZO-1 interaction is to control hemichannel to GJ transition [57]. ZO-1 may, therefore, control the balance between hemichannel-mediated communication with the outside of the cell and GJIC. Accordingly, these studies showed that decreased Cx43-ZO-1 interaction led to increased GJ-mediated dye transfer between cells and decreased hemichannel dye uptake [57]. This parallels the long-held view that GJs are assembled from connexons added at the edges of the GJ plaque [67,87].

Another important type of intermolecular interaction of the Cx43 C-terminus is that of the numerous enzymes that can interact to phosphorylate residues of the tail. These are involved in regulating gating of connexins. Most connexins are phosphoproteins [88], and most phosphorylation events occur after membrane delivery [89]. While the phosphorylation events of connexin proteins are too extensive to be covered in depth here, the focus will be on phosphorylation of Cx43, as this is where most study of this phenomena has been done. A metabolic labeling study showed that Cx43 arrived at the membrane mostly unphosphorylated, and progressive phosphorylation of Cx43 paralleled incorporation into GJs [90]. Along these lines, dephosphorylation of connexins has been linked to degradation [42]. Phosphorylation plays roles in connexin turnover, GJIC, and cell and tissue pathophysiology, though this varies by cell type [88].

The Cx43 C-terminus has 12 serine residues and two tyrosine residues that are known to be phosphorylated (Fig. 1-7A) [91]. The phosphorylation events of the Cx43 C-terminus are reviewed extensively by others and can be found here: [35,91–94]. Phosphorylation of Cx43 happens at different points throughout its lifecycle [90,95]. Various degrees of phosphorylation lead to changes in electrophoretic ability, and the protein separates into three major bands on Western blots: P0, P1, and P2. P0 is non-phosphorylated, and P1 and P2 are progressively phosphorylated and migrate more slowly (Fig. 1-7B). To some extent, Cx43 may be phosphorylated before it is inserted into the membrane [96,97]. Cx43 is known to be phosphorylated by non-receptor- and receptor protein tyrosine kinases, mitogen-activated protein (MAP) kinase, and elevated cAMP [91]. Protein kinase C (PKC) is known to increase Cx43 phosphorylation and decrease GJIC in numerous cell types [98–101]. Previous reports in NRVMs suggest that PKC activation increases [102] or causes no change to GJIC [103].

PKC phosphorylates Cx43 at S368 and S372. S368 is likely responsible for reduced GJIC and changes in single channel behavior [92], as PKC activation decreased single channel conductance of Cx43 to ~50 pS, whereas in cells with a Cx43-S368A mutation (i.e., substitution of serine for a non-phosphorylatable alanine (A) residue), the ~100 pS channel conductance state was present. Our lab has shown that PKCε activity is increased by αCT1, with a subsequent increase in Cx43 pS368 [104,105]. Though various diseases and compounds alter the phosphorylation status of Cx43, the biophysics of this process is not well

understood. For example, pS368 is often associated with the P0 band in Western blots, though it is unknown when this event occurs and whether this alters GJ plaque structure.

1.4 Cardiac tissue organization and function in the normal heart

Myocytes are responsible for the contractile function of the heart, while fibroblasts serve to generate the extracellular matrix (ECM) on which the heart is organized. While myocytes comprise up to 75% of the volume of the heart, non-myocytes are far more numerous, accounting for nearly two thirds of cells by number in rat [106] and human [107,108], although these cells may only account for 30% of cells by number in mice [109].

Myocytes are organized into sheets that are 3-5 cells thick and these muscle layers can slide against each other during ventricular contraction. ‘Fiber orientation’ or the orientation of myocytes along their long axis, varies from -45 in the epicardium to +45° in the endocardium relative to the ventricle horizontal plane [110,111]. Connexins are located primarily at the IDs on the short ends of myocytes, with some localized to lateral myocyte borders (Fig. 1-8A). This arrangement promotes anisotropic propagation of electrical signal through the myocardium [112].

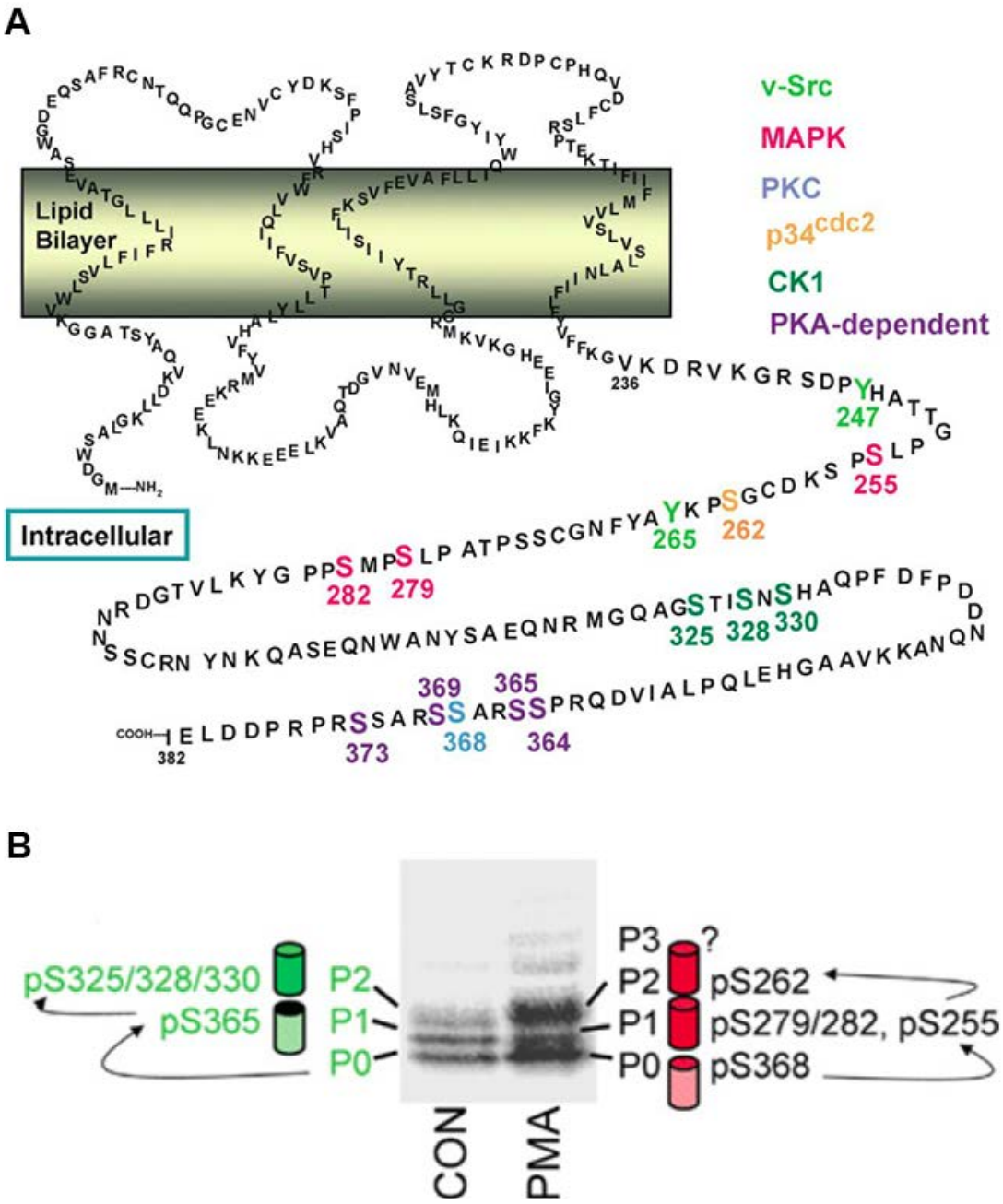

Figure 1-7. Cx43 C-terminal phosphorylation sites. A) There are many phosphorylatable amino acids on the Cx43 C-terminal tail. Each is highlighted here in colors corresponding to the enzyme responsible for its phosphorylation. B) Phosphorylation events are associated with changes in electrophoretic mobility of Cx43, and three bands result on Western blots. The P0 band migrates fastest and is thought to correspond to nonphosphorylated Cx43. The P2 band migrates slowest and incorporates multiple phosphorylation events. P1 is an intermediate band. Reproduced from [91] and [35].

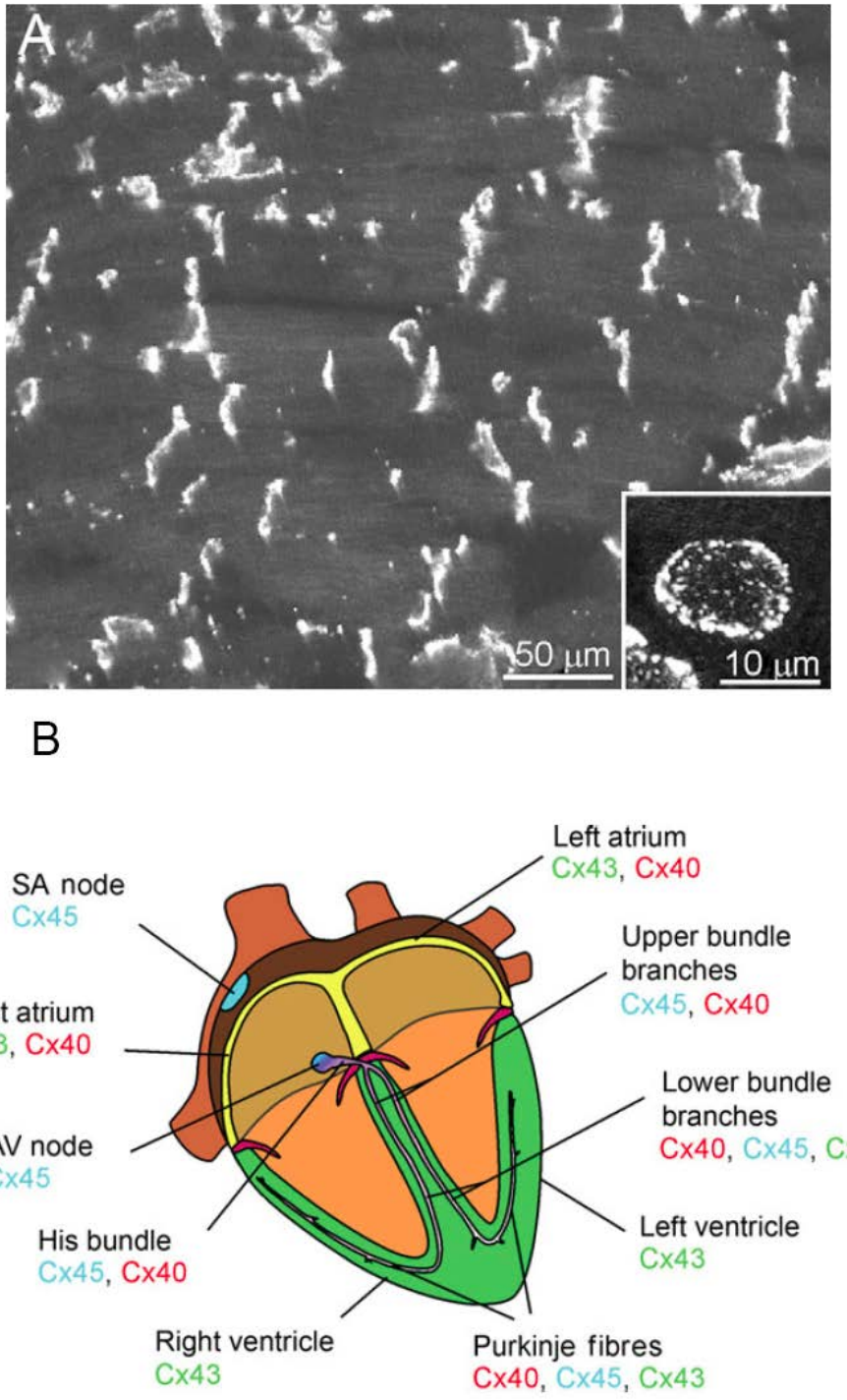

Figure 1-8. Connexin organization in the heart. A) Cx43 is localized primarily at the intercalated discs (IDs), and electrically connects adjacent myocytes. Inset: Cx43 is present in higher density at GJ plaque edges. B) Connexins 40, 43, and 45 are all found in heart and their expression varies by region of the heart, with Cx43 being the predominant connexin in the ventricle. Reproduced from [330].

Connexins in the heart are thought to be responsible for the spread of electrical signals. Conduction starts in the sino-atrial (SA) node and travels through the atria to the atrio-ventricular (AV) node. Here, conduction is delayed while the ventricles are filled, then electrical activation is propagated though the His-Purkinje system, down to the apex of the heart. Waves of excitation then travel from the apex up to the base through ventricular myocardial tissues, being conducted through myocytes that are highly interconnected at IDs. The ID allows for sequential activation and contraction of the muscle syncytia by allowing the passage of ions.

The mammalian heart contains three types of connexin proteins in abundance: Cx40, Cx43, and Cx45 [113–116]. Local conduction differences and electrophysiological properties in the heart are thought to be largely accounted for by the variation in connexin distribution (Fig. 1-8B) [116]. Analysis of connexin localization using myocyte and fibroblast specific markers in rabbit ventricle showed that 95% of Cx43 was associated with myocytes, 7% with fibroblasts, and 3% was found at the interface between the two cell types (Fig. 1-9A) [117].

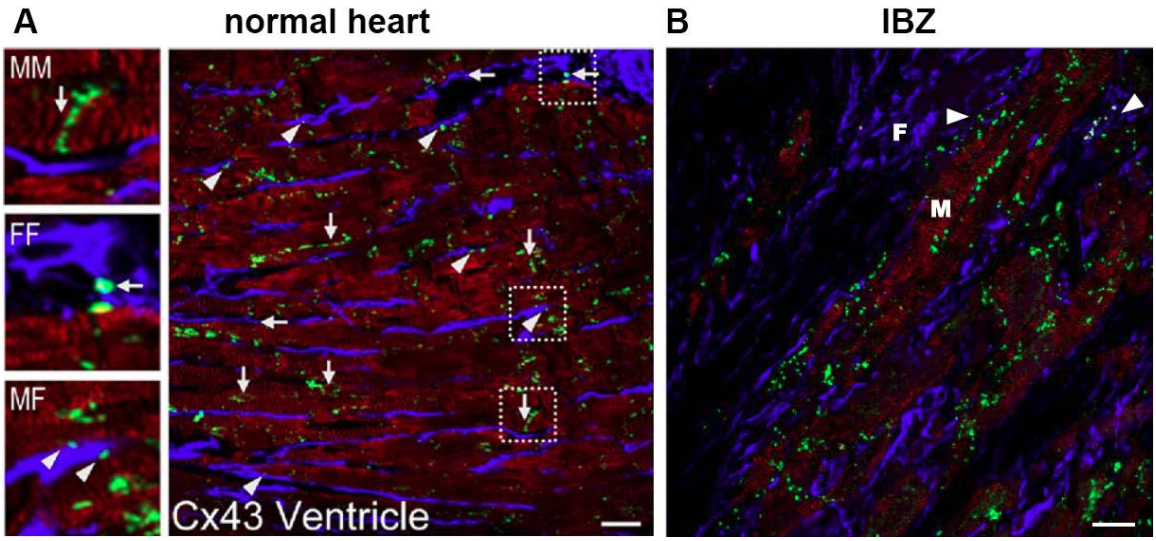

Figure 1-9. Cx43 localization in the ventricle in normal heart and disease. A) In the normal heart, Cx43 (green) is highly expressed in myocytes (red). Fibroblasts (blue) also express some amount of Cx43 and can interact with myocytes via this protein. Vertical arrows show myocyte-myocyte connections (MM), horizontal arrows show fibroblast-fibroblast (FF) connections, and angled arrowheads show MF connections. B) In the injury border zone (IBZ) of infarcted myocardium, Cx43 organization is disrupted and is increasingly found in myocyte-fibroblast interactions (left arrowhead), and in fibroblasts (angled arrowhead). Reproduced from [331] and [173].

While the long-held view of electrical activation in the heart involves ion transport through GJs, ephaptic coupling – in which local ion concentration gradients are responsible for activation of adjacent cells – may also play a role [118]. Studies from our lab have demonstrated the presence of the cardiac voltage-gated sodium channel, $Na_v1.5$, in the perinexus along with other structural, functional, and *in silico* data that provides evidence for this non-electrotonic form of coupling in the heart [119,120]. Computer models have shown that ephaptic effects may be seen in all areas of extracellular space, not just at the IDs between myocytes [121], leaving open the possibility for fibroblast involvement.

Cardiac fibroblasts are organized into thin sheets, interspersed between myocytes in the myocardium. Fibroblasts *in situ* have a large surface area, with electron microscopy studies estimating their surface area at >1500 μm^2 [122]. A large membrane surface area would enable fibroblasts to extensively interact with adjacent cells.

Cardiac fibroblasts were once thought of as a homogeneous population of cells, though recent studies have shown that these cells of mesenchymal origin derive from a number of sources. The majority of fibroblasts derive from the pro-epicardium [123]. Fibroblasts also originate from the epicardium and endothelium by epithelial-to-mesenchymal transformation (EMT) [124,125] and endothelial-to-mesenchymal transformation (EndoMT) [126–128], respectively, though the species-specific relative contribution of these populations is presently unknown.

One caveat to studying cardiac fibroblasts that may directly relate to their developmental heterogeneity is the lack of a marker that is inclusive and specific. Proteins that have been used to identify fibroblasts – of both normal and activated phenotypes – include discoidin domain receptor tyrosine kinase-1 (DDR2) [129,130], vimentin [131–133], Transcription factor-21 (TCF21) [134,135], fibroblast specific protein-1 (FSP1) (which has turned out not to be fibroblast specific) [136], fibroblast activation protein (FAP) [137–139], Wilm's Tumor 1 (WT1), and α-smooth muscle actin (αSMA) [140,141]. Lack of a specific marker has made studying these cells in health and disease challenging. While one of the

primary functions of a fibroblast is to produce collagen, few studies have used this as a benchmark for identifying fibroblasts in either health or disease, though more recent studies have demonstrated the utility of collagen as a genetic marker of cardiac fibroblasts [141].

Fibroblasts, as a mesenchymal cell, have been pegged as having the primary structural role of producing the ECM ‘skeleton’ of the heart into which the cardiac cells are organized. While this function is required for maintenance of the normal myocardium, and for preventing rupture of the infarct area due to myocyte death after myocardial infarction, fibroblasts are known to have many other roles. Fibroblasts are extensively involved in biochemical signaling in the heart (reviewed here: [142–144]), but also contribute to electro-mechanical signal transduction [145,146], and can be electrotonically coupled to myocytes [21,147–149], as fibroblasts have been shown to express Cx40, 43, and 45 [150,151]. The field of myocyte-fibroblast electrotonic coupling, while far from new (some of the first reports of myocytes coupling to non-myocytes were by Goshima [152] in the late 1960s), still has a lot of open questions.

1.5 Changes in the post-myocardial infarction heart

The myocardium does not have the ability to regenerate, so after MI, the significant loss of cardiac muscle is replaced by a scar. The healing response in the

myocardium has been reviewed extensively elsewhere (see: [153,154]). A brief review will follow. Cells in the ischemic area of the myocardium die and cardiac repair begins with the inflammatory response that clears the infarcted region of tissue of dead cells and debris and provides the proper biochemical signaling to heal the infarct. Fibroblasts are activated in the process and migrate into the wound to replace the lost myocytes and deposit excess ECM. This healing and scarring response, as in other wounds in the body, changes over time, though it rarely reaches an equilibrium state as this type of scarring injury is generally associated with declining (and irrecoverable) cardiac function. As the heart is less able to efficiently pump due to the loss of myocytes, the heart begins to dilate and myocytes hypertrophy, a process that can eventually deteriorate into heart failure – an ultimately fatal disease [6].

Fibroblasts post-MI release chemotactic factors like transforming growth factor-β (TGF-β) that recruit inflammatory cells into the ischemic tissue and activate fibroblasts [155–158]. Activation of fibroblasts leads to transdifferentiation to myofibroblasts and includes an initial increase in proliferation and migration, followed by increased synthesis of ECM proteins [159]. While this helps prevent the heart wall from rupturing after MI, these changes can alter normal conduction through the heart [160]. As described in the previous section, fibroblasts in the heart comprise a heterogeneous population of cells. Recent studies in various injury models have shed some light on the contribution of these relative

populations to pressure overload-induced fibrosis in the heart [141,161], though it is presently unknown how these populations contribute to healing after MI.

Bone marrow derived cells are known to be recruited to the site of injury in many tissues in the body. Several studies of MI suggest that bone marrow derived cells make a large contribution (up to 60%) of fibroblast-like cells in the scar [162–165], though there is some debate as to whether the labeled cells in these models truly represent bone marrow derived cells.

The IBZ is often the site of reentrant arrhythmia generation and there are several structural factors that contribute to this, including changes in cell and tissue organization and changes in Cx43 distribution. While the myocytes in the ischemic area die and are replaced with fibroblasts and the ECM these cells deposit, some of the myocytes in the IBZ survive. Structural remodeling in the IBZ involves an interspersion of myocytes with fibroblasts and ECM, leading to separation of myocytes and increased coupling between myocytes and fibroblasts (Fig. 1-9B) [11,166,167]. Additionally, increased deposition of ECM proteins leads to an altered structure that can separate cells, interrupting patterns of electrical coupling. Alterations in cell organization and coupling may contribute to the arrhythmogenic propensity of the IBZ [168].

In addition to reorganization of cells and increased deposition of ECM proteins post-MI, Cx43 reorganization to the lateral borders of myocyte membranes in the IBZ, as seen in Figure 1-9B, is thought to contribute to arrhythmias [112,169–171].

One of the alterations in fibroblasts post-MI is an increase in connexin expression [167,172,173], which increases the ability for fibroblasts to be coupled to myocytes via GJs [167]. While myocyte-fibroblast coupling is relatively rare in the uninjured myocardium, immunolabeling studies show that this coupling is increased in the IBZ (Fig. 1-9) [173,174]. In multiple experimental animal models, conduction slowing is measured in the IBZ and scar [104,160].

In addition to its known function in transmission of electrical signals in the heart, Cx43 is known to be involved in the spread of injury signals. GJs in skin are implicated in the spread of injury signals [175], and are involved in inflammation, wound closure, and scarring (reviewed here: [176,177]). Accordingly, the knockdown of Cx43 in mouse skin has led to smaller wound sizes and faster rates of closure [178]. In our lab, application of the αCT1 peptide to excisional skin wounds in rats and pigs led to shorter times to wound closure and scar tissue with more normal histo-architecture [179]. This peptide has completed Phase I and Phase II clinical trials for wound healing in chronic non-healing diabetic foot ulcers [180] and venous leg ulcers [181], where the peptide led to significant decreases in ulcer size versus standard of care treatment alone. In other studies from our lab, cryo-injury size was increased in streptozotocin (STZ) diabetic mice compared to control mice receiving insulin, and this increase in injury size was associated with a decrease in Cx43 pS368 [182], suggesting that Cx43 pS368 is likely decreasing the conductance state of GJ channels and the subsequent injury spread in the heart.

A decrease in GJIC has been observed in the myocardium post-MI [183]. After ischemia or during cardiac hypertropy, density of GJs decreases in the ischemic area compared to the remote regions of myocardium [184]. Changes in GJ distribution in the IBZ seem to contribute to reentrant arrhythmia generation [185]. Decreased electrical coupling during acute MI has been correlated with dephosphorylation and reorganization of Cx43, as well as translocation from the cell surface to intracellular pools [186,187].

In the population of Cx43 that remains at the ID in an ischemic setting, there is an increase in phosphorylation at S368 (Fig. 1-10) [94]. Additionally, ischemic preconditioning has been shown to increase PKCε–mediated Cx43 phosphorylation of S262 and S368, and prevent Cx43 lateralization following an ischemic insult [188]. Phosphorylation events in Cx43 are known to regulate channel effects like unitary conductance, so it may be that communication is reduced as a protective mechanism against injury spread from the ischemic area.

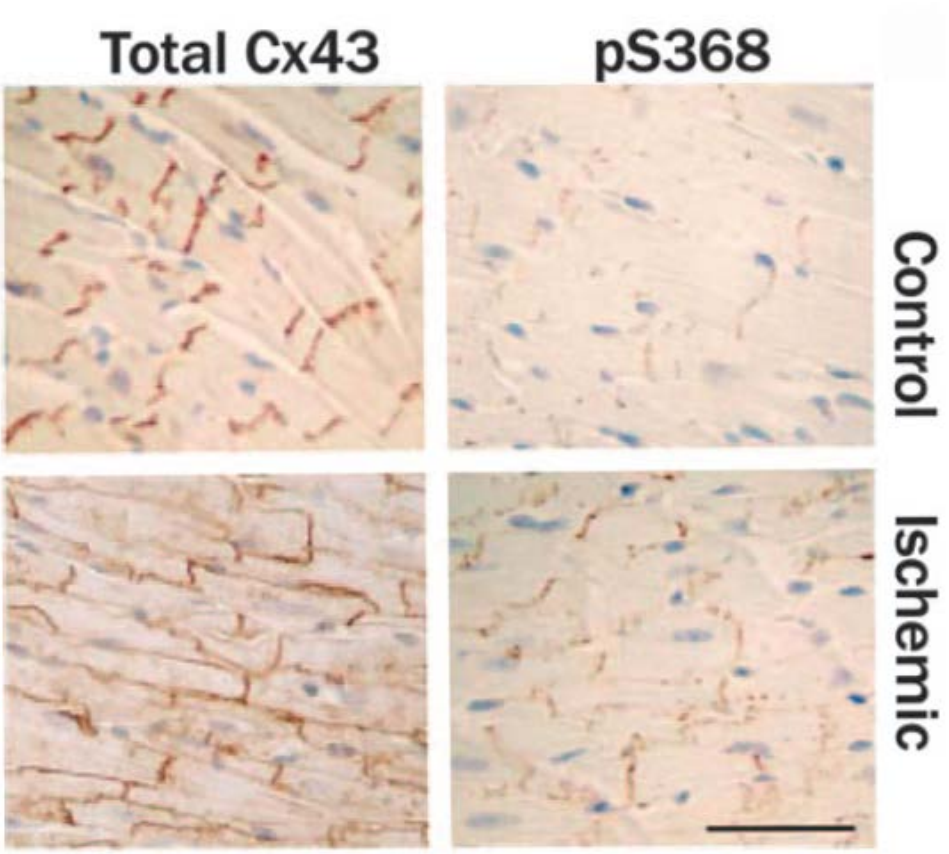

Figure 1-10. Cx43 phosphorylation in ischemic disease. Cx43 that is phosphorylated at serine 368 (pS368) is maintained at the IDs in ischemic conditions while Cx43 reorganizes to the lateral myocyte borders. Reproduced from [94].

1.6 Attempts to heal the heart

Cardiac disease models

Models of cardiac disease – both *in vivo* and *in vitro* – are used extensively in research not only to better understand disease processes, but also as a model for testing pharmaceutical compounds. The commonly used left anterior descending (LAD) coronary artery experimental model of acute MI in mice is closely

representative of ischemic cell death as seen in humans [189,190]. However, due to differences in branching of the coronary arteries and collateral circulation in rodents, this model often leads to differences in size and shape of the infarct area and scar [191]. First reported by van den Bos and colleagues [190], a cryo-injury model of infarction is generated by creating an injury area by freezing the left ventricle. While the mechanism of cell death is different in the cryo-injury model from the ischemic model, cryo-injury creates an extensive IBZ that is a few cell layers thick, and an injury that is of repeatable size and shape, making it ideal for testing therapeutic compounds targeted at altering IBZ properties. More clinically relevant models include dog, pig [192,193], and sheep infarction [194], since these animals are closer to humans in size, structure, and heart rate. However, these large animal models are expensive, low throughput, and time consuming.

Many *in vitro* models have been used to study cardiac disease processes. These models use NRVMs, embryonic chick myocytes, human embryonic stem cell-derived cardiomyocytes, and induced pluripotent stem cell (iPSC)-derived cardiomyocytes [195]. These models include natural hydrogel-based models, synthetic scaffold-based models, and microdevice-based models [196]. An advantage of iPSC cardiac disease models is that they can often reproduce genetic cardiac diseases, as has been observed with familial dilated cardiomyopathy [197] and familial hypertrophic cardiomyopathy [198]. More recently, *in vitro* models of cardiac disease have been used to test pharmaceutical compounds that are already used clinically in order to develop models relevant to

certain cardiac disease conditions. Human iPSCs have been used to test both an ion channel blocker (verapamil) [199] and a β-blocker (metoprolol), using beat rate and mechanical motion to assess cardiac tissue function. Additionally, another β-blocker (isoproterenol) and a human Ether-à-go-go-Related Gene (hERG) blocker (E-4031) were tested in this model [200]. However, further development of these models for testing of pharmaceutical compounds relevant to cardiac disease is needed.

Cardiac tissue engineering

Nearly 20 years ago the first engineered cardiac tissues were created from embryonic chick cardiomyocytes [201]. The field has seen immense growth since then with hundreds of papers being published each year on the subject, including the first report of cell sheets being implanted in a patient [202]. The history, development, and state of the art of this field have been reviewed extensively elsewhere (see: [203,204]). The following is a brief summary on the successes and challenges of the various techniques used to engineer cardiac tissue.

Cardiac tissue engineering has its roots in culture of aggregated cardiac cells, generated by rotating culture by Moscona in 1959 [205]. These heart cells formed heart-like tissue that generated beating aggregates.

Hydrogels have been used since the 1980s and include a gelling matrix of natural proteins like collagen or Matrigel in a casting form [201]. These proteins induce cells to spread and form intercellular connections. The cells can contract and remodel the matrix in which they reside. Hydrogels that are anchored induce alignment of cells and enable constant mechanical strain of engineered tissues. The first anchored studies demonstrated the importance of mechanical forces in alignment of cells and proper engineered tissue development [206]. More recent studies have shown that electrical stimulation can also induce proper cell alignment and development of tissue structure [207].

A classical engineering approach to cardiac tissue engineering involves creation of a prefabricated matrix that is seeded with cardiac cells or cardiac progenitor cells. Various materials used to create matrices include natural and synthetic materials like alginate [208] and collagen [201], or polyglycolic acid [209], and poly-L-lactic acid/polyglycolic acid composites [210], among others. These matrices can be made to any dimensions and easily manipulated in culture. This being said, synthetic scaffolds are challenged by limited diffusion capacity, inability to be remodeled (though some can be degraded), and toxic degradation products.

Decellularizing whole hearts with detergents that do not affect matrix structure can provide natural cues to cardiac cells or cardiac progenitor cells for repopulation, though repopulation of these structures has proven difficult [211].

Temperature-sensitive coatings on culture dishes allows cells to be grown in sheets and then detached [212]. These sheets can be stacked to generate beating 3D tissues. While this scaffold-free technology generates a tissue that is suitable for transplantation, these tissues can be difficult to manipulate because of their mechanical properties. However, this technique continues to be developed for cardiac repair [213,214].

In addition to mechanical strain and electrical signals, *in vitro* development of cardiac tissues has indicated the importance of non-myocytes in the formation of functional tissues. Tissues using a combination of myocytes and fibroblasts develop higher forces [215] and better tissue structure and electrical activation threshold [216].

Another approach to cardiac tissue engineering involves injection of cells in a matrix *in situ* and relies on native signaling within the myocardium to induce differentiation and maturation of injected cells [217]. Many of these techniques have been used in some variation or combination to create engineered cardiac tissue. However, there are remaining challenges to developing and treating an injured heart to regain function, including cell sourcing, standardization of protocols, serum-free culture, tissue maturation, and testing to ensure consistency across various methods [204].

Pharmaceutical development

There a great number of pharmaceutical compounds used for cardiac disease. General classes of these drugs include anticoagulants, antiplatelet agents, ACE-inhibitors, angiotensin II receptor blockers, angiotensin receptor neprilysin inhibitors, β-blockers, combined α- and β-blockers, calcium channel blockers, cholesterol lowering medications, digitalis preparations, diuretics, and vasodilators [218]. In 2010, global market sales reached $170 billion for cardiovascular drugs alone and growth was projected to hit $187 billion by 2016 [219]. Development of new drugs, however, is expensive and inefficient. For most compounds, it takes over a decade of research and nearly $5 billion per drug [220–222]. Additionally, in order to launch a single drug per year, 9 compounds on average need to enter Phase I clinical trials, 5 need to enter Phase II, and 2 need to enter Phase III trials [221].

Before drugs reach the preclinical animal-testing phase, they are typically screened *in vitro* using established and well-characterized cell lines. 2D *in vitro* cultures are not representative of the 3D tissue microenvironment in either health or disease, making this a poor model for investigation. Additionally, preclinical animal models are expensive, poorly predict outcomes due to interspecies variation in cardiac electrophysiology [223,224], and have led to drugs being withdrawn from the market because of previously unobserved cardiotoxic effects [225,226]. Human heart cells and tissue would provide more relevant models, but

are difficult to obtain and challenging to maintain in culture, so they are an unrealistic testing platform [227].

There is a great need for design of new testing platforms with the goals of reducing cost and time to approval, decreasing the number of drugs that make it past approval and are then removed from the market because of toxic effects, and reducing side effects. In the last 20 years, the US Food and Drug Administration approved 113 drugs for cardiology and vascular diseases, many of them generics of drugs that had come off patents [228]. Not a single one of these drugs is aimed at healing the heart, restoring lost cardiac function, or regenerating the myocardium. Much preclinical testing directly targeting regeneration or disease-related signaling cascades exists [229]. A combination of these new therapies and development of novel testing platforms has the potential to transform the development of cardiovascular therapeutics.

The effect of Cx43 C-terminal mimetic peptide on the healing heart

We adapted the cryo-injury model for use in our lab [104], and we have determined that it produces an injury of reproducible size and shape, making it useful for testing of therapeutic compounds as fewer animals can be used to detect differences between treatments. We have shown that treatment of a murine cryo-injury with αCT1 led to reduced LV dilation, fewer inducible arrhythmias, lower arrhythmia

severity scores, increased ventricular depolarization times, and maintenance of Cx43 at intercalated discs between myocytes, which was associated with an increase in Cx43 pS368 [104,230].

To further investigate the changes in the myocardium that could be responsible for the improvements in physiological function, TTC staining of hearts 8 weeks after cryo-injury showed a trend of decreased scar volume for αCT1-treated hearts relative to reverse peptide and vehicle controls [231]. The difference was significant ($p < 0.02$) for the αCT1 and reverse comparison. Images through the base-apex axis along the middle of each scar were used to quantify scar depth and thickness of underlying myocardium. There was a trend of decreased scar depth and increased depth of underlying myocardium for αCT1-treated hearts, but the differences between treatment and controls were not significant.

Masson's trichrome staining of histological sections of the scar also indicated that fibrous organization of the scar in αCT1-treated hearts was more uniform than in control mice (Fig. 1-11A) [231]. This was seen as a more regular pattern of collagen deposition and increases in collagen alignment along the scar. Vascular structures in the scar tissue appeared to increase scar non-uniformity by acting as obstacles that caused local variations in the orientation of collagen fibers.

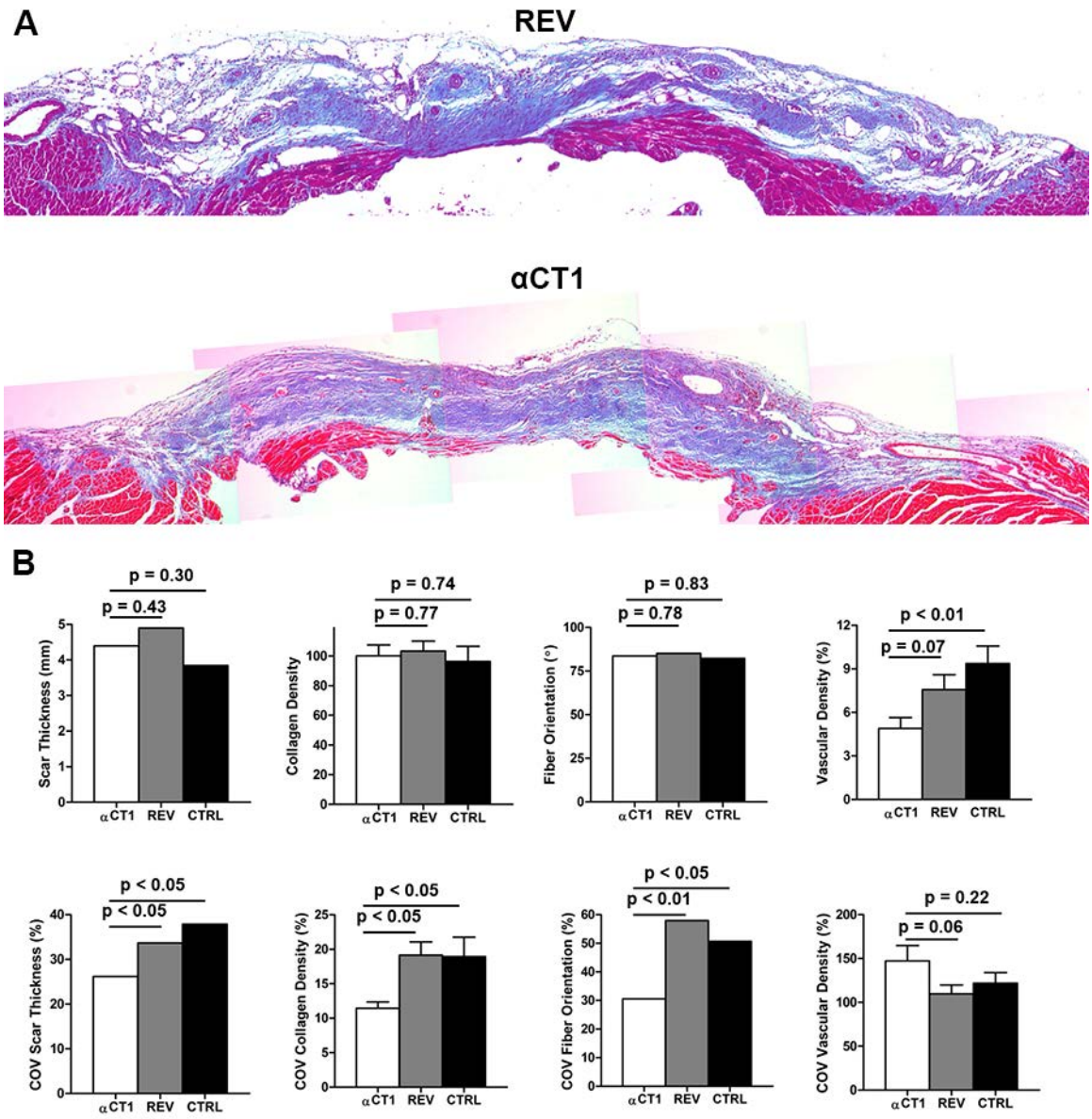

Figure 1-11. Masson's trichrome images of cryo-injured hearts indicates a more uniform scar structure. A) αCT1 treated hearts (bottom) show a more uniform fibrous structure than reverse inactive peptide controls (top). B) This was quantified by examining parameters of the scar substructure. While no differences were seen between αCT1 and controls in scar thickness, collagen density, or fiber orientation, the coefficient of variation (COV) of these measurements was significantly lower in αCT1-treated hearts compared to controls, meaning scars were more uniform. While COV of vascular density did not differ between groups, the vascular density was significantly reduced in αCT1-treated hearts versus controls – a factor that may contribute to more uniform collagen fiber orientation.

A survey of scar structure parameters showed that scar thickness (measured as the epicardial to endocardial thickness through multiple points along the scar) was not significantly different between groups (Fig. 1-11B). Collagen density was measured as the area of collagen tissue normalized to total scar area in Masson's stain. Collagen fiber orientation was measured at 20 different points within the scar. None of these measurements were significantly different between treatments and controls.

We measured the coefficient of variation (COV = SD/mean) of each of these measurements (Fig. 1-11B). The COV of scar thickness is significantly reduced in αCT1-treated scars compared to controls, meaning that scar thickness is more uniform. The COV of collagen density is lower in αCT1-treated hearts, meaning collagen density is more uniform. The COV of collagen fiber orientation is lower in αCT1-treated hearts compared to controls, meaning collagen is more organized in a uniform direction. In all of these parameters, αCT1-treated hearts showed less variation than either reverse or vehicle controls. This suggests that, in hearts treated with αCT1, scars were more uniform. We measured vascular density and the COV of vascular density and found fewer vessels in the αCT1-treated scars. It may be that this reduction in vascular density is one of the reasons for lower variation in collagen orientation, as with decreasing vessel density, there are fewer structures for collagen fibers to negotiate. Overall, the quantitative data indicated that the histo-architecture of 8-week LV cryo-scars in αCT1-treated hearts was more uniform than that of controls.

At 8 weeks after cryo-injury, a definite IBZ approximately 5-10 myocyte diameters wide differentiated adjacent to cryo-injury scars. This narrow zone of myocardial cells exhibited increases in MLC2a immunolabeling and this was significantly increased in αCT1-treated hearts compared to controls (Fig. 1-12A,B). The IBZ was also characterized by interdigitation of collagen fibrils projecting from the scar between border zone myocytes (Fig. 1-13A). There were striking differences in IBZ structure between αCT1-treated and control hearts. In picrosirius red staining of control mice, collagen tended to interdigitate in fine patterns between myocytes in the IBZ, while in the IBZ of αCT1-treated hearts, groups of myocytes appeared grouped together in coherent bundles, with myocytes less separated by strands of interstitial collagen than in controls (Fig. 1-13A). Additionally myocytes in the IBZ in αCT1-treated hearts appeared to be slightly larger and more uniformly sized than controls (Fig. 1-13B). When quantified in a 4 cell-thick layer adjacent to the scar, αCT1-treated hearts also showed significantly decreased variability (COV) of IBZ myocyte width (Fig. 1-12B). There was a tendency for the mean size of IBZ myocytes to be increased in the αCT1 group, but this trend was not significant (data not shown). The extent of both MLC2a immunolabeling was also significantly increased in the IBZ myocardium of the αCT1-treated group, as compared to control (Fig. 1-13A,B).

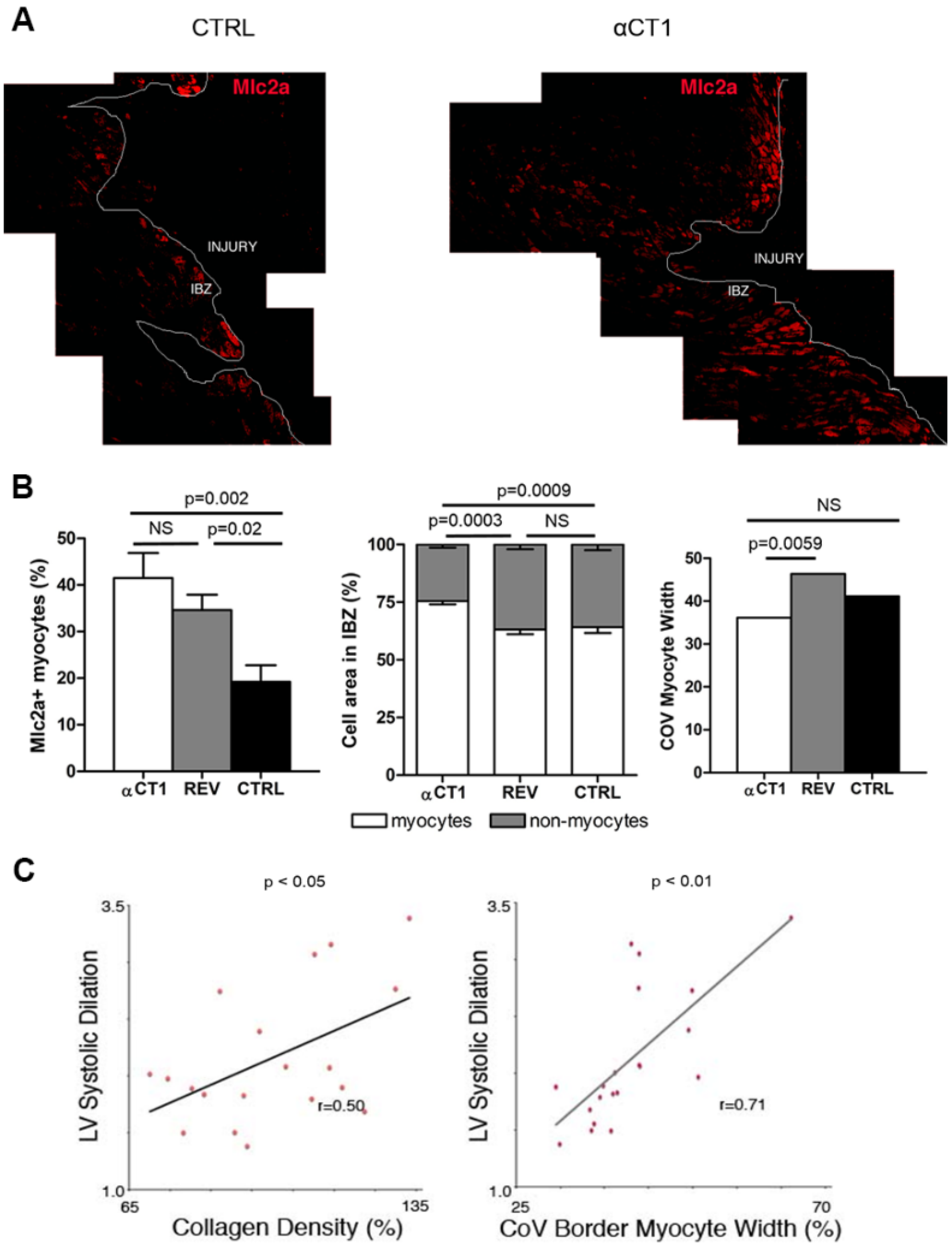

Figure 1-12. αCT1 treatment of cryo-injured hearts alters myocytes. A) αCT1-treated hearts (right) have an increased expression of Mlc2a in the IBZ 8 weeks after injury compared to controls (left). B) αCT1-treated hearts have an increased expression of Mlc2a (left), are comprised of a higher percentage of myocytes (center), and have more uniform myocyte size than control hearts (right). C) Reduced collagen density and less variation in myocyte size in the IBZ are associated with reduced systolic dilation. These histological changes are seen in αCT1-treated hearts.

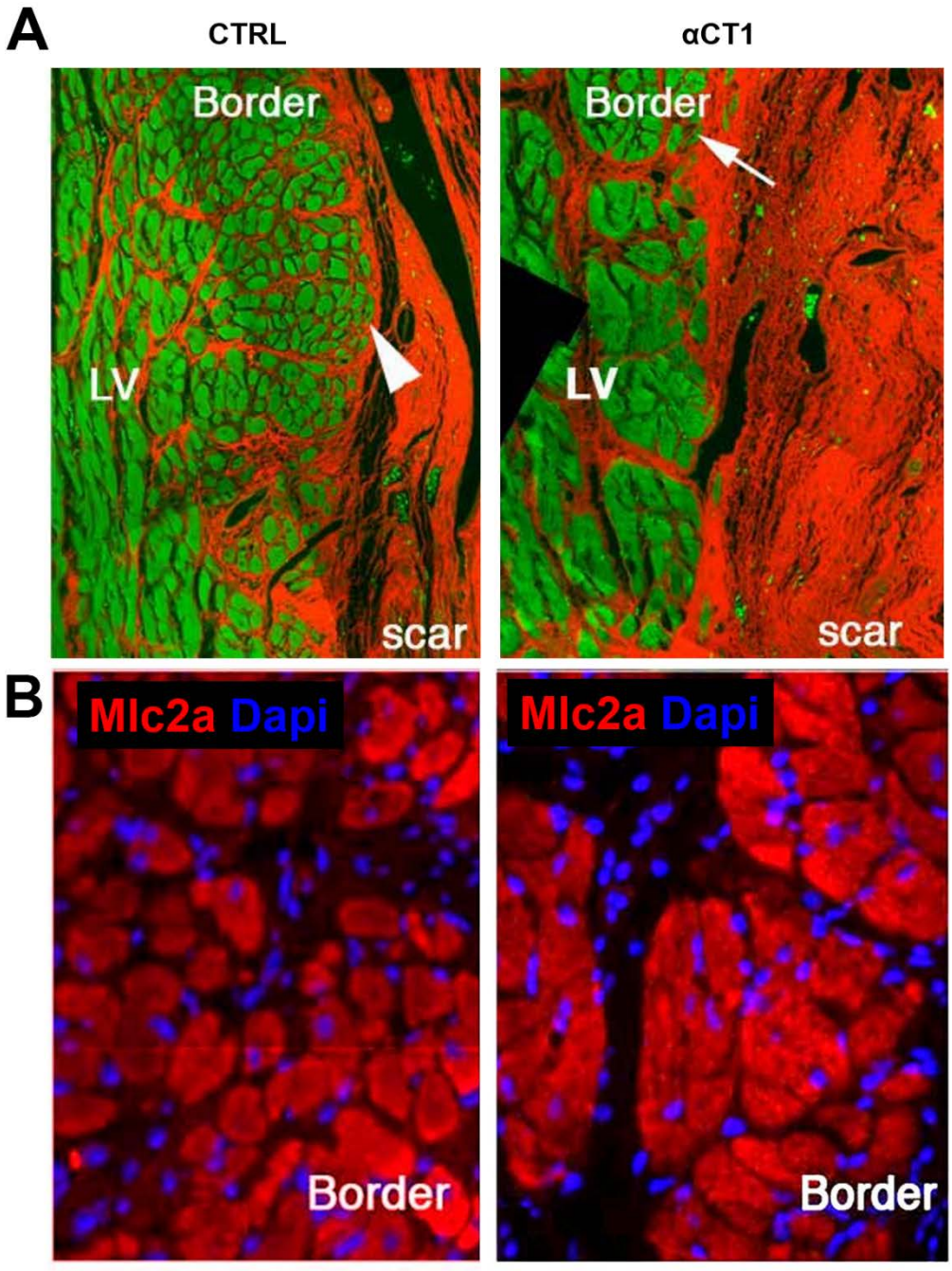

Figure 1-13. αCT1 alters cell organization in the IBZ. A) Picrosirius red staining of scars revealed collagen deposition that separates individual myocytes in CTRL hearts, and this occurred to a lesser extent in αCT1-treated hearts. B) Mlc2a labeling of myocytes in the IBZ indicated more cohesive bundles of myocytes in αCT1-treated hearts while in CTRL IBZ, myocytes appear to be separated by non-myocytes.

Both echocardiography and scar morphometry were undertaken on mice subject to the cryo-injury. If we look at how these histological changes correlate with changes in physiological function, we find significant positive correlations between LV systolic dilation and collagen density, as well as LV systolic dilation and the coefficient of variation of myocyte width in the border zone (Fig. 1-12C). The first correlation may reflect that with increased collagen density the ability of the heart to dilate at systole is being impaired. More uniform myocyte size was also found to correlate with LV systolic dilation. A more uniform myocyte size signifies less variation in the contractile ability of these myocytes in the IBZ, and more even application of mechanical forces. Overall, this suggests that a lower collagen density in the scar and a lower variation in myocyte width in the IBZ are associated with improved physiological outcomes and both of these are changes seen in the αCT1-treated hearts.

Overall the changes in cell organization and scar profile the IBZ with αCT1-treatment raised the question as to whether αCT1 was altering cellular interactions in a way that led to improved physiological outcome.

Study objectives and rationale

Our objective is to develop an *in vitro* model of the IBZ that can be 1) validated against an animal model of infarction, 2) used as a platform for high-throughput

testing of potential therapeutic candidates to target the IBZ, and 3) used to gain a better understanding of heterocellular interactions in IBZ.

The rationale for these studies is the need for disease-relevant and tissue structure-relevant *in vitro* testing platforms for candidate compounds and the lack of understanding of how heterocellular interactions render the IBZ a pro-arrhythmic substrate. Important design criteria for *in vitro* testing of pharmaceutical compounds of relevance to cardiac disease include: 1) A disease model system that sufficiently recapitulates key aspects of the cardiac disease; and 2) A disease model system that can accurately reproduce the drug response seen *in vivo*.

Chapter 2 describes the development and validation of our novel model of the IBZ. It covers changes that we see in the model that reflect the changes in a cryo-injury model of infarction in mouse and begins exploration of the mechanism behind these changes.

Chapter 3 describes the conduction-related changes in cryo-injured hearts treated with our Cx43 mimetic peptide in the presence of varying extracellular ion concentrations, the contribution of recruited bone marrow cells to the healing IBZ, and the effect of the peptide on GJIC.

Chapter 4 describes the changes in myocyte-fibroblast interactions via Cx43 *in vivo* and *in vitro* and examines the GJ plaque sub-domain organization.

Chapter 5 is a stand-alone chapter. It briefly examines the role of Cx43 in healing and regeneration of skeletal muscle, and serves as a proof of principle in modulating the immune response to skeletal muscle satellite cells for muscle regeneration.

Chapter 6 contains conclusions, discusses challenges and limitations, and gives future directions and recommendations.

Significance and innovation

Generation and validation of a novel *in vitro* IBZ model will provide a platform that enables us to better understand heterocellular interactions in the IBZ and the basis for future testing of novel therapeutic compounds. While 3D models have been used extensively to study tumor microenvironment and treatments, to our knowledge, no studies have been done in a 3D model of cardiac cells to examine cellular interactions. This project addresses a critical barrier to progress in development of cardiovascular therapeutics focused on regeneration and altering intercellular interactions. Successful completion of this project will change our knowledge of the disease state and will provide a better model for testing of therapeutics for post-MI patients that is directed at disease mechanism.

These studies are innovative in that they seek to challenge the clinical paradigms by shifting treatment from a focus on prolonging life of post-MI patients to one of

cardiac regeneration and understanding mechanisms that go beyond attempting to stabilize cardiac function. A goal of this work is to also shift current research paradigms for drug development to using more clinically relevant models of disease for testing of therapeutic compounds. This has the potential to decrease cost by finding better treatments, making additional and ongoing treatments for patients unnecessary, and also to identify and remove non-efficacious or toxic compounds in development more quickly, reducing the cost of the drug development pipeline. These studies will accomplish this by creating novel methods for analysis that could lead to further development of instrumentation. Some of these methods are novel to the cardiovascular field, having been used in other fields for therapeutic development, while others are novel across all fields.

CHAPTER 2: DEVELOPMENT AND VALIDATION OF A NOVEL IN VITRO MODEL OF THE CARDIAC INJURY BORDER ZONE

2.1 Introduction

The leading cause of death in the Unites States is cardiovascular disease (CVD), which was responsible for 787,000 deaths in 2011 [3]. Myocardial infarction (MI) alone caused over 157,000 deaths in 2011. Estimated direct and indirect costs of heart disease in 2010 was $204.4 billion, with MI being one of the most expensive diagnoses ($11.5 billion) [3]. While current clinical interventions have increased patient survival [3], there are few new candidate compounds for cardiovascular disease [232], not to mention the lack of available drugs focused on restoring heart function [229]. To shift treatment of cardiac disease from a focus on prolonging life to a focus on curing disease, development of new compounds directed at underlying disease mechanisms is critical. Until we understand disease mechanism better, have more disease-relevant models for evaluating drugs, and develop mechanistically based drugs, the therapeutic pipeline will continue to be challenged by a low number of candidate drugs.

Mechanistically speaking, the injury border zone (IBZ) – typically no more than a few cell layers thick – is often the site of lethal arrhythmia generation [11,233]. While cellular heterogeneity at the border zone is a critical predictive factor for arrhythmogenesis [234], the mechanism of this contribution remains to be

understood. Altered patterns of Cx43 protein [233] and changes in organization of myocytes and fibroblasts are key variations of the IBZ compared to healthy myocardium [173], though how these changes contribute to the re-entrant arrhythmias that occur at these pathogenic tissue loci remains to be understood.

Our lab previously showed the effects of a Cx43 C-terminal mimetic peptide (αCT1) on healing of a cryo-injury model of infarction [104]. αCT1-treated hearts showed reduced LV dilation, fewer inducible arrhythmias, lower arrhythmia severity scores, increased ventricular depolarization times, and maintenance of Cx43 at intercalated discs between myocytes [104,230]. Examination of patterns of collagen deposition and myocyte and fibroblast localization in the IBZ of cryo-injured hearts displayed a difference in patterns of cell organization (Chapter 1). It may be that αCT1 is altering heterocellular interactions in the IBZ in a way that decreases arrhythmogenesis, though this needs to be investigated directly.

While animal models of infarction are used extensively and can accurately recapitulate important aspects of human disease (i.e. arrhythmias), these models are expensive, time-consuming, and low-throughput. These models are also not feasible for initial screening studies. Before drugs reach the pre-clinical animal model stage, extensive *in vitro* testing is involved in screening new candidate drugs, though most of this is done on cell lines in 2D culture, which is far from representative of actual human tissues. Frequently, drugs that demonstrate effectiveness in these systems are not clinically effective and contribute to the

meager 16% of compounds that make it through drug development and into the clinic and market [235].

In vitro testing allows direct control of cell types and can readily accommodate co-culture models. Unlike *in vivo* systems, where many cell types are involved and cannot be controlled, *in vitro* co-culture models allow isolation of effects based on interactions of specific cell types. Additionally, 2D *in vitro* systems lend themselves to simple methods of examining cell interactions by technologies such as live cell imaging. While 2D cultures have a limited ability to simulate 3D tissue processes, development of a 3D *in vitro* heterocellular model of the IBZ would greatly contribute to the drug development pipeline and would provide a platform to examine myocyte-fibroblast interactions in disease. Development of a model that simulates disease-relevant tissue processes may help screen out ineffective compounds before they reach the expensive pre-clinical stage, leading to huge cost savings in drug development.

The objective of the present study was to: 1) Develop and optimize a 3D *in vitro* model of the IBZ using primary cardiac cells; 2) Validate this model against known parameters of the IBZ; and 3) Evaluate the response to a small peptide therapeutic that was previously shown to improve cardiac function after experimental MI in mice [104]. This model is optimized to generate large numbers of technical replicates that are highly reproducible, to create aggregates of cells that are sufficiently small so they are not subject to necrotic cell death from oxygen

starvation, and to allow high-throughput live imaging in order to obtain relevant time-dependent data when testing a therapeutic compound. This model may be used as a platform to study new compounds.

2.2 Methods

Preparation of HeLa cell aggregates in rocking culture: HeLa and HeLa-Cx43 cells were cultured in DMEM (Hyclone) supplemented with FBS (Hyclone), 10 U/ml penicillin and 10 µg/ml streptomycin (Hyclone), and 2 mM L-alanyl-L-glutamine (Gibco) and maintained in an incubator at 37°C, 5% CO_2. HeLa and HeLa-Cx43 cells were mixed 1:1, seeded at $1x10^6$ cells/well in agarose-covered chamber slides, and rocked at 0.25, 0.5, or 1 Hz. Media was changed daily. To image, aggregates were removed from wells, washed in PBS, fixed for 10 minutes at room temperature in 4% paraformaldehyde, washed in PBS, dried on gasketed slides, mounted in SlowFade Gold reagent (Life Technologies), and imaged on a Leica SP5 laser scanning confocal microscope (LSCM).

Preparation of acrylamide and agarose micromolds: Micromolds (24-96 – small spheroids) from microtissues.com were filled with 2% UltraPure™ Agarose (Life Technologies) in normal saline. Molds were extracted and equilibrated in myocyte complete medium for 3 medium changes. For acrylamide micromolds, a 20% acrylamide mix was made of acrylamide stock, bis-acetate, PBS, water, and

TEMED. Fresh 2% ammonium persulfate was added and solution immediately pipetted into the micromolds and allowed to gel. Acrylamide micromolds were sterilized with 70% ethanol, rehydrated in PBS, and equilibrated with myocyte complete medium before use.

Cell seeding and culture in micromolds: H9C2 cells (ATCC), an embryonic rat myocardium-derived cell line, were cultured in DMEM High glucose (4500 mg/L) with sodium pyruvate (110 mg/L) (Hyclone) supplemented with 10% FBS (Hyclone), 10 U/ml penicillin and 10 µg/ml streptomycin (Hyclone), and 2mM L-alanyl-L-glutamine (Fisher) and maintained in an incubator at 37°C, 5% CO_2. Aggregates were labeled with CellTracker Orange (CMRA) (Life Technologies), and seeded at 1,440-324,000 cells per micromold. This should result in aggregates from 50-300 µm diameter. To image, aggregates were spun out of the micromolds at 800 rpm for 5 minutes, washed in PBS, and resuspended in glycerol on a depression slide, or in a home-built gasket slide, making the gasket as thin as possible to accommodate the aggregates but still be able to image. Cells were then imaged on a Leica SP5 and aggregate diameters were measured from these images.

Cell isolation and labeling: Primary cardiac neonatal rat ventricular myocytes and neonatal rat ventricular fibroblasts (NRVFs) were isolated from 2-day neonatal rats by digestion in trypsin (Worthington), Pancreatin (Fisher), Collagenase II (Worthington), and elastase (Fisher) in HBSS (Hyclone). Cells were separated on

a Percoll (GE Healthcare) gradient, and washed. Fibroblasts were seeded and cultured in DMEM (Hyclone or Gibco) supplemented with FBS (Hyclone), 10 U/ml penicillin and 10 µg/ml streptomycin (Hyclone), and 2 mM L-alanyl-L-glutamine (Fisher) and maintained in an incubator at 37°C, 5% CO_2. Myocytes were labeled immediately in 2.5 µM CellTracker Orange (CMRA) (Life Technologies) in OptiMEM (Gibco) for 30 minutes and washed in myocyte complete medium (M199 supplemented with 0.16% glucose (Sigma), 1x MEM vitamins (Gibco), 1x NEAA (Gibco), 1x MEM Amino acids (Gibco), 10 U/ml penicillin and 10 µg/ml streptomycin (Hyclone), 10% horse serum (Gibco), and 5% FBS (Hyclone). Myocytes were seeded at 30,000 cells per mold and allowed to aggregate for 48 hours. Before seeding, fibroblasts were washed in PBS, labeled with 2.5 µM CellTracker Green (CMFDA) in OptiMEM (Gibco) for 30 minutes and washed in fibroblast medium. Fibroblasts were added at 48 hours at 30,000 cells per mold. Culture medium (including treatments) was changed every 24 hours. Aggregates were treated with 100 µM αCT1, reverse control peptide, or vehicle control.

Cx43 mimetic peptides and aggregate treatment: Two peptides (American Peptide) were generated: αCT1 and a reverse sequence peptide (REV). These peptides contain an N-terminal biotin tag followed by the 16-amino acid antennapedia internalization vector (RQPKIWFPNRRKPWKK). Linked to the C-terminal K of the antennapedia sequence is either the C-terminal 9-amino acids of Cx43 (RPRPDDLEI; αCT1) or the Cx43 C-terminal 9-amino acids in reverse

(IELDDPRPR; REV; Fig. 1-6). Aggregates were treated with 100 μM αCT1 or REV peptide in culture medium with daily medium changes.

Live imaging of aggregates: Aggregates were imaged at 24, 48, and 72 hours after fibroblasts were seeded. An upright Leica SP5 LSCM equipped with a 20x dipping lens (Leica HCX Apo L 20x/0.5 UVI, 506147) was submerged in the well of a 24-well plate containing each micromold (each micromold contained 96 wells, each with a single aggregate). Alternatively, an inverted Leica SP8 LSCM equipped with a heated, humidified, and CO_2–injected incubation system and a 10x lens (Leica HC Plan Apo 10x/0.4 NA) was used to image aggregates in micromolds sitting in MatTek plates with no loss of optical clarity. 15 aggregates were imaged live and analyzed for various model parameters including size, cell migration, and cell number.

Immunolabeling: Aggregates were washed in PBS, fixed for 10 minutes at room temperature in 4% paraformaldehyde, and washed 3x in PBS. The depression at the top of the micromold was filled with molten agarose and allowed to gel in order to prevent aggregates from being lost from micromold wells. Micromolds were placed in 30% sucrose (company) overnight, embedded in OCT and frozen. Micromolds were cryosectioned at 10 μm and dried on positively charged slides for 30 minutes prior to immunolabeling. Slides were either stored at -80°C or were immunolabeled immediately. Sections of aggregates were blocked with 1% BSA (Fisher Scientific), 0.1% Triton-X-100 (Fisher Scientific) in PBS. Sections were

immunolabeled for vimentin (Millipore) (1:1000), MF20 (DSHB) (1:100), pan-cadherin (clone CH-19, Sigma C1821, 1:1000), or Cx43 (Sigma or Abcam). Labeling was viewed with AlexaFluor secondary antibodies and stained with Hoechst 33342 (Sigma; nuclear labeling), mounted, and imaged on a Leica SP5 or SP8 LSCM equipped with a Leica Plan Apo 63x/1.4 NA oil immersion objective.

Statistical analyses: All data were checked for normality by Shapiro-Wilk [236–240]. Non-normal data were transformed to normality using Box-Cox. If data could not be transformed to normality, non-parametric tests were used. Normal data were examined by ANOVA. All statistical analyses were performed in Statistical Package for the Social Sciences (SPSS).

2.3 Results

Agarose micromolds allow generation of a high number of reproducible aggregates of uniform size that can be subjected to live imaging

To produce a 3D heterocellular model of the IBZ, multiple techniques to generate cell aggregates were examined. HeLa cells and HeLa cells stably expressing Cx43 (HeLa-Cx43) were used initially. The parental HeLa cell line is not known to express connexin proteins, though the HeLa-Cx43 cell line has been transduced to stably and heterologously express Cx43 [241]. These cells are representative

of myocytes and fibroblasts in the heart, as cardiac fibroblasts express low levels of connexin proteins [167,242], and myocytes express Cx43 abundantly [243,244].

First, hanging drop culture was tested by mixing equal numbers of myocytes and fibroblasts and pipetting them into holes punched in the silicone-coated lid of a 48-well plate. Cells aggregated over time, and could be spun down into the wells. This method allowed only mixed-cell aggregates to be formed, and made manipulation of aggregates difficult (data not shown). Also, this method produced relatively small numbers of aggregates limiting progress rate. Second, rocker culture was tested on a heterocellular population of aggregrates. Agarose-coated chamber slides at various rocking speeds were seeded with HeLa-Cx43 and WT HeLa cells. A rocking speed of 0.25 Hz resulted in clumps with 10-20 cells. Increasing the rocking speed to 0.5 Hz resulted in clumps of 4-10 cells, with a few larger aggregates. Increasing rocking speed further to 1 Hz resulted in clumps of 15-20 cells with many larger aggregates of cells. These larger aggregates of cells appeared to be ~150-275 μm in diameter (Fig. 2-1A), though size could not be precisely controlled. It also appeared that these larger clumps of cells likely aggregated from smaller clumps of similar cells, resulting in cell separation within the aggregates that could not be accurately regulated (Fig. 2-1B). Aggregates generated by rocker culture were fixed, washed in PBS, and dried onto slides with a gasket, then mounted and imaged. While this method did allow cells to be imaged at a magnification that nearly enabled discrimination of individual cells (Fig. 2-1),

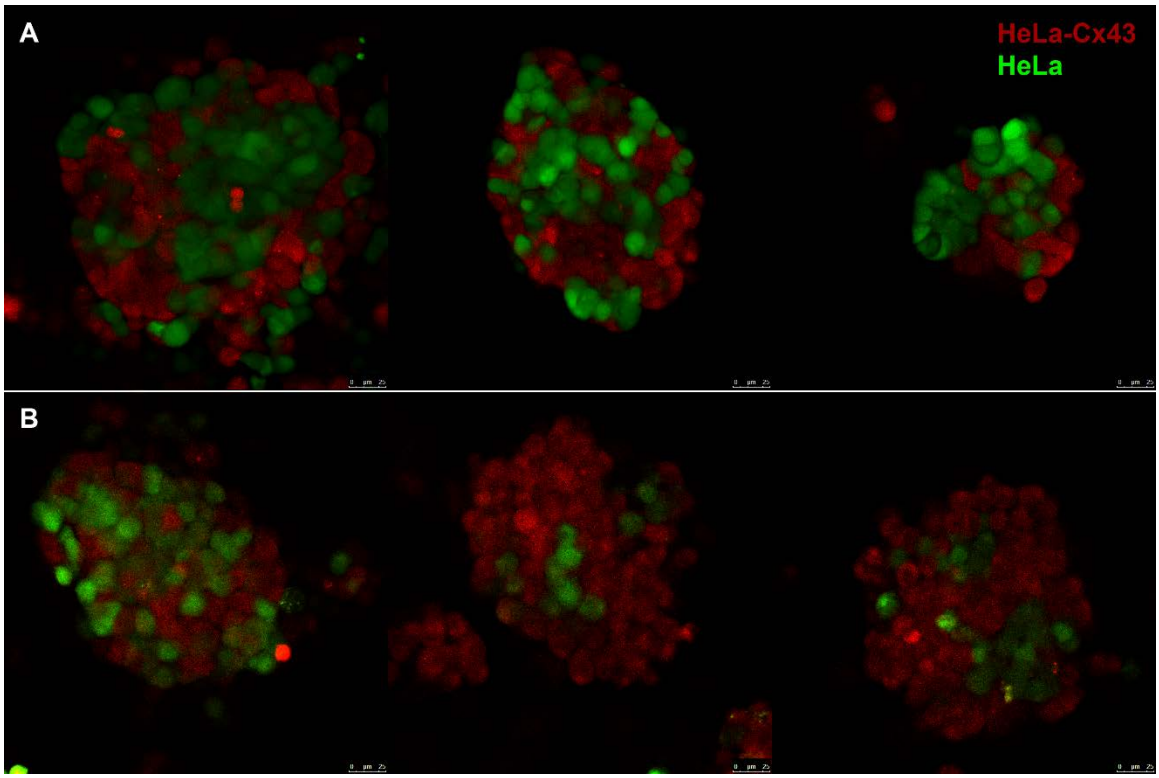

Figure 2-1. Heterocellular aggregate generation by rocker culture. A) Aggregate size cannot be precisely controlled at 1 Hz. B) Even mixing of heterocellular populations cannot be controlled at 1 Hz.

this proved a relatively low-throughput method. Aggregates were also not able to be imaged live, as they could not be efficiently immobilized.

In order to create cell aggregates of more precisely controlled and consistent size, micromolds from microtissues.com were tested (Fig. 2-2A) [245,246]. These molds can be filled with a non-adhesive, permeable material and a cell suspension can be seeded into the depression on the top of the mold. The cell suspension is allowed to settle and aggregate over time. One of the objectives in developing this model was to create a simple way to image live cells within these aggregates, as we would be able to track their organization over time. Therefore, we wanted a

material for the micromolds that was optically transparent. While acrylamide was more transparent than Ultrapure agarose, tested cells frequently failed to properly aggregate, adhering to the sides of acrylamide microwells (Fig. 2-2B). Ultrapure agarose (Fig. 2-2C) was found to provide an optimal substrate for promoting formation of aggregates, thus, we used this material for further development of our model of the IBZ.

Optimization of aggregate size for the IBZ model involved testing a variety of cell seeding densities. To do this, we used a more cardiac-relevant cell line – H9C2 cells – which are derived from embryonic rat myocardium. Aggregates of varying cell densities were seeded into micromolds and images were obtained (Fig. 2-3).

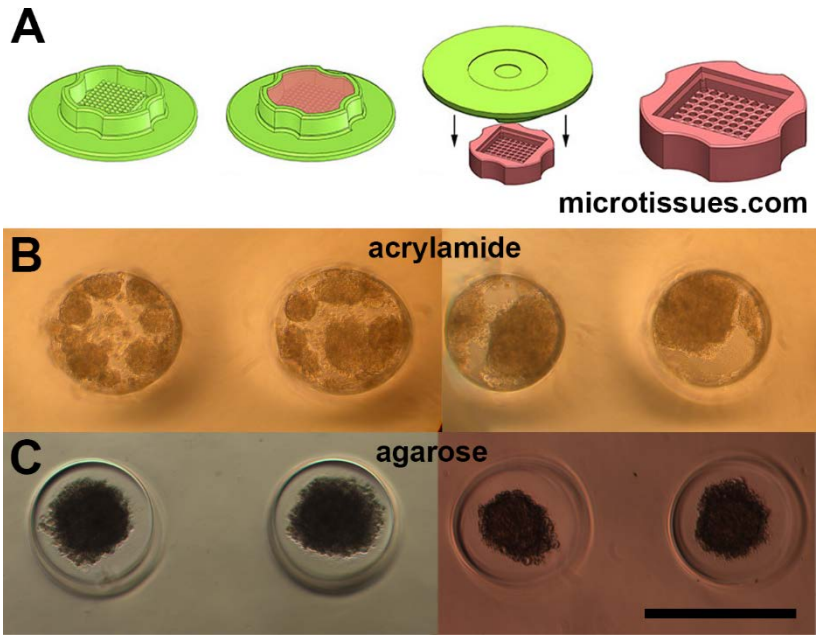

Figure 2-2. Silicone molds can be used to generate microwells of optically transparent, permeable materials (A). B) Cells did not aggregate efficiently in acrylamide, and often adhered to the microwells. C) Cells in agarose micromolds aggregated efficiently and formed aggregates of uniform size. Scale = 200 µm.

The critical diffusion length of oxygen in tissues is around 200 µm [247], so this placed an upper limit on the size of aggregates, such that cells were able to exchange nutrients and waste and avoid the formation of necrotic zones at the center of aggregates [248]. Furthermore, while we determined that generating aggregates in a large range of sizes was possible, light scattering and lack of laser penetrance constrained our ability to image into H9C2 cell aggregates deeper than 100 µm (Fig. 2-3). Thus, maintaining cell viability and the demands of the imaging technologies available to us set our optimal aggregate size limit at ~100 µm.

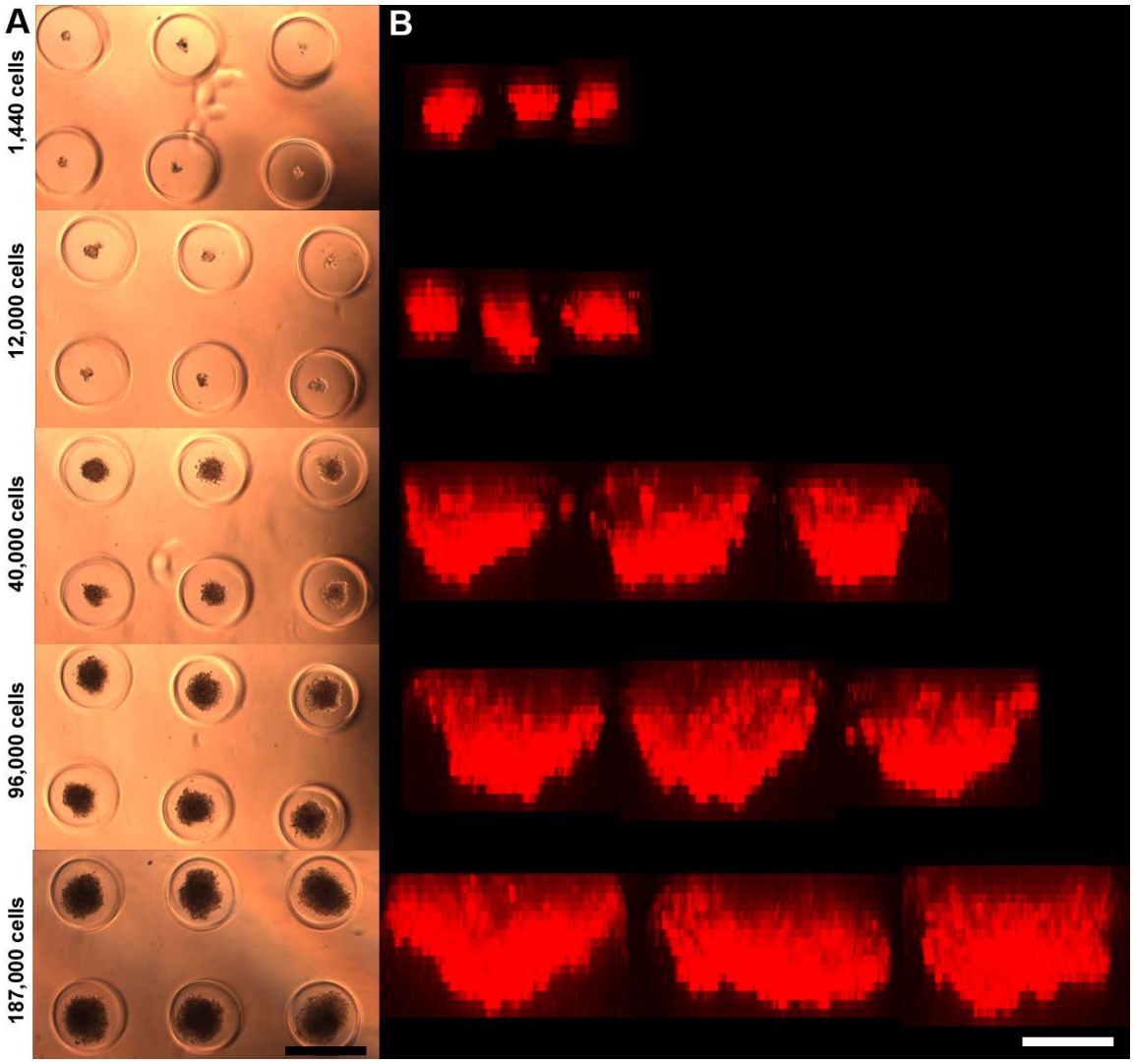

Figure 2-3. Aggregate size can be controlled by varying cell seeding density into the micromolds (A). B) Imaging of larger aggregates was challenged by laser penetrance and light scattering when using standard confocal techniques. Scale = 200 µm and 100 µm in A and B, respectively.

To generate a more cardiac-relevant model of the IBZ, we used neonatal rat ventricular myocytes (NRVMs) and neonatal rat ventricular fibroblasts (NRVFs) isolated from 2-day old rat pups. Aggregates were generated by two seeding

methods. In both methods, equal numbers of myocytes and fibroblasts were used. First, myocytes were labeled with CellTracker Orange (CMRA) dye and mixed in equal parts with fibroblasts that were labeled with CellTracker Green (CMFDA). This mixed-cell population was then seeded into equilibrated agarose micromolds and allowed to settle and aggregate (Fig. 2-4A). In the second method, myocytes were labeled with CellTracker Orange (CMRA) dye and seeded into micromolds to form a core of myocytes. Fibroblasts were cultured, then labeled with CellTracker Green (CMFDA), and seeded into the micromolds on top of the already

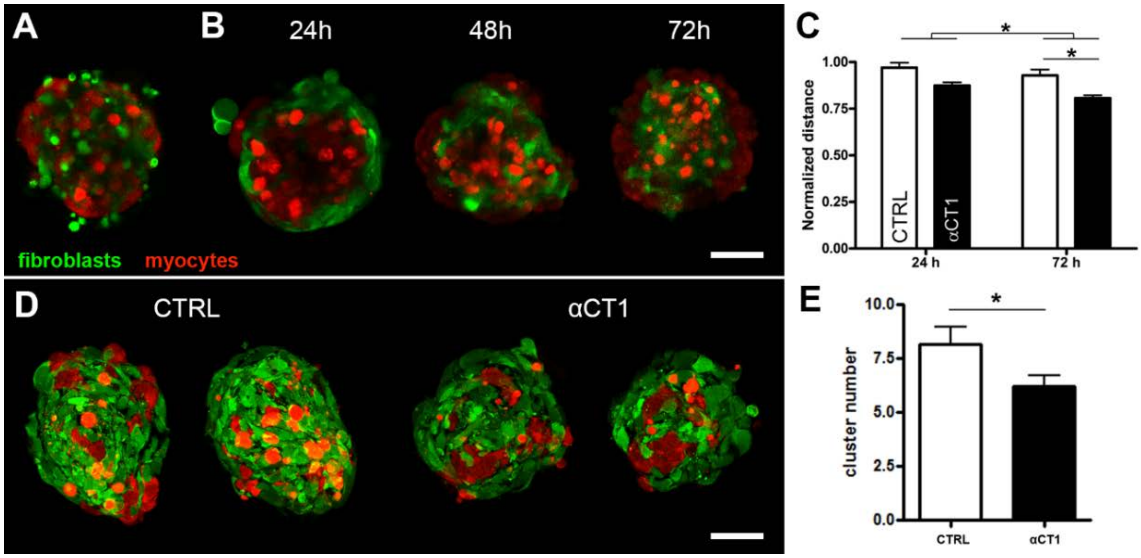

Figure 2-4. 3D IBZ model incorporating myocytes and fibroblasts. A) Aggregates of evenly mixed cells maintained this organization in culture. B) Layered aggregates with a core of myocytes and a shell of fibroblasts led to changes over time in cell organization, as fibroblasts migrated to the center of aggregates. C) Treatment of the IBZ model with αCT1 led to increased fibroblast migration ($p<0.05$) over time. D) Myocytes appeared to be more cohesive in αCT1-treated aggregates, whereas fibroblasts separated individual myocytes in CTRL aggregates. This tendency could be measured by counting cluster number ($p<0.05$; E). Scale = 50 µm.

formed myocyte aggregates. This novel approach enabled the formation of an external shell (mantle) of fibroblasts around a central core of myocytes (Fig. 2-4B).

Figure 2.5 shows immunolabeling for myocyte and fibroblast-specific proteins. MF20 and vimentin signal overlapped with the CellTracker labeling based on the Percoll separation of cells (e.g. vimentin labeling overlapped with CellTracker Green-loaded fibroblasts and MF20 labeling overlapped with CellTracker Orange-loaded myocytes). This indicated that bona-fide myocyte and fibroblast populations were being isolated and maintained in our aggregates.

Aggregates were imaged live on a confocal microscope 24, 48, and 72 hours after fibroblast seeding. Aggregates of mixed cells showed no changes in patterns of cell organization (Fig. 2-4A). Though previous studies of similar aggregates reported that cells separated by cell type [249,250], this phenomenon did not occur in our hands. In multi-layer aggregates of myocytes and fibroblasts, fibroblasts migrated toward the center of the aggregates over time, pushing the myocytes outward (Fig. 2-4B).

Treatment with a peptide mimetic of connexin43 altered fibroblast migration and patterns of cellular cohesion, which was not correlated with adhesion molecule changes

Previous data from our lab shows that treatment with a peptide mimetic of Cx43 can improve cardiac function in an experimental model of MI [104]. To better understand the mechanism by which this happens, we treated myocyte-fibroblast aggregates in the IBZ culture model with this peptide (αCT1). Analysis of fibroblast migration in these aggregates showed that this effect could be measured, and occurred to a greater degree in fibroblasts treated with αCT1, as the average distance of fibroblasts from the center of the aggregate decreased significantly over time (Fig. 2-4C, $p < 0.05$).

Since cellular organization changes in the IBZ, we examined the *in vitro* model for patterns of cellular cohesion. In CTRL aggregates, individual myocytes appeared to be separated by fibroblasts (Fig. 2-4D). By contrast, in aggregates treated with αCT1, myocytes and fibroblasts tended to remain more clustered together in cohesive groups. To measure this, the number of myocyte clusters in each aggregate was counted at the 72 hour time point, as this was the stage at which changes in cell organization were stabilized. αCT1-treated aggregates had significantly fewer clusters of myocytes, indicating that myocytes were more clustered together in treated aggregates compared to controls (Fig. 2-4E, $p < 0.05$).

Since adhesion molecules are known to influence patterns of cell sorting [39,40], we examined levels of adhesion molecules using a pan-cadherin antibody that cross reacts with all known members of the cadherin family (including N-, E-, and P-cadherin) in fixed sections of the aggregates at 72 hours. Labeling for proteins in whole mount aggregates was not feasible due to limitations of light penetrance and working distance of objectives. In fixed sections of aggregates, no significant differences in pan-cadherin levels were found between αCT1-treated aggregates and controls (Fig. 2-6; $p = 0.404$ and $p = 0.494$). When we investigated these phenomena further, it was found that these sorting effects were strongly correlated to differences in levels of Cx43 in heterocellular interactions between treatment and control (described and discussed in detail in Chapter 4). Though classical adhesion molecule adhesive forces are much stronger than connexins, in the absence of adhesion molecules, cells are known to sort based on connexin proteins [41].

Extensive analysis of other model parameters revealed important markers

Other system parameters were measured that may indicate drug mechanism. All of these changes were measured as a difference between 24 and 72 hours, though none was significant by time or treatment. These include aggregate size and cell number, which showed decreases of ~25% and ~20%, respectively (data not shown). This slight reduction in aggregate size observed in response to αCT1 is

likely accounted for by compaction of the cells within the aggregates. Though fibroblasts moved toward the aggregate center (measured as cell distance from the aggregate center) by ~30% over time and showed a significant treatment effect, myocytes did not show this same change (data not shown). Another parameter measured was ratio of red to green cells. This parameter was neither significant by time, nor did it show a treatment effect (data not shown). These results indicate that the Cx43 mimetic peptide likely did not significantly affect cell proliferation or death rates. Since these are all parameters that can be measured in live cell aggregates, these determinations can be made quickly from this model.

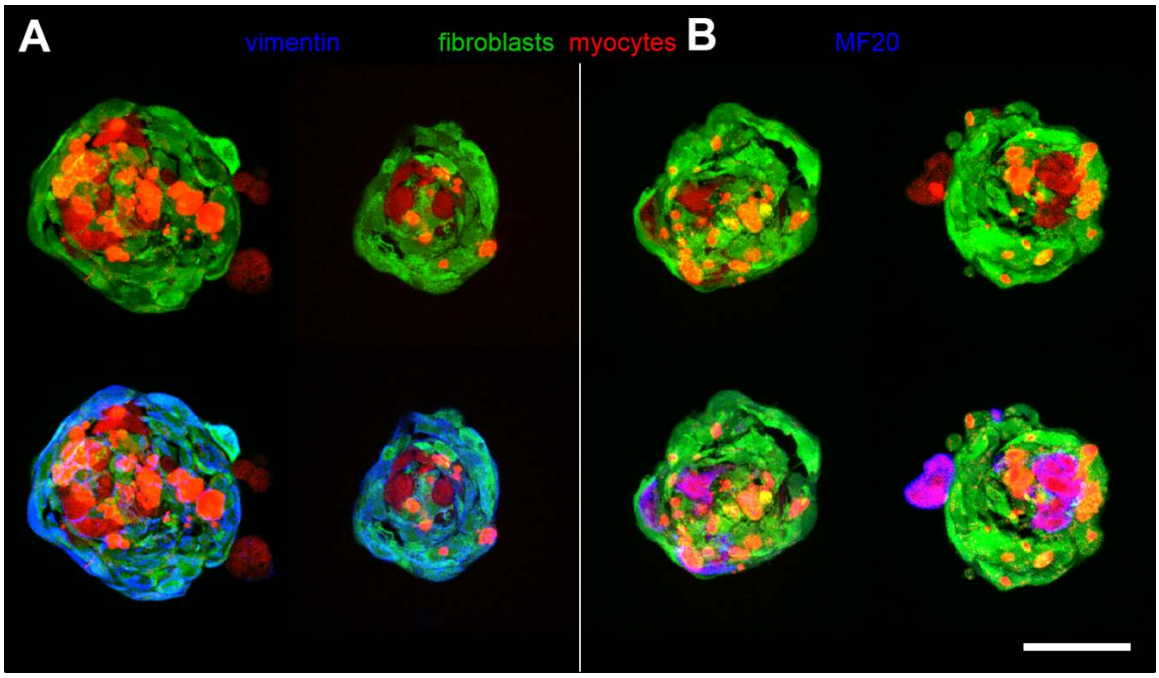

Figure 2-5. Verification of cell type by immunolabeling. Fibroblasts (green) are loaded with CellTracker Green dye and myocytes (red) are loaded with CellTracker Orange dye. A) Vimentin labeling (blue) for fibroblasts overlaps with green signal. B) MF20 labeling (blue) for myocytes overlaps with red signal. Scale = 50 µm.

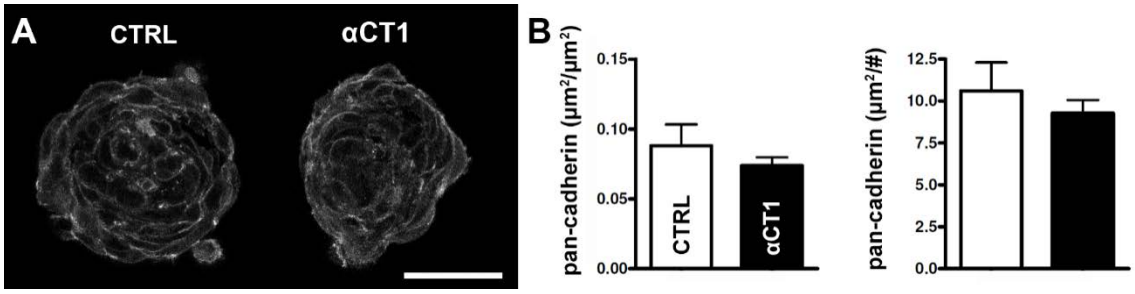

Figure 2-6. Cadherin levels were not affected by treatment with αCT1. Immunolabeling for pan-cadherin (A) and subsequent quantification (B) indicated no treatment effect on levels of these adhesion molecules whether normalized to aggregate size (left) or cell number (right). Scale = 50 µm.

2.4 Discussion

Using non-adhesive, optically transparent micromolds, we have developed a model of the IBZ that incorporates myocytes and fibroblasts – i.e., the dominant cellular constituents of this pathogenic tissue *in vivo*. The micromolds used allowed generation of up to 96 nearly identical cell aggregates. Larger formats would also be feasible in theory, permitting more aggregates to be made through a single cell seeding. The sizes of aggregates optimized in this model were within the diffusion limit of oxygen in tissues, which would prevent the center of the aggregates from becoming necrotic. Sequential seeding of myocytes and fibroblasts allowed the formation of a two-layered aggregate, which could be imaged live over several days to examine the changes in patterns of cell organization. Fibroblasts migrated to the center of heterocellular aggregates over time, forming a more or less coherent core of cells and pushing the myocytes outward. This effect occurred regardless of treatment, though treatment with αCT1 increased the fibroblast migration to a greater degree. Myocytes were also found to be more clustered together in αCT1-treated aggregates than controls, suggesting a cellular cohesive-promoting effect of the peptide. Immunolabeling on fixed sections of aggregates was performed, as whole mount immunolabeling did not enable visualization of desired proteins due to physical limits. Similar levels of cadherin immunolabeling were observed in both αCT1-treated aggregates and controls, so it appeared that the cell sorting and clustering effects were likely not cadherin-based. Though a number of other parameters were measured in this model, none of them showed

statistically significant time or treatment effects. However, the ability to measure these parameters may prove important in future evaluation of novel drug compounds.

Cx43-ZO-1 interaction has been implicated in cardiac disease as reorganization of Cx43 is frequently associated with arrhythmias in the heart. Many studies of heart failure in animal models and humans have shown that Cx43-ZO-1 co-localization is altered and Cx43 expression is reduced [79,83,251]. αCT1, a Cx43 mimetic peptide that inhibits Cx43-ZO-1 interaction, increases GJ plaque size and decreases association of Cx43 with ZO-1 at the plaque border [77]. Application of αCT1 to cardiac injury may, therefore, beneficially alter Cx43-ZO-1 interaction and reduce arrhythmogenesis. Indeed, it was found that when applied to a murine cryo-injury model of infarction, this peptide improved several metrics of cardiac physiological function [104,230].

The mechanism by which altered cell organization contributes to arrhythmias in the border zone is not fully understood, though these studies revealed that application of this peptide can affect cell organization. These changes are in parallel with the changes seen in the IBZ of our cryo-injury model of infarction, where myocytes in the IBZ were more clustered together and appeared to be separated by fewer fibroblasts in αCT1-treated hearts than in controls (Chapter 1). Changes in cellular cohesiveness in this study were not found to be based on cadherin effects, though it would be pertinent to further test the effect of cadherin-

based sorting through knockdown experiments or using anti-cadherin antibodies in the generation of these aggregates. We did find changes in Cx43 in heterocellular interactions in treated aggregates versus controls that may account for the cell sorting effect seen here (Chapter 4). Further investigation may reveal a mechanism by which this peptide can therapeutically alter cell organization in the IBZ *in vivo* to reduce arrhythmia incidence [234].

In the IBZ model, αCT1 increased migration of fibroblasts in the 3D aggregates. This resembles a response previously seen in 2D scratch wound assays of fibroblasts in our lab, in which cells treated with αCT1 showed a significant positive dose-dependent migration response in a 24 hour assay. This effect was reproduced in our 3D heterocellular model in the presence of myocytes.

While our purpose in this study was to generate a model of the IBZ, a similar heterocellular model could be used to study other cardiac fibrotic diseases. For example, instead of the focal scar that forms in the ischemic area in MI, diffuse interstitial fibrosis develops in the pressure overloaded heart, with no drastic change in cell organization. The mixed-cell aggregates where a 1:1 suspension of myocytes and fibroblasts is seeded in the micromolds would more accurately represent the cellular tissue structure of the pressure overloaded heart. Additionally, ischemia could be simulated in either of these models by culturing aggregates in a low-oxygen environment.

3D *in vitro* models have been frequently used to study tissue processes and drug development. Multicellular spheroids have been utilized to study tumor microenvironment and growth since 1988 [252,253], and have been used more recently to bridge the gap between *in vitro* and pre-clinical models in development of cancer therapeutics [254]. A cardiac spheroid model has also been developed in Mende's lab [255]. While our work has been validated by a number of their observations in this model, their work has focused primarily on modeling electrophysiological properties and calcium handling in these microtissues, and they do not report changes in heterocellular interactions.

While *in vitro* models cannot reproduce *in vivo* disease processes, this model serves to simulate, at least in part, the changes in myocyte-fibroblast interaction happening in 3D at the IBZ. Additionally, other factors important to the healing and scar formation process may be added to this *in vitro* model at a relevant time point. For instance, inflammatory cells are recruited to the heart after MI and, along with the resident cells, release inflammatory molecules [153,256]. Bone marrow cells are often recruited to the site of injury in tissues, though the extent of this effect in the case of cardiac injury is debated [257–259]. These cell types – or even others engineered to provide a therapy – could be added to this *in vitro* model for analysis.

This novel 3D *in vitro* model of the IBZ provides a reproducible method to study changes in heterocellular interactions in live cells using an optically transparent, porous micromolded material to form large numbers of aggregates. Using this

model, we have shown a treatment effect of a Cx43 mimetic peptide on fibroblast migration and cellular cohesion. Immunolabeling in fixed sections of these aggregates may be used to identify proteins relevant to these and other processes. Taken together, this model provides an efficient platform for efficacy testing and mechanistic evaluation of therapeutic compounds for treating cardiac disease processes.

CHAPTER 3: αCT1 ALTERS CONDUCTION AND INTERCELLULAR COMMUNICATION, BUT NOT BONE MARROW-DERIVED CELL RECRUITMENT TO THE CRYO-INJURED HEART

3.1 Introduction

The changes in histoarchitecture, connexin distribution, and cell phenotypes that occur in the IBZ after MI alter the electrophysiological properties of this tissue substrate and contribute to generation of arrhythmias [160,233,260–262]. Previous studies demonstrate action potential slowing through the IBZ [160,233], increased coupling of myocytes and fibroblasts via connexin proteins [167,173], and altered tissue architecture with increased collagen deposition [11,140]. Fibroblasts are activated by injury in the myocardium and proliferate and migrate (or arrive from extra-cardiac sources, like the bone marrow [162–165]) into the scar. Fibroblast proliferation in the IBZ can separate myocytes from each other. There is a need to understand the interplay between these structural changes in order to develop targeted therapies.

While intercellular communication of myocardial cells is well-established, as conduction spread through the myocardium is thought to rely on passage of ions through GJs [263,264], the presence and function of heterocellular coupling via connexins is not well understood. Heterocellular coupling is well established *in*

vitro, as cells removed from the native myocardium increase their expression of connexin proteins [152,155,265,266], and is increased in disease [173], as the phenotype of cardiac fibroblasts changes in response to injury [267–269]. The overall effect of this increased coupling in the context of other changes to the post-MI environment is currently unknown. It may be that altered myocyte-fibroblast coupling is responsible for changes in conduction in the IBZ. However, presence of connexin immunolabeling used to probe heterocellular interactions in these studies does not necessarily imply functional GJ channels. Previous work from our lab has shown that treatment of cryo-injured hearts with αCT1 led to a reduced propensity for inducible arrhythmias and lower arrhythmia severity score [104]. These changes were associated with an increased tendency for Cx43 to be maintained at the IDs in the IBZ. Additionally, there was an increase in Cx43 that was phosphorylated at serine 368 in the IBZ.

S368 phosphorylation is associated with a decrease in unitary conductance of the GJ channel [58], perhaps as a protective mechanism against the spread of injury signal in the heart [94,175,188,270]. Somewhat paradoxically, increased pS368 (i.e. decreased communication) in αCT1-treated hearts was associated with fewer arrhythmias and lower arrhythmia severity scores in our studies [104]. This suggests that communication is altered in the IBZ, though there is a need to better understand the cellular and molecular mechanism for this.

Cells recruited to the site of MI may also affect electrophysiological properties. Since the first report in 2001 [271], bone marrow derived cells (BMCs) – a recruited cell type – have been extensively studied for their utility in cardiac repair. Reports in the literature suggest a range of contribution of BMCs – which can be mobilized by injury signals and recruited to the site of injury – to healing of the injured heart [162–165]. Clinical trials of exogenously applied BMCs post-MI suggest modest benefit from paracrine factors [272] and exosome release [273,274] (i.e. the presence of the cells themselves is not required). However, there is further room for improvement of this type of therapy, as the BMCs could be used as a delivery vehicle. For example, if sufficient numbers of cells are recruited to the scar and IBZ, BMCs could be engineered to express increased levels of connexins (they already express some [275]) and ion channels in order to improve electrophysiological properties of the IBZ and scar.

To assess whether αCT1 alters conduction in the IBZ and can alter GJIC, we studied the effect of the peptide on conduction velocity through the IBZ in cryo-injured hearts and examined direct intercellular communication in an *in vitro* parachute communication assay. To determine the contribution of endogenous recruited BMCs to the IBZ and scar, we transduced the femoral cavity of mice after delivery of a cardiac cryo-injury to assess the efficiency with which labeled cells were recruited to the site of injury.

3.2 Methods

Animal care and use: All animal research was conducted under the guidance of the Institutional Animal Care and Use Committee at Virginia Polytechnic Institute and State University and conform to the *NIH Guide for the Care and Usage of Laboratory Animals*.

Cryo-injury: CD-1 Mice (12-24 weeks old, Charles River Labs) were anesthetized by exposure to 5% isoflurane in oxygen. The mice were placed in supine position and the trachea intubated, under direct visualization, with a 22-gauge angiocatheter over a blunt introducer. The mice were ventilated with 2% isoflurane in oxygen at a tidal volume of 250 µl and 150 cycles/minute. Mice were given buprenorphine pre-operatively (50-100 mg/kg SC). Maintaining sterile technique, a left thoracotomy was performed at the fourth intercostal space, using a (MZ75, Leica) dissecting scope. All muscles overlying the intercostal space were dissected free and retracted with a home-built retractor. After opening the thorax, the pericardial sack was opened and the left lung was reflected to allow a clear view of the heart. The left ventricular free wall was cryo-injured by direct exposure to a prechilled (10 sec) 3mm flat-tip circular probe of a cryo-gun for 5 seconds (CRY-AC-3, Brymill). Treatments were delivered to the surface of the heart in methylcellulose patches containing 100 µM αCT1 or reverse peptide, or water for vehicle control. After cryo-injury, the incision was closed in layers using 6-0 Prolene sutures (Ethicon) and the skin sealed with Gluture skin glue (Abbott). Mice

remained on the ventilator receiving oxygen until they began spontaneous respiration. After surgery, the mice were given carprofen (2-5 mg/kg SC) for analgesia and placed on a warming blanket until recovery from anesthesia was complete. Mice were then returned to their cages where they received treatment with buprenorphine every 12 hours for 48 hours and carprofen every 24 hours for 48 hours. Animals were sacrificed 1 week after surgery, hearts collected, and fresh frozen in OCT.

Lentiviral transduction of bone marrow cells: After cryo-injury was performed, a small incision was made in the skin over the mouse hindlimb patella. The knee was placed in flexion and a 27 gauge needle was used to bore a hole through the end of the femur into the bone marrow cavity. A 30 ga needle was used to inject 20 µL of lentiviral TurboGFP (Penn State Vector Core).

Langendorff perfusion: 8 weeks after cryo-injury and bone marrow transduction, mice were anesthetized via isoflurane inhalation and cervically dislocated. The hearts were quickly excised, the aorta cannulated, and retrogradely perfused. Hearts were perfused with solutions (pH 7.4) described in Table 3-1 at a flow rate of 1 to 1.5 ml/min maintaining the perfusion pressure at approximately 65 mmHg. The temperatures of the perfusate and the bath were maintained at 37 °C. Electrophysiology was quantified in hearts perfused with either low sodium and high potassium, or high sodium and low potassium as described in Table 3-1 (5 CTRL and 4 αCT1-treated animals).

Optical mapping: Hearts were optically mapped with the voltage-sensitive dye, Di-4-ANEPPS, perfused at a concentration of 4 μM for approximately 5 min. Motion was arrested with the electromechanical uncoupler, 2,3-butanedione monoxime, or blebbistatin (BDM) at the concentrations listed in Table 3-1. Hearts were stabilized against the front glass of the bath by applying slight pressure to the back of the heart. The center of the anterior ventricular surface was paced with a unipolar silver wire with a reference electrode at the back of the bath. Hearts were stimulated at ~1V for 1 ms at a burst cycle length of 150 ms. Excitation light from a halogen light source (MHAB-150W, Moritex Corporation) was filtered by a 510-nm filter (Brightline Fluorescence Filter) before it reached the heart. The emitted light was filtered by a 610-nm filter (610FG01-50(T257), Andover Corporation) before it was recorded using aMiCam Ultima CMOS L-camera at a sampling rate of 1000 frames/s. The camera captured optical signals from an area of 1 cm^2 in a 100×100 pixel array with an interpixel resolution of 0.1 mm.

Activation times were assigned to the maximum rate of rise of an action potential as previously reported [276] and conduction velocity was calculated using the Bayly et al. algorithm [277]. In short, activation time was determined from the maximum rate of optical action potential rise at each pixel, and a parabolic surface was fit to activation times in order to determine a conduction velocity vector at each pixel. Activation delay was calculated at multiple points along a line drawn through the pacing site and the scar, normal to the IBZ.

Primary cell isolation: Primary cardiac neonatal rat ventricular myocytes and neonatal rat ventricular fibroblasts (NRVFs) were isolated from 2-day neonatal rats by digestion in trypsin (Worthington), Pancreatin (Fisher), Collagenase II (Worthington), and elastase (Fisher) in HBSS (Hyclone). Cells were separated on a Percoll (GE Healthcare) gradient, and washed. Fibroblasts were seeded and cultured in DMEM (Hyclone or Gibco) supplemented with FBS (Hyclone), 10U/ml penicillin and 10µg/ml streptomycin (Hyclone), and 2mM L-alanyl-L-glutamine (Fisher) and maintained in an incubator at 37°C, 5% CO_2. Myocytes were seeded in myocyte complete medium (M199 supplemented with 0.16% glucose (Sigma), 1x MEM vitamins (Gibco), 1x NEAA (Gibco), 1x MEM Amino acids (Gibco), 10 U/ml penicillin and 10 µg/ml streptomycin (Hyclone), 10% horse serum (Gibco), and 5% FBS (Hyclone)).

Density gradient centrifugation: Due to their differences in densities, myocytes and fibroblasts can be separated by density gradient centrifugation. As such, Percoll (GE Healthcare) was used to generate a two-layer gradient in which a layer of Percoll of 1.060 g/mL density was underlaid with a layer of Percoll of 1.080 g/mL density. Cells from no more than 4 digested rat pup hearts were suspended in 1x ADS solution, laid onto the top of the gradient, and centrifuged at 3000 rpm for 30 minutes with no brake. Myocytes sink to the bottom density interface and fibroblasts remain at the top interface. Cells are then collected and washed in complete medium for the respective cell type.

Parachute assay: Myocyte or fibroblast acceptor cells were seeded and grown to confluence on 2-well glass chamber slides coated with gelatin (myocytes) or poly-L-lysine (fibroblasts). Donor fibroblasts were grown in 6-well plates. Donor and acceptor cells were treated with 100 μM αCT1 or reverse control peptide or HBSS vehicle control for 48 hours with daily media changes. At the time of parachute, donor cells were loaded with 5 μM calcein AM (Life Technologies) and 2.5 μM CellTracker Orange (CMRA) (Life Technologies) in OptiMEM (Gibco) for 45 minutes at 37°C. Donor fibroblasts were washed in PBS, trypsinized, and parachuted in complete medium with 100 μM treatments. Transfer was allowed to progress for 4 hours at 37°C and cells were mounted in OptiMEM and imaged on an Olympus BX61VS slide scanner. Only transferring cells were counted.

Statistics: 2-way ANOVA was performed on optical mapping data. Comparisons between treatment groups in a parachute assay was performed with a mixed model design. After it was determined that interaction effects could be eliminated, experiments were split by cell type for analysis. ANOVA was performed with Least Significant Difference (LSD) for inter-group comparisons.

3.3 Results

αCT1 reduces conduction delay at the IBZ

Cryo-injured hearts were optically mapped 8 weeks after injury with the voltage sensitive dye Di-4-ANEPPs. Extracellular ion concentration was varied during the mapping procedure by using perfusates of different composition (Table 3-1). In control hearts, optical maps showed a crowding of isochrone lines at the approximate location of the IBZ with low sodium and high potassium, but not with high sodium and low potassium (Fig. 3-1A). αCT1-treated hearts showed relatively uniform conduction through the IBZ and did not exhibit this conduction delay in low sodium and high potassium (Fig. 3-1A). Conduction delay through the IBZ was calculated at points along a line through the pacing site and normal to the IBZ. In control hearts, a low sodium concentration and high potassium concentration unmasked a significant delay that was not seen when mapped with a high sodium concentration and low potassium concentration (Fig. 3-1B; $p = 0.002$). In hearts treated with αCT1, neither solution altered conduction delay at the IBZ with respect to the other (Fig 3-1B; $p = 0.176$). While αCT1-treated hearts and CTRL hearts were not directly compared, it appears that αCT1 protected against non-uniform conduction slowing in the IBZ in the presence of varying extracellular ion concentration while controls did not.

Table 3-1. Perfusate composition for optical mapping (in mM).		
	Solution 1	**Solution 2**
NaCl	130	118.3
$NaHCO_3$	24	29
NaH_2PO_4	1.2	
Total [Na^+]	155.2	147.3
KCl	4	4.7
K_2HPO_4		1.4
Total [K^+]	4	6.1
$MgCl_2$	1	
$MgSO_4$		1
Glucose	5.6	10
$CaCl_2$	1.8	3.4
BDM	15	10

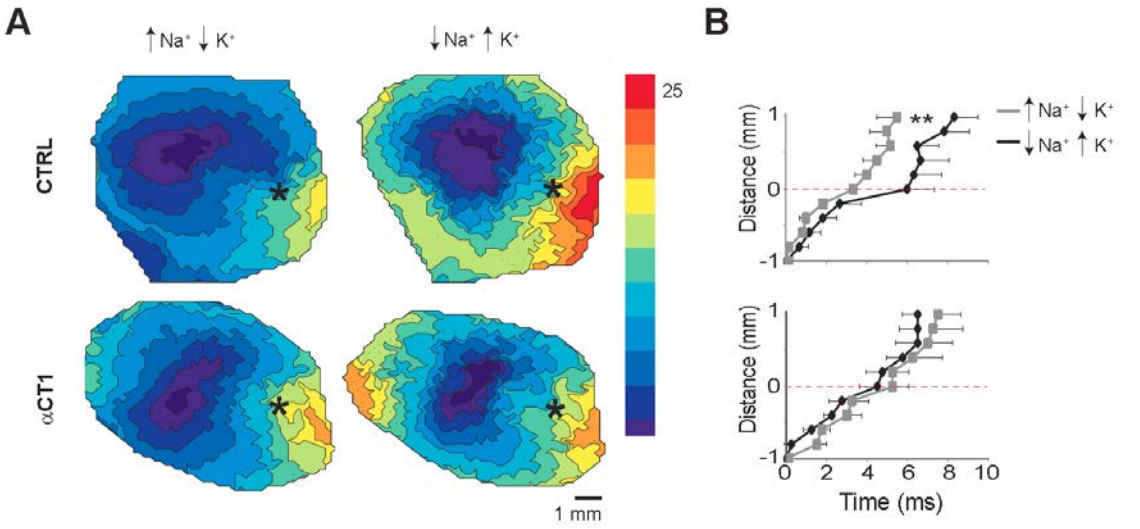

Figure 3-1. αCT1 reduces conduction delay at the IBZ. A) Optical maps of cryo-injured hearts in either high sodium and low potassium (left) or low sodium and high potassium (right). An asterisk marks the approximate IBZ area. B) Low sodium and high potassium solution unmasks a significant conduction delay at the IBZ in controls that is not seen in αCT1-treated hearts.

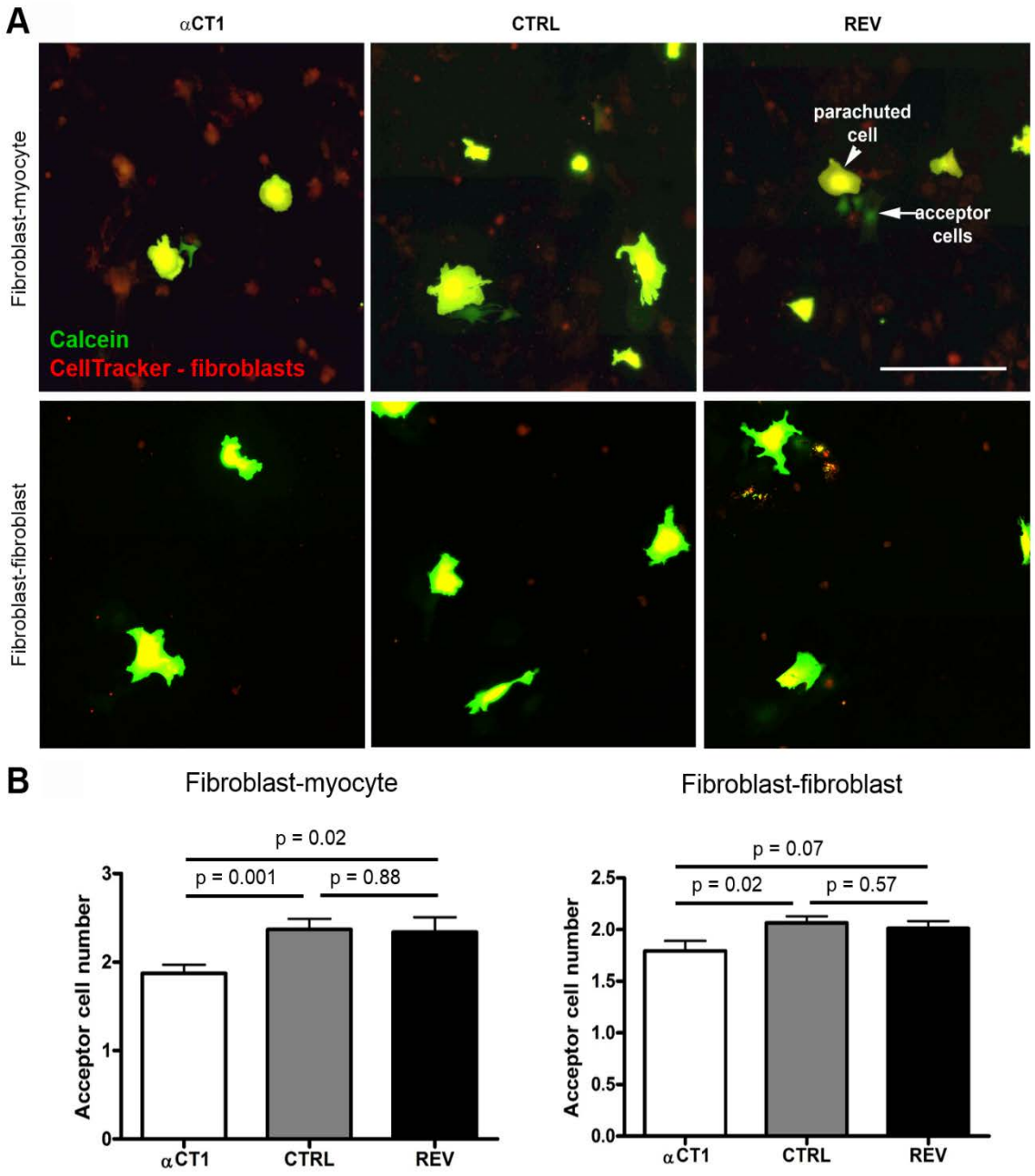

Figure 3-2. Parachute assay of gap junctional intercellular communication (GJIC). A) Communication was assessed in myocyte-fibroblast interactions and fibroblast-fibroblast interactions. Arrowheads show calcein (green) and CellTracker (red) parachuted cells. White arrows show acceptor cells that have received calcein (green) from the parachuted cells. B) αCT1 decreased communication between myocytes and fibroblasts and in fibroblast homocellular connections compared to reverse and vehicle controls. Scale = 250 µm.

αCT1 decreases GJIC between homocellular and heterocellular contacts

Since we saw alterations in conduction at the IBZ with varying ion concentrations in treated hearts versus controls, and previous data (Chapter 1) showed that treating cryo-injured hearts with αCT1 led to changes in patterns of cellular organization in the IBZ, we assessed GJIC in a parachute communication assay to examine myocyte-fibroblast communication and fibroblast-fibroblast communication. To perform the parachute assay, an acceptor cell layer of NRVMs was plated near confluence in glass chamber slides and allowed to form mature GJs over several days in culture, as evidenced by synchronous beating of cells. For 48 hours before the assay was performed, both donor and acceptor cells were treated with 100 μM αCT1 or reverse or vehicle control with daily medium changes. Donor cells were then loaded with the GJ-permeable dye Calcein green and the GJ-impermeable dye CellTracker Orange (CMFDA) and parachuted at a 1:15 dilution on top of the confluent acceptor layer of NRVMs. The parachuted NRVFs settled and adhered to the NRVMs. If functional GJs were formed between the donor and acceptor cells, Calcein green, but not CellTracker Orange, was transferred to the acceptor cells (Fig 3-2). As a measure of communication, the acceptor cells to which dye was transferred were counted. All non-transferring cells were excluded from the analysis.

Surprisingly, it appeared that αCT1 treatment of cultures led to a decrease in GJIC in heterocellular parachute assays (Fig 3-2). This suggests that αCT1 treatment

Previous data from the Gourdie lab showed that αCT1 treatment of hearts led to an increase in pS368 and this effect was maintained *in vivo* for several hours after application of the peptide [104]. Phosphorylation of Cx43 at serine 368 is known to be associated with a decrease in unitary conductance of the GJ channel. So it may be that the peptide is inducing phosphorylation of Cx43 in myocyte-fibroblast connections and in fibroblast-fibroblast connections, leading to a decrease in GJIC.

Contribution of recruited bone marrow cells to healing after cryo-injury

In order to investigate the effect of αCT1-treatment on efficiency of recruitment of BMCs, and subsequently examine whether there is a difference in GJ coupling in the heart, we labeled the femoral bone marrow cavity of cryo-injured mice. Mice were subjected to cryo-injury, then lentiviral Turbo-GFP was injected into the femoral bone marrow cavity to label the cells. Theoretically, any transduced cell in the bone marrow cavity that was recruited outside of the bone marrow would express GFP in its new location. Mice were allowed to recover for 8 weeks before the hearts were excised and examined.

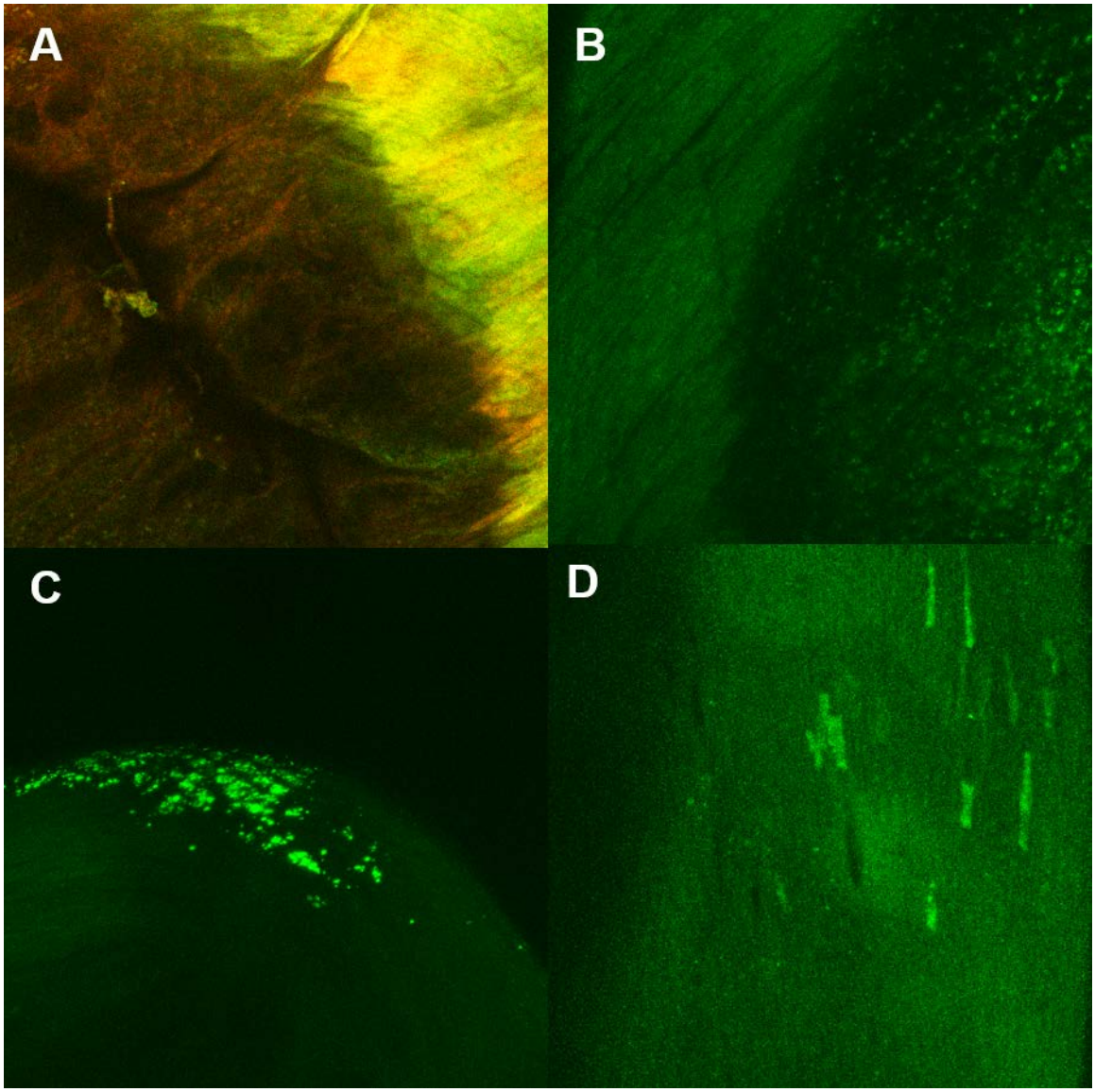

Figure 3-3. Recruitment of bone marrow derived cells to the healing infarct. A&B) Little evidence of GFP-positive cells were seen in the scar area. C) GFP-positive cells were found on the apex of the heart. D) Adjacent to the IBZ, several brick-shaped weakly-GFP positive cells were found.

For gross examination of recruited BMCs, hearts were cannulated and placed on gravity perfusion and imaged on a confocal microscope with motion arrested by BDM. Figure 3-3 depicts several scans taken from different hearts. While we did find a few green cells on the epicardial surface of cryo-injured hearts (Fig. 3-3C&D), we could not find clear GFP signal in the IBZ of these hearts (Fig. 3-3B). In the apex of the heart, there appeared to be several GFP positive cells, though this area was not injured (Fig. 3-3C). Additionally, there was little evidence for GFP-positive cells anywhere in the cryo-injury scar (Fig. 3-3A). Interestingly, we did find some brick-shaped cells (possibly myocytes) that were weakly GFP-positive in the myocardium adjacent to the IBZ (Fig. 3-3D), though the significance of these cells is unknown. Overall it appeared that recruitment of GFP-positive BMCs to the site of cryo-injury was low.

3.4 Discussion

These studies describe data elucidating the cellular determinants of reduced arrhythmogenicity in the IBZ of αCT1-treated hearts. αCT1 was shown to reduce conduction delay in the IBZ in the context of altered extracellular ion concentration, and decrease myocyte-fibroblast heterocellular communication and fibroblast homocellular communication, though it appeared to have no effect on BMCs recruited to the cryo-injury.

αCT1 protected against conduction delay in the IBZ in varying extracellular ion concentrations, while control hearts showed a significant delay in conduction through the IBZ. These results indicate that αCT1 may be contributing to the generation of a more uniform electrophysiological substrate in the IBZ. Previous data from the cryo-injury model in our lab show altered patterns of cellular localization in the IBZ of αCT1-treated hearts compared to controls (Chapter 1). In the IBZ of control hearts, collagen deposition and fibroblasts separated individual myocytes from each other, interrupting patterns of electrical coupling. In contrast, myocytes in the IBZ of αCT1-treated hearts were more clustered together in cohesive groups and showed less evidence of intercalated non-myocytes. αCT1 treatment also led to a higher percentage of myocytes to non-myocytes in the IBZ. This correlates with experimental modeling data that shows that increasing fibroblasts in the IBZ can exacerbate arrhythmia propensity, though this study did not incorporate effects of cellular organization [260]. Similarly, a report by Miragoli et al. found that ectopic activity in cultured strands of ventricular myocytes was increased with increasing fibroblast concentrations [278].

Cardiac myocytes and fibroblasts have vastly different electrophysiological properties, and alterations in coupling between these cell types could contribute to arrhythmia generation. Fibroblasts – a non-excitable cell type – have a more depolarized resting membrane potential compared to myocytes [21,242,279], and higher membrane resistance [21,279,280] and capacitance [281,282]. *In vitro* and *in silico* studies suggest that a fibroblast may act as a current sink when coupled

to a myocyte [21,283], potentially giving rise to arrhythmias [284]. Studies in the sheep heart have shown an increase in structural coupling by connexins in heterocellular interactions in the IBZ [173], suggesting the possibility of increased myocyte-fibroblast functional coupling in the IBZ, though the only functional *in vivo* studies on heterocellular coupling were done in the sinoatrial node of healthy rabbit heart [285]. Previous studies from our lab on the αCT1 peptide suggested an increase in GJIC and a decrease in hemichannel-mediated communication [57]. By contrast, in our dye coupling studies, αCT1 reduced GJIC between myocytes and fibroblasts, and among fibroblasts. Our previous data on studies of the heart demonstrate the ability for αCT1 to increase pS368 [104,105], which decreases communication. While this result was unexpected, reduced communication in heterocellular contacts (which are rare in healthy myocardium [117,122]) may be accountable for more uniform conduction in the IBZ. For example, reduced electrotonic coupling between myocytes and fibroblasts (in which fibroblasts could act as a current sink) would lead to more normal electrophysiological properties of the IBZ. Interestingly, we found a large increase in the amount of Cx43 in heterocellular interactions between myocytes and fibroblasts in our *in vitro* model, though, in light of the dye coupling data presented here, it would suggest a mechanical role for Cx43 in those interactions (see Chapter 4).

Injection of lentiviral Turbo-GFP into the femoral cavity of cryo-injured mouse yielded few GFP-positive cells on the surface of the heart 8 weeks after injury. BMCs are thought to be mobilized by injury signals, though they need to

subsequently home to and engraft in the injured tissue [162–165]. This process is not always efficient, though strategies using heterospecific homing antibodies are being developed to improve this, and have been shown to increase engraftment of intravascularly injected cells in the heart [286]. These antibodies are engineered to be specific for the antigens of two cell types. In this case, they first bind to the target cardiac cells, and then to specific antigens on the injected cells. This strategy holds promise with both administered cell types, as well as those recruited to the site of injury.

It is also possible that lentiviral injection into the bone marrow cavity of cryo-injured mice did not efficiently label cells in that compartment. The percentage of BMCs that are recruited to injured tissue is low, and this would be further challenged by a low labeling efficiency in the bone marrow cavity. While some reports suggest the ability of BMCs to differentiate into a myocyte-like phenotype [271], this seems to be a rare event, if possible at all [287,288]. It is more likely that these GFP-positive brick shaped cells arose as a cell-fusion event [289]. Overall, our attempt to study the contribution of BMCs to the cardiac cryo-injury did not yield conclusive results. Other reporter systems exist that may provide more robust methods to study this effect. These include bone marrow chimeras in which animals are irradiated to kill native bone marrow, followed by subsequent transplantation of reporter bone marrow cells in the bone marrow cavity [257,290] or a transgenic reporter model. Robust reporter models of monocytes [291] and hematopoetic

stem cells [292] have been developed, though tracking bone marrow mesenchymal cells is challenged by lack of a specific marker for this cell type [293].

CHAPTER 4: αCT1 ALTERS MYOCYTE-FIBROBLAST INTERACTIONS VIA CONNEXIN43 AND CONNEXIN43 GAP JUNCTION PLAQUE SUBDOMAIN ORGANIZATION

4.1 Introduction

MI induces several changes in heterocellular interactions in the IBZ and scar. One of the best known is the reorganization of Cx43 to the lateral borders of myocytes in the IBZ, which is thought to contribute to arrhythmia generation. While the traditional role of connexin proteins is in intercellular communication, there are several studies suggesting their importance in cell adhesion [36–38]. Cadherins are known to be responsible for cell sorting as per the differential adhesion hypothesis [39] and subsequent substantiating research [40]. Even though cadherin adhesion forces are stronger than that of connexins, connexin-based cell sorting effects have also been demonstrated, and these effects seem to have a similar influence as cadherin-based effects [41]. Work from Chapter 2 suggests that this could be the case in our models with αCT1, as altered patterns of cell organization were seen in aggregates with no detectable treatment-induced differences in cadherin levels.

In EM and immunolabeling studies of the heart, Cx43 can be found in interactions between myocytes and fibroblasts [117,122]. An immunolabeling study in the

rabbit ventricle indicated that as much as 3.2% of Cx43 was localized to the interface of these heterocellular interactions [117], and that this percentage increased in the IBZ after MI in the sheep [173]. Though one study in canine infarction found a heterogeneous decrease in Cx43 in the border zone and no evidence of heterocellular coupling [294]. However, the ability of myocytes and fibroblasts to couple via GJs is supported by the increased expression of connexin proteins in activated fibroblasts, which are present in the IBZ [167,172,173]. There is further work to be done to understand the presence and distribution of myocyte-fibroblast coupling via Cx43 in both healthy and diseased myocardium.

Cx43 phosphorylation at serine 368 results in a decrease in unitary conductance of the GJ channel [58]. In the post-MI heart, Cx43 pS368 is associated with the Cx43 that is maintained at the ID, both in our studies and those of others [104,295]. Other reports have suggested that Cx43 phosphorylation is a protective mechanism against injury spread in the heart [94,175,188,270].

Some of the first studies from our lab examining inhibition of the Cx43-ZO-1 interaction by αCT1 peptide showed that this led to an increase in GJ plaque size [77]. Subsequent work confirmed that Cx43-ZO-1 interaction regulated GJ size by controlling the rate at which hemichannels waiting in the perinexus flowed into the GJ plaque [57]. Hemichannels are known to be added to the GJ at the periphery of the plaque [26,52,56], and progressive phosphorylation seems to be associated with their incorporation into the plaque [90]. However, some reports suggest the

possibility that Cx43 may be phosphorylated to some extent before it reaches the membrane [96,97]. This may affect the GJ plaque substructure, though to date, there are no reports on GJ plaque substructure with respect to connexin phosphorylation. Immuno-confocal images currently provide the best detail available on the localization of proteins within the GJ. However, the majority of these studies display findings that suggest co-localization of proteins. Super resolution microscopy techniques are becoming more readily available and shed some light onto the localization of proteins in the GJ plaque at the single molecule level [120].

The previous chapter examined the presence and function of communication in the cryo-injured hearts. Here, we aim to understand whether and how myocytes and fibroblasts are coupled via Cx43 GJs. To examine the presence and extent of myocyte-fibroblast coupling via GJs and the differences in structure induced in the Cx43 GJ plaque, we use an approach based on immuno-confocal and immuno-super resolution techniques. Importantly, for the development of a robust *in vitro* IBZ model, the drug responses observed *in vitro* are validated against the physiological responses seen in the disease model *in vivo*.

4.2 Methods

Cell isolation and labeling: Primary cardiac neonatal rat ventricular myocytes and neonatal rat ventricular fibroblasts (NRVFs) were isolated from 2-day neonatal rats by digestion in trypsin (Worthington), Pancreatin (Fisher), Collagenase II (Worthington), and elastase (Fisher) in HBSS (Hyclone). Cells were separated on a Percoll (GE Healthcare) gradient, and washed. Fibroblasts were seeded and cultured in DMEM (Hyclone or Gibco) supplemented with FBS (Hyclone), 10U/ml penicillin and 10µg/ml streptomycin (Hyclone), and 2mM L-alanyl-L-glutamine (Fisher) and maintained in an incubator at 37°C, 5% CO_2. Myocytes were labeled immediately in 2.5 µM CellTracker Orange (CMRA) (Life Technologies) in OptiMEM (Gibco) for 30 minutes and washed in myocyte complete medium (M199 supplemented with 0.16% glucose (Sigma), 1x MEM vitamins (Gibco), 1x NEAA (Gibco), 1x MEM Amino acids (Gibco), 10U/ml penicillin and 10µg/ml streptomycin (Hyclone), 10% horse serum (Gibco), and 5% FBS (Hyclone)). Myocytes were seeded at 30,000 cells per mold and allowed to aggregate for 48 hours. Before seeding, fibroblasts were washed in PBS, labeled with 2.5 µM CellTracker Green (CMFDA) in OptiMEM (Gibco) for 30 minutes and washed in fibroblast medium. Fibroblasts were added at 48 hours at 30,000 cells per mold. Culture medium (including treatments) was changed every 24 hours. Aggregates were treated with 100 µM αCT1, reverse control peptide, or vehicle control.

Cx43 mimetic peptides: Two peptides (American Peptide) were generated: αCT1 and a reverse sequence control peptide (REV). These peptides contain an N-terminal biotin tag followed by the 16-amino acid antennapedia internalization vector (RQPKIWFPNRRKPWKK). Linked to the C-terminal lysine (K) of the antennapedia sequence is either the C-terminal 9-amino acids of Cx43 (RPRPDDLEI; αCT1) or the Cx43 C-terminal 9-amino acids in reverse (IELDDPRPR; REV).

Animal care and use: All animal research was conducted under the guidance of the Institutional Animal Care and Use Committee of Virginia Polytechnic and State University and conforms to the NIH *Guide for the Care and Usage of Laboratory Animals.*

Cryo-injury: CD-1 Mice (12-24 weeks old, Charles River Labs) were anesthetized by exposure to 5% isoflurane in oxygen. The mice were placed in supine position and the trachea intubated, under direct visualization, with a 22-gauge angiocatheter over a blunt introducer. The mice were ventilated with 2% isoflurane in oxygen at a tidal volume of 250 µl and 150 cycles/minute. Mice were given buprenorphine pre-operatively (50-100 mg/kg SC). Maintaining sterile technique, a left thoracotomy was performed at the fourth intercostal space, using a Leica MZ75 dissecting scope. All muscles overlying the intercostal space were dissected free and retracted with a home-built retractor. After opening the thorax, the pericardial sack was opened and the left lung was reflected to allow a clear view

of the heart. The left ventricular free wall was cryo-injured by direct exposure to a prechilled (10 sec) 3mm flat-tip circular probe of a cryo-gun for 5 seconds (CRY-AC-3, Brymill). Treatments were delivered to the surface of the heart in methylcellulose patches containing 100 μM αCT1 or reverse peptide, or water for vehicle control. After cryo-injury, the incision was closed in layers using 6-0 Prolene sutures (Ethicon) and the skin sealed with Gluture skin glue (Abbott). Mice remained on the ventilator receiving oxygen until they began spontaneous respiration. After surgery, the mice were given carprofen (2-5 mg/kg SC) for analgesia and placed on a warming blanket until recovery from anesthesia was complete. Mice were then returned to their cages where they received treatment with buprenorphine every 12 hours for 48 hours and carprofen every 24 hours for 48 hours. Animals were sacrificed 1 week after surgery, hearts collected, and fresh frozen in OCT.

Immunolabeling: At 72 hours, aggregates were fixed in 4% paraformaldehyde for 10 minutes at room temperature, washed, and embedded in OCT for frozen sectioning. Aggregates were cut in thin sections of 5-10 μm and allowed to dry for 30 minutes. Cryo-injured hearts were cut in thin sections of 10 μm. Sections of aggregates or hearts were blocked with 1% BSA (Fisher Scientific), 0.1% Triton-X-100 (Fisher Scientific) in PBS. Cells were labeled for Cx43 (1:2000 Sigma, 1:100 Abcam, or 1:100 Chemicon), Cx43 pS368 (1:200 Cell Signaling), or 1:1000 pan-cadherin (Sigma). Hearts were counterstained with vimentin (Millipore) (1:1000) and MF20 (DSHB) (1:100). Labeling was viewed with AlexaFluor secondary

antibodies and stained with Hoechst 33342 (Sigma; nuclear labeling). For gSTED immunolabeling, proteins were visualized with goat anti-rabbit Chromeo 505 (1:100) and anti-mouse biotin (1:200) followed by streptavidin- conjugated Horizon V500 (1:100) secondary antibodies. For single molecule localization, cells and tissue were fixed in 4% paraformaldehyde, reduced in 0.1 M glycine, permeabilized in PBS with 0.2% Triton-X-100, and blocked in goat serum. Samples were labeled for Cx43 (Chemicon) and Cx43 pS368 overnight at 4°C, washed and visualized with AlexaFluor 647 (1:4000) and Cy3b (1:50).

Confocal, gSTED, and single molecule localization microscopy: For confocal, immunolabeled samples were imaged on a Leica SP8 LSCM with a Plan Apochromat 63x/1.4 NA oil immersion objective and Leica HyD hybrid detectors. For gSTED, immunolabeled samples were imaged on a Leica SP8 LSCM equipped with a gated stimulated emission depletion (gSTED) modules, a Plan Apochromat 63x/1.4 NA oil immersion objective, Leica HyD hybrid detectors and a 592-nm STED depletion laser. Fluorophores were imaged sequentially by frame. Two-color gSTED super-resolution images were obtained sequentially as z-stacks (with a step size of 10 nm) and processed using Huygens STED deconvolution software (Scientific Volume Imaging, Hilversum, The Netherlands). This enabled a maximum lateral full width at half maximum resolution of 22 nm using gSTED. For single molecule localization, immunolabeled samples were imaged on a Bruker Vutara 350 Single Molecule Localization system equipped with 555 nm and 647

nm lasers, and 100x objective. Two-color images were obtained sequentially as z-stacks with a step size of 10 nm and processed with Vutara software.

Confocal Cx43 quantification: Cx43 was quantified from images of Cx43 using the Sigma and Abcam antibodies for total Cx43 and an antibody for Cx43 pS368 (Cell Signalling). Image masks were created of the Cx43 labeling, myocytes (from CellTracker Orange or MF20 immunolabeling), and fibroblasts (from CellTracker Green, or vimentin immunolabeling) using ImageJ (NIH). Cx43 was quantified as fibroblast, myocyte, or fibroblast-myocyte interface.

Statistical analyses: All data were checked for normality by Shapiro-Wilk [236–240]. Non-normal data were transformed to normality using Box-Cox. If data could not be transformed to normality, non-parametric tests were used. For Cx43 area comparisons in myocytes, fibroblasts, and the zone of interaction of the two, factorial ANOVA (2 x 3) was performed with posthoc analysis by Least Significant Difference (LSD). Cx43 linear density was analyzed by ANOVA with posthoc analysis by LSD. Cx43 pS368 linear density was analyzed by Mann-Whitney U.

4.3 Results

αCT1 increases myocyte-fibroblast interactions via Cx43 in an *in vitro* IBZ model

As described in Chapter 2, we observed changes in cell organization in the *in vitro* IBZ model that correlated with changes in cell organization in a cryo-injury model of infarction (i.e. more cohesive groups of myocytes with αCT1 treatment compared to controls). Since we observed no differences in levels of pan-cadherin immunolabeling between treatments that would have suggested an effect of classical adhesion molecules on the cell sorting behavior, we hypothesized that changes in Cx43 – which also has adhesive properties – were responsible for changes in myocyte cohesion. The greatest change in myocyte-fibroblast organization was seen at 72 hours, so we looked for Cx43 at this time point. For analysis of Cx43 in myocyte and fibroblast compartments, image masks were used to separate the Cx43 immunolabeling signal into these compartments. The highest Cx43 particle density of total Cx43 was found in the myocyte compartment, which was expected, since myocytes have the greatest Cx43 expression in the heart (Fig. 4-1A&B). A zone of myocyte-fibroblast interaction showed the next greatest particle density of total Cx43, and this was significantly lower than the myocyte compartment (Fig. 4-1B; $p < 0.001$). Not surprisingly, the lowest levels of Cx43 were found in the fibroblast compartment and this was significantly lower than either the myocyte compartment or the myocyte-fibroblast interaction zone (Fig. 4-1B; $p < 0.001$). In both the fibroblast compartment and in the myocyte-fibroblast

compartment, αCT1 led to a significant increase in total Cx43 particle density (Fig. 4-1B; $p < 0.001$ and $p < 0.05$, respectively). When we measured linear Cx43 density, where the number of Cx43 particles was normalized to the length of myocyte-fibroblast interaction, total Cx43 density was significantly increased in αCT1-treated aggregates compared to controls (Fig. 4-1B; $p < 0.05$).

This analysis was repeated to examine the presence and extent of Cx43 pS368 in myocyte-fibroblast interactions. The highest Cx43 particle density of Cx43 pS368 was found in the myocyte compartment, though this was not significantly greater than in the myocyte-fibroblast compartment (Fig. 4-1C). Not surprisingly, the lowest levels of Cx43 pS368 were found in the fibroblast compartment and this was significantly lower than either the myocyte compartment or the myocyte-fibroblast interaction zone (Fig. 4-1C; $p < 0.001$). In both the myocyte compartment and in the myocyte-fibroblast compartment, αCT1 led to a significant increase in total Cx43 particle density (Fig. 4-1C; $p < 0.05$ and $p < 0.05$, respectively). There was no difference in Cx43 pS368 levels in the fibroblast compartment between αCT1-treated aggregates and controls. Linear density of Cx43 pS368 was significantly increased in αCT1-treated aggregates compared to controls (Fig. 4-1C; $p < 0.05$).

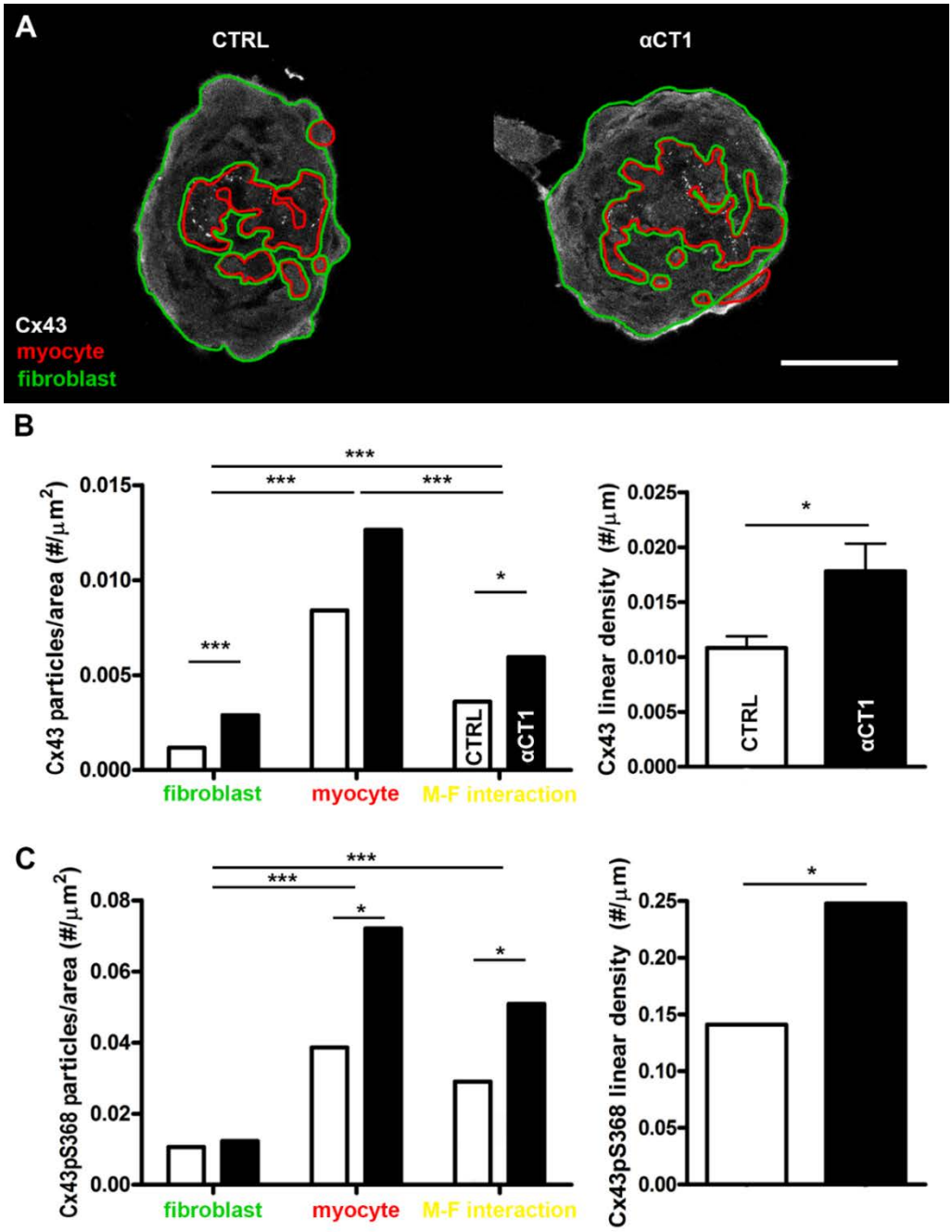

Figure 4-1. Myocyte-fibroblast interactions via Cx43 are increased in the IBZ *in vitro* model. A) Cx43 (white) immunolabeling is mostly within the myocyte compartment (red outline), though some is present in the fibroblast compartment (green outline). There seems to be more punctate Cx43 in αCT1-treated aggregates. Cx43 was measured from immunolabeled aggregates in the myocyte compartment, the fibroblast compartment, and a zone of interaction between the two. B and C) Myocyte-fibroblast interactions via Cx43 and Cx43 pS368 were significantly increased in αCT1-treated aggregates compared to controls. ***$p < 0.001$, **$p < 0.01$, *$p < 0.05$; Scale = 50 μm.

Overall, immunolabeling for Cx43 at the 72 hour time point showed that treatment with αCT1 significantly increased the amount of Cx43 in myocyte-fibroblast interactions compared to controls (Fig. 4-1). Interestingly, though Cx43 was increased in myocyte-fibroblast heterocellular interactions, phosphorylation of Cx43 at serine 368 was also increased. It is likely that there is a decrease in communication in these heterocellular contacts, as we also saw a decrease in heterocellular GJIC (Chapter 3). Increased clustering of myocytes was also seen in the aggregates at 72 hours (Chapter 2), suggesting that instead of Cx43 playing a role in intercellular communication, it may be serving an adhesive function in heterocellular interactions in the IBZ.

αCT1 alters myocyte-fibroblast interactions via Cx43 in the cryo-IBZ

As another method to validate our *in vitro* IBZ model and to further examine the changes in heterocellular interactions in the IBZ, we examined these interactions in the cryo-injury model at 7 days. Immunolabeling of Cx43 pS368 was undertaken on sections of cryo-injured mouse heart (Fig. 4-2). Confocal images demonstrated an increase in fibroblast infiltration into the IBZ, leading to separation of myocyte connections. Cx43 also appeared disordered in the IBZ compared to the regions remote from the injury. There was a trend toward increasing myocyte-fibroblast interactions via Cx43 in the IBZ.

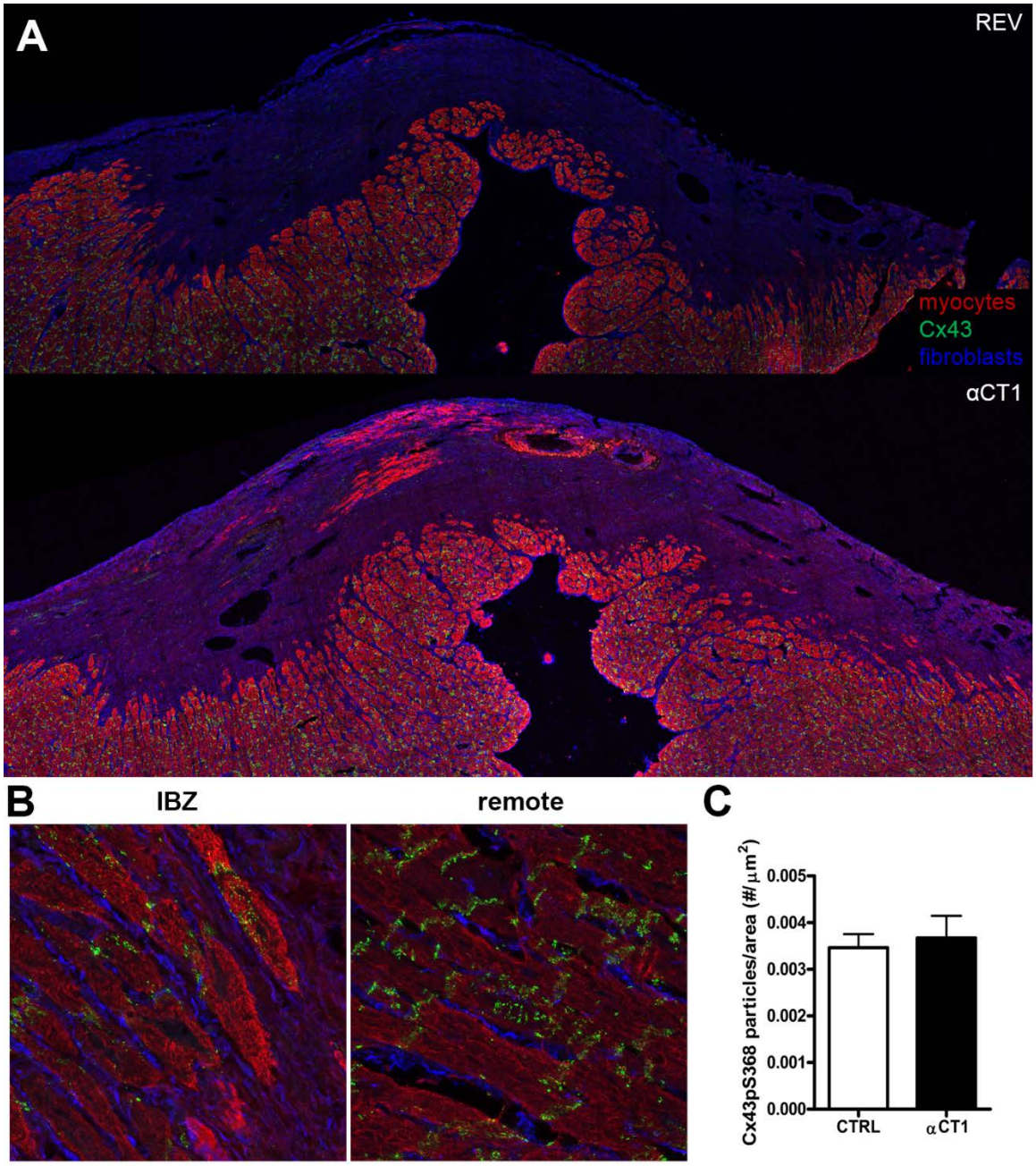

Figure 4-2. Murine cryo-injury model of infarction demonstrated lateralized Cx43 in the IBZ. A) High-resolution tile scans of the cryo-IBZ and scar in reverse control and αCT1 peptide-treated hearts. Scar area is largely comprised of fibroblasts (blue), which appear to separate myocytes (red) in the IBZ. Cx43 (green) appears decreased and lateralized in the IBZ. B) Fibroblasts infiltrate normal myocyte connections in the IBZ, but not in regions of the myocardium remote from the injury. C) There was a trend toward increased myocyte-fibroblast interactions via Cx43 when measured in the IBZ.

A novel gap junction plaque phosphorylation subdomain organization

Previous studies from our lab have shown that αCT1 increases Cx43 pS368 in a PKC-dependent manner [104,105]. In order to better understand how these changes influence the GJ plaque structure in terms of subdomain organization, we undertook immuno-confocal and immuno-super-resolution imaging studies in cultures of NVRMs and NRVFs and in cryo-injured mouse heart tissue. Cells and tissues were labeled with antibodies directed against the non-phosphorylated form of Cx43 and against Cx43 pS368. Confocal images of myocyte-fibroblast co-cultures demonstrated presence of small, punctate GJs between myocytes and fibroblasts (Fig. 4-3A). Signal from non-phosphorylated Cx43 and Cx43 pS368 appeared to mostly overlap in these images (Fig. 4-3B).

To get a more detailed picture of the structure of the GJ plaques in myocyte-fibroblast contacts in these co-cultures, we used gSTED microscopy. However, we were unable to obtain images of these punctate plaques in myocyte-fibroblast connections as the high laser power used for gSTED microscopy quickly extinguished the fluorescent antibody under imaging parameters that allowed capture of larger GJ plaques. This technique did allow us to obtain images of larger myocyte-myocyte gap junctions (Fig. 4-3C&D). These images revealed a never-before-seen GJ subdomain organization with respect to non-phosphorylated Cx43 and Cx43 pS368 (Fig. 4-3C,D,E). Interestingly, co-cultures treated with αCT1 showed larger GJ plaques, though there did not appear to be a difference in

subdomain organization between treated and control cultures. Figure 4-3E shows the detail of non-phosphorylated Cx43 and Cx43 pS368 subdomain organization, where it appears that these two forms of Cx43 are organized into a mosaic pattern in the GJ plaque.

In order to understand the structure of myocyte-fibroblast Cx43 interactions in adult tissue, we used gSTED microscopy to look for this same protein pair in sections of cryo-injured adult mouse heart tissue. gSTED was not sufficiently robust to image into these tissues, so we repeated this imaging study using a single molecule localization technique. Again, we found it difficult to image myocyte-fibroblast connections because of their small size. Images obtained of GJ plaques between adjacent myocytes in the remote (uninjured) region of the myocardium (Fig. 4-3F) displayed a similar GJ subdomain structure to that seen in cultures of neonatal myocytes.

Figure 4-3. (Following page) A novel GJ plaque subdomain structure revealed by super-resolution imaging. A) Myocytes and fibroblasts interact in culture via Cx43 GJs. B) Inset of (A). It appears that the non-phosphorylated form (green) and Cx43 pS368 (red) are co-localized when examined with standard confocal microscopy. C&D) αCT1 increased GJ size at the myocyte-myocyte interface. Cx43 (green) and Cx43 pS368 (red) appeared to be organized into a mosaic pattern when imaged with super-resolution techniques. E) Inset of (C) via gSTED microscopy. F) Structure of an ID in adult mouse heart via single molecule localization technique.

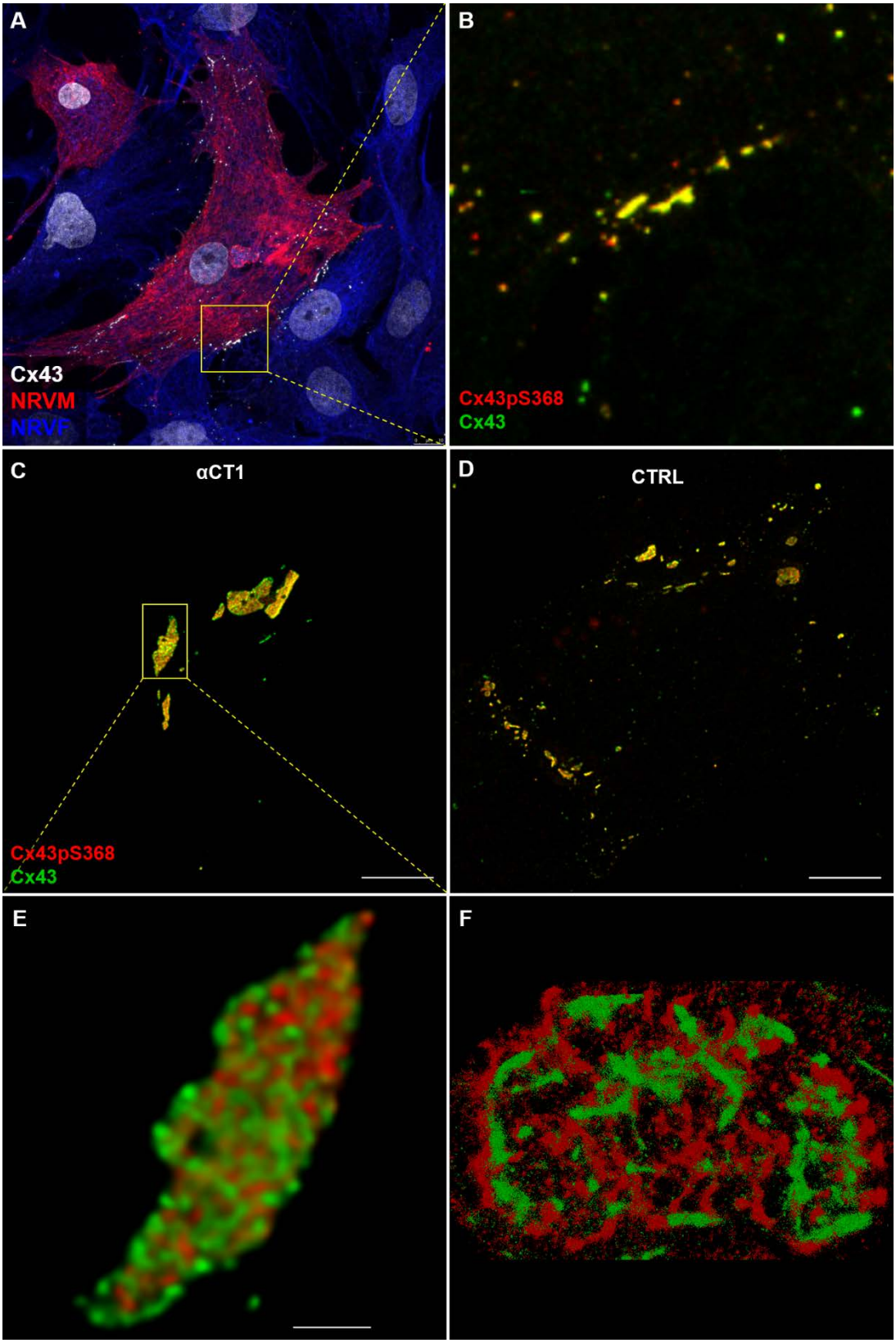
A
Cx43
NRVM
NRVF
B
Cx43pS368
Cx43
C
αCT1
Cx43pS368
Cx43
D
CTRL
E
F

4.4 Discussion

In this chapter, we describe the presence of Cx43 in myocyte-fibroblast interactions in our *in vitro* model of the IBZ and modulation of these interactions by the Cx43 mimetic peptide αCT1. In the IBZ model, total Cx43 and Cx43 that is phosphorylated at serine 368 were found to be significantly increased by treatment with the αCT1 peptide *in vitro*. Subsequent examination of these interactions by returning to the cryo-injury model of infarction suggested that αCT1 may alter interactions in the IBZ to some extent *in vivo* as well. In light of these increased myocyte-fibroblast interactions via Cx43, further examination of Cx43 GJs by super-resolution microscopy techniques revealed a never-before-seen subdomain organization of the GJ plaque where the non-phosphorylated form of Cx43 and Cx43 pS368 organize into a mosaic pattern within the plaque.

Importantly, the work detailed in this chapter provide further validation of the *in vitro* model of the IBZ and suggest that αCT1 may be an important tool for modulating cellular interactions via Cx43. Data from previous chapters suggest that this peptide has an overall beneficial effect on modulating arrhythmias, and this chapter suggests that one of the cellular mechanisms involved may involve Cx43 GJs.

Studies on the GJ plaque structure indicate that connexons waiting in the non-junctional perinexus zone are added to the GJ from the edge of the plaque. It is thought that Cx43 is inserted into the membrane mostly unphosphorylated and

connexin incorporation into GJ plaques is associated with increasing phosphorylation. In light of the novel GJ plaque sub-domain organization described in this chapter, connexons may be either differentially phosphorylated by PKC at S368 as they are inserted into the cell membrane, resulting in a mosaic pattern as they are incorporated into the plaque, or they are differentially phosphorylated as sub-domains within the GJ plaque. Studies on trafficking of Cx43 may provide more insight into the GJ phosphorylation sub-domain organization.

CHAPTER 5: IMMUNE MODULATION FOR IMPROVED SURVIVAL AND ENGRAFTMENT OF STEM CELLS FOR SKELETAL MUSCLE REGENERATION

5.1 Introduction

Though heart muscle and skeletal muscle are both of mesenchymal origin, skeletal muscle has remarkable ability to regenerate after injury, while injury to the heart typically results in a scar. While numerous populations of muscle stem cells have been identified in the skeletal muscle, it is the satellite cell (SC) that is primarily responsible for regeneration and muscle re-growth. SCs are normally quiescent, contributing to homeostasis of muscle tissue [296]. When muscle is injured, SCs are activated by various signals [297], proliferate, and fuse to generate mature myofibers [298] that replace lost or damaged muscle. There is, however, a limit to the regenerative capacity of muscle. In volumetric muscle loss (VML), which typically occurs from injuries due to traumatic accidents or explosions like those seen in the battlefield, large amounts of muscle tissue are lost or damaged and scarring of the injured area results [299]. Chronic degenerative diseases like muscular dystrophies also involve extensive scarring [300]. These conditions are subject to reparative fibrosis, in which muscle does not fully regenerate and is partially replaced by scar tissue, leading to impaired muscle function and patient disability.

Therapies for regeneration of lost or damaged muscle tissue include tissue engineering approaches with both natural and synthetic scaffold materials [301,302], using a variety of cells to either populate scaffolds or inject directly as cell-based therapies (Fig. 5-1) [302–305]. For the purpose of this project, we have focused on cell-based therapies, which allow the biochemical and biophysical signals from the tissue environment to direct regeneration. Cell-based therapies are challenged by low survival of implanted cells – typically, only 5-10% of cells survive. This low survival rate would require an extremely large number of cells to be injected in order to regenerate a large amount of tissue, resulting in high cost of these therapies.

One factor influencing the low survival rate of implanted cells, especially in non-autologous therapies, is the immune system attack and destruction of these cells. Major histocompatibility complex class I (MHC-I) molecules are expressed by all cells in the body. In healthy cells, the MHC-I molecules presented are derived from the cell's own proteins, so the immune system recognizes these cells as 'self.' When infected, the cell presents some molecules derived from the proteins of the pathogen, which activates cytotoxic T lymphocytes against those proteins and results in killing of the infected cell [306].

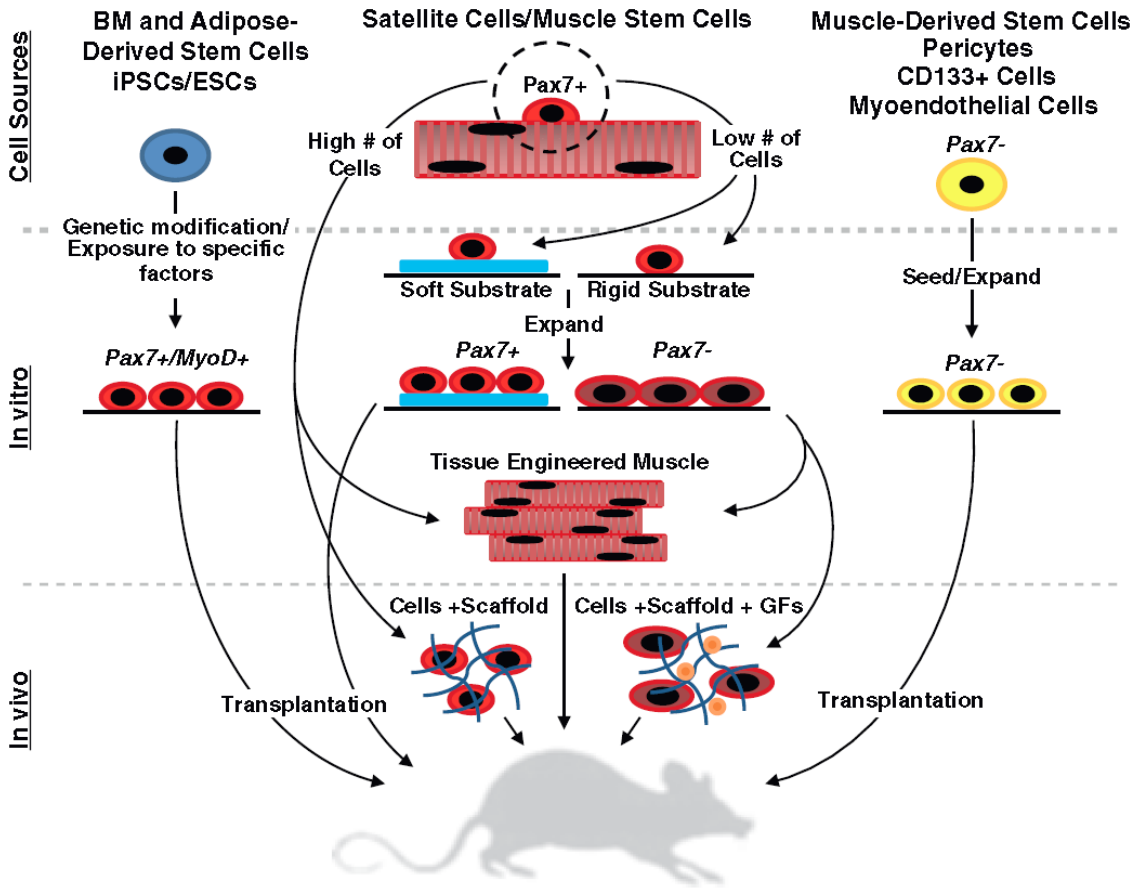

Figure 5-1. Cell sources and regenerative strategies for skeletal muscle. A variety of cell sources are used for experimental muscle regeneration, including those derived from the muscle itself, as well as sources outside the muscle, like bone marrow and adipose tissue. These cells can be cultured *in vitro* on various substrates to form tissue engineered muscle for transplantation. Cell may also be modified genetically and expanded in culture for transplantation *in vivo.*

Bone marrow mesenchymal stem cells (BMSCs) are thought to be an 'immune-privileged' cell type, making them a good candidate for increasing survival in cell-based therapies [307]. BMSCs express intermediate levels of MHC-I and lack MHC-II entirely, enabling them to evade the immune system in allogeneic transplantation [308]. Additionally, BMSCs are known to differentiate into multiple

tissue types, including muscle [309–312], and have been shown to have modest beneficial effects on healing of the heart after MI. While BMSCs can evade immune system attack to some extent, other studies report that rejection of these cells does occur, and it is likely because of MHC-I mismatch between the donor and recipient [313,314].

Human cytomegalovirus (HCMV) is ubiquitously expressed in humans. It has developed strategies to evade the immune system by downregulating MHC-I surface molecules through production of proteins that code for the Unique Short (US) region of the HCMV genome [315,316]. Human BMSCs genetically engineered to express these US proteins have downregulated surface levels of MHC-I, are protected against NK killing, and result in a 1.5 fold to 1.8 fold increase in engraftment when implanted in fetal sheep [317]. These results suggest that modulating MHC-I expression is a viable strategy for reducing immune system response to implanted cells and increasing their survival.

The goal of these studies was to improve survival and engraftment of satellite cells implanted for cell-based skeletal muscle regeneration. Here we describe genetically engineered rat BMSCs expressing human US proteins as a proof of principal of downregulation of MHC-I. We have also engineered a skeletal muscle satellite cell line to express human US proteins, though further examination is required. This method of decreasing the immune response is novel to the field of skeletal muscle regeneration, but has been used in other fields.

5.2 Methods

Animal care and use: All animal research was conducted under the guidance of the Institutional Animal Care and Use Committee of Virginia Polytechnic and State University and conforms to the NIH *Guide for the Care and Usage of Laboratory Animals.*

BMSC isolation and culture: Bone marrow mesenchymal stem cells were isolated from adult rat femurs. Femur heads were clipped off using bone reamers, and DMEM medium was used to flush the bone marrow cavity with a syringe and 22 gauge needle. Bone marrow was collected into a 15 mL conical tube. Cells were triturated and plated on 100 mm dishes. Non-adherent cells were removed after 24 hours. Cells were passaged no more than 5 times in DMEM (Hyclone) supplemented with 10% FBS (Hyclone), 10 U/ml penicillin and 10 µg/ml streptomycin (Hyclone), and 2 mM L-alanyl-L-glutamine (Fisher) and maintained in an incubator at 37°C, 5% CO_2.

H2K cell culture: H2K cells [318,319] were isolated by Terry Partridge's lab at the Children's National Medical Center in Washington, DC. H2K cells were grown to a density of 10,000/cm^2 in DMEM (Hyclone) supplemented with 20 U/mL IFN-γ (Millipore), 20% HI-FBS (Atlanta Biologicals), 2% chick embryo extract (Accurate Chemical), 2 mM L-alanyl-L-glutamine (Fisher), 10 U/ml penicillin and 10 µg/ml streptomycin (Hyclone) and maintained in an incubator at 33°C, 10% CO_2.

PT67 cell culture: PT67 cells transfected with constructs for HCMV Unique Short (US) proteins US2, US3, US6, US11, and an empty vector were a gift from the lab of Dr. Graça Almeida-Porada at the Wake Forest Institute for Regenerative Medicine. Briefly, US2, US3, US6, and US11 DNA sequences were PCR amplified from a clinical HCMV isolate, introducing EcoRI and XhoI restriction sites for US3, US6, and US11 and EcoRI and SalI for US2. The purified PCR products were then ligated into the pMSCV-Neo retroviral vector backbone (Clontech, Mountain View, CA) that had been previously digested with EcoRI and XhoI. These recombinant plasmids were transformed into One Shot Top10 chemically competent cells (Life Technologies), and transformed Top10 cells were selected with ampicillin (Sigma; 50 µg/mL). Positive clones were confirmed by PCR using primers for the US insert, miniprep digestions, and sequencing. For US3, US6, and US11 cloning, digestion was performed with EcoRI and XhoI restriction enzymes. For US2 cloning, EcoRI and BglII restriction sites were digested, as US2 cloning generated a SalI/XhoI hybrid restriction site. Each US recombinant plasmid and an empty plasmid were transfected into the RetroPack™ PT67 Packaging Cell Line (Clontech) using Lipofectamine 2000 (Life Technologies) according to the manufacturer's instructions. Stable transfectants were selected for 5 days with 500 µg/mL G418 (Fisher), starting at 72 hours after the transfection. Supernatants were collected and filtered with 0.2 µm low protein binding syringe filters (Pall Corporation, Ann Arbor, MI). PT67 cells are cultured in DMEM (Hyclone) supplemented with 10%

FBS (Hyclone), 10 U/ml penicillin and 10 µg/ml streptomycin (Hyclone), and 2 mM L-alanyl-L-glutamine (Fisher) and maintained in an incubator at 37°C, 5% CO_2.

BMSC transduction: Subconfluent cultures of BMSCs were transduced for 6 hours with filtered supernatant containing either US recombinant or empty MSCVneo retrovirus diluted in serum-free QBSF60 medium (Quality Biological, Gaithersburg, MD) and 8 µg/mL protamine sulfate (Calbiochem, San Diego, CA). After transduction, stable US-recombinant BMSCs were selected with 500 µg/mL G418 (Fisher) for 5 days, replacing the selection media every 2 to 3 days. Therefore, after the antibiotic selection, all the cells were transduced and consequently expressing NeoR and the corresponding US HCMV gene.

H2K cell transduction: Subconfluent cultures of H2K cells were transduced for 6 hours with filtered supernatant containing either US recombinant or empty MSCVneo retrovirus diluted in serum-free QBSF60 medium (Quality Biological, Gaithersburg, MD) and 8 µg/mL protamine sulfate (Calbiochem, San Diego, CA). After transduction, stable US-recombinant H2K cells were selected with 500 µg/mL G418 (Fisher) for 5 days, replacing the selection media every 2 to 3 days. Therefore, after the antibiotic selection, all the cells were transduced and consequently expressing NeoR and the corresponding US HCMV gene. Transmitted light images of transduced and untransduced H2K populations were captured on a Life Technologies EVOS FL microscope.

Flow cytometry analysis: BMSC, BMSC-E, BMSC-US2, BMSC-US3, BMSC-US6, and BMSC-US11, prior to confluence, were detached by cell scraping in 1x PBS, in order to preserve extracelluluar epitopes. Cells were counted and their viability checked using Trypan Blue reagent. $1x10^6$ cells were incubated for 15 minutes at room temperature with FITC-tagged mouse anti-rat RT1A (BD Pharmingen™, Clone OX-18) or FITC-tagged mouse IgG1$_\kappa$ isotype control antibodies. Cells were washed, fixed with 0.1% azide in PBS, centrifuged and fixed with 1% paraformaldehyde. Forward and side scatter plots were generated and used to exclude the few dead cells and debris from the histogram analysis plots.

5.3 Results

HCMV US proteins downregulate MHC-I on rat bone marrow MSCs

Rat bone marrow MSCs were transduced with retroviral vectors expressing US2, US3, US6, and US11. Non-transduced BMSCs and BMSCs transduced with an empty vector (BMSC-E) were used as controls. 48 hours after transduction, BMSCs were selected with 500 µg/mL G418 for 5 days with media changes every 2 to 3 days. Only cells expressing neomycin resistance (NeoR), and hence, the expression vector for the protein of interest, survived. The morphology of the BMSCs was not changed by transduction with the US protein constructs (data not shown).

Expression of MHC-I was measured by flow cytometry in cells transduced with US proteins and their controls. Scatter plots of BMSCs from the initial experiment are shown in Figure 5-2 with isotype controls subtracted. Figure 5-2B summarizes the percentage of MHC-I positive cells with Median Fluorescent Intensity (MFI) ratios in Figure 5-2C. MFI ratio was obtained by dividing MHC-I's MFI by the respective isotype's MFI. Transduction of BMSC with MSCVneo empty retroviral vector resulted in a decrease in the percentage of transduced cells expressing MHC-I from 94.75% to 76.45%. Transduction of BMSCs with US6 and US2 resulted in the largest decrease in surface expression of MHC-I to 62.45% and 68.36%, respectively. This represented a ~34% and a ~28% decrease, respectively. This reduction in MHC-I expression was also reflected in the decreased MFI ratio in US6 and US2 transduced cells (Fig. 5-2C). Transduction of BMSCs with US3 and US11 also resulted in decreased MHC-I expression, though to a lesser extent (74.64% and 75.04%, respectively).

H2K cells can be transduced and selected for US-protein expression

H2K cells were transduced with retroviral vectors expressing US2, US3, US6, and US11. Non-transduced H2K cells and H2K cells transduced with an empty vector (H2K-E) were used as controls. 48 hours after transduction, H2K cells were

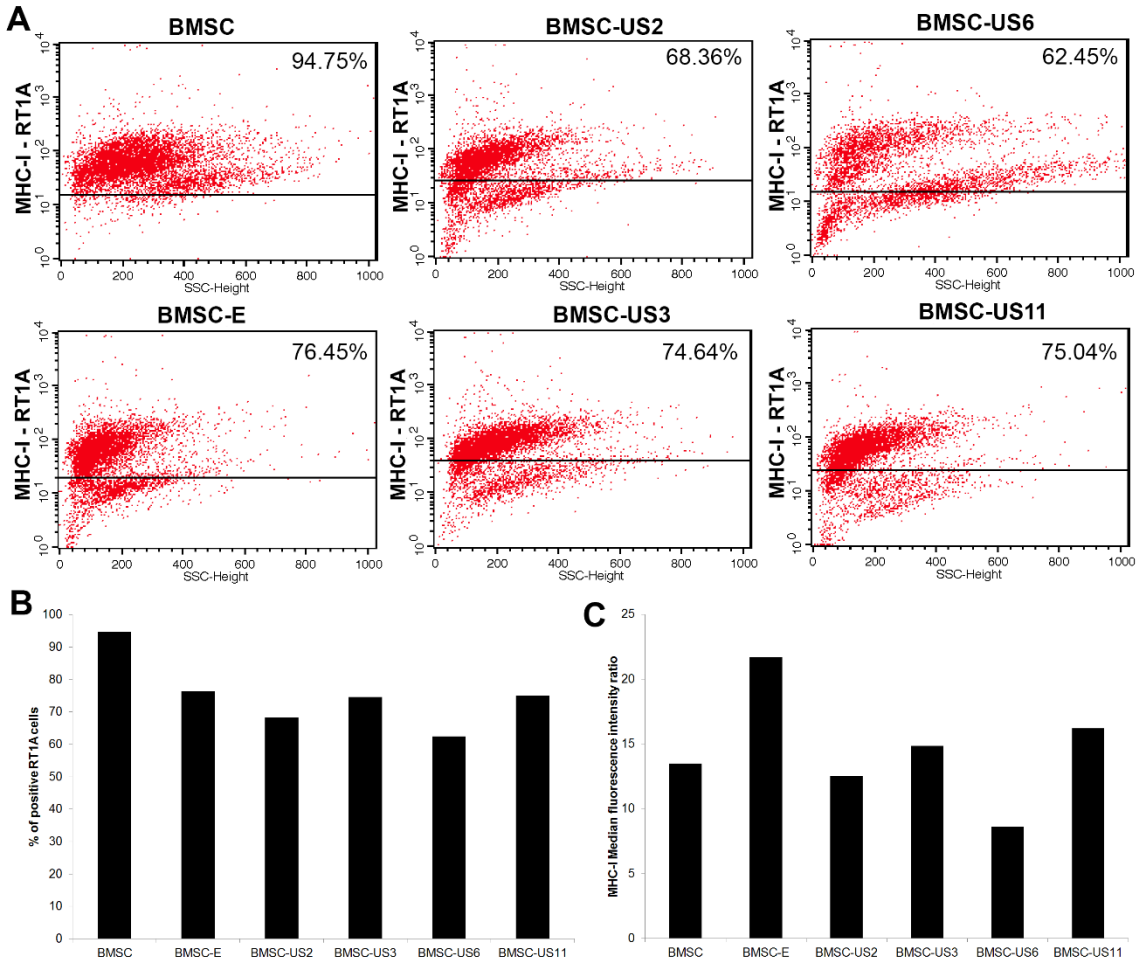

Figure 5-2. Forced expression of human US proteins in rat BMSCs reduced cell surface presentation of MHC-I. A) Flow cytometry scatter plots showed reduced MHC-I presentation by ~30% in US2 and US6, which is reflected in (B). C) The median fluorescent intensity ratio reflects the alteration in MHC-I surface expression.

selected with 500 µg/mL G418 for 5 days with media changes every 2 to 3 days. Only cells expressing neomycin resistance (NeoR), and hence, the expression vector for the protein of interest, survived. The morphology of the H2K cells was not changed by transduction with the US protein constructs (Fig. 5-3).

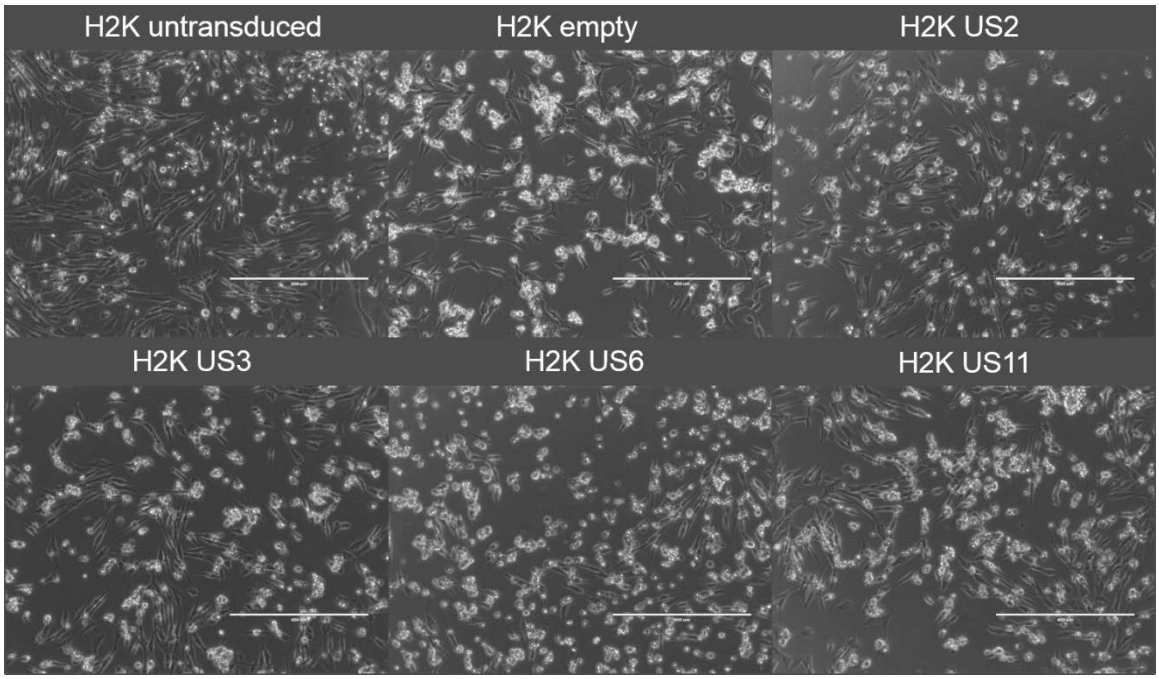

Figure 5-3. H2K cells can be transduced with US protein viral constructs with no change to their morphology. Cells under selection with G418 have several rounded, dying cells that were not transduced.

5.4 Discussion

Satellite cells have the ability to regenerate lost muscle tissue, though VML and muscular dystrophies typically result in scarring that can inhibit muscle function. Satellite cells have been used for tissue engineering and cell-based regenerative medicine approaches, but these therapies are challenged by low survival and engraftment of injected cells. One of the reasons for low cell survival is attack of the implanted cells by the immune system, in particular, MHC-I molecule mismatch between the donor and the recipient [313,314]. Previous studies have shown that

downregulation of MHC-I molecules through US protein expression can improve cell survival [317].

Here, we demonstrated proof of principal of downregulation of MHC-I on rat BMSCs, resulting in ~30% decrease in cell surface levels of MHC-I molecules. Additionally, we transduced H2K cells with US protein constructs and selected for cells expressing the constructs. Further work needs to be done to examine the relative levels of MHC-I on H2K cells by flow cytometry. Additionally, studies of survival and engraftment need to be completed. H2K cells are particularly well-suited to studies of this type, as they are a conditionally immortal cell type [319,320]. These cells, isolated from the *H-2K^{b}-tsA58* immortomouse, have a temperature sensitive immortalizing gene, where at lower temperatures the cells are continually mitotic, and at higher temperatures the cells terminally differentiate and fuse into myotubes [319,320].

The immortomouse system provides the highest reproducibility across animal experiments, as cells from a single isolation can be expanded extensively in culture, eliminating variability due to multiple isolation of primary cells. For animal implantation models, cell death and regeneration can be measured using the Y chromosome – which is conserved in the immortomouse system, proving a distinct advantage over other mouse cell lines.

Cell-based therapies for MI have included both satellite cells [321,322] and bone marrow cells [272]. Satellite cells, a muscle progenitor, were believed to be a good

candidate for differentiation into a contractile cell phenotype that would confer functionality to the infarcted myocardial scar [323]. In addition to their ability to differentiate into muscle cells, these cells can be easily expanded *in vitro*, are resistant to ischemia, and have a low risk of tumorigenesis [6]. Studies of this kind have been met with only moderate success due to the inability of satellite cells to efficiently transdifferentiate into a cardiomyocyte-like phenotype [324,325].

The studies completed and outlined here examine the development of a technique that can modulate the immune response to cells implanted for regenerative therapies with the goal of improving survival and engraftment of cells.

CHAPTER 6: CONCLUSIONS

6.1 Summary

Cardiovascular disease is the leading cause of death worldwide. Myocardial infarction – a subset of CVD – is responsible for over 150,000 deaths each year in the United States alone [3]. Current clinical therapies for MI are focused on prolonging life and few new drugs make it to market due to the inefficiencies in the drug development pipeline. In order to get more efficacious drugs to patients faster with a focus on improving cardiac function and regenerating tissue lost to the ischemic insult, there is a need for better platforms for testing of new therapeutics.

The IBZ is frequently the site of lethal reentrant arrhythmia generation, likely caused by the changes in cellular and molecular remodeling that occur after MI [11,233]. Alterations in patterns of organization of myocytes and fibroblasts, increased fibrosis, and changes in localization of Cx43 are all thought to contribute to the generation of a pro-arrhythmic substrate, though the mechanism of each of these is not fully understood.

The major focus of my work is the development and validation of an *in vitro* model of the IBZ with the goals of generating a disease-relevant and tissue structure-relevant model that can be used for high-throughput *in vitro* testing of therapeutic compounds to target the arrhythmogenic propensity of the IBZ and utilizing this

model to gain a better understanding of heterocellular interactions in the IBZ. The research presented in this dissertation has generated novel contributions to the fields of drug development and mechanistic targets for cardiac regenerative therapies.

In chapter 2 we developed a novel *in vitro* model of the IBZ. This model recapitulates disease-relevant alterations in cell organization in response to the small peptide therapeutic (αCT1) reported in previous studies of cardiac cryo-injury from our lab [231], and suggests an adhesive role for Cx43 in this process. Of relevance to drug discovery is the generation of a high-throughput 3D model, which is more tissue-relevant than the 2D *in vitro* testing paradigms often used prior to pre-clinical animal models. Other experimental *in vitro* models of cardiovascular disease have been used to test drugs, though these platforms are not widely used, have not been standardized, and have not been validated against disease or drug responses [195]. To our knowledge, none of these is an image-based platform. Our novel *in vitro* model advances the field of drug development by providing a model relevant to tissue that can be validated against disease and drug responses. Additionally, it is the first model of its kind used to examine cell interactions in real time.

In chapter 3 we described a delay in action potential propagation through the cryo-IBZ in conditions of altered extracellular ion concentrations, though acutely treating cryo-injured hearts with αCT1 abolished this delay when measured in 8-week

healed hearts. A communication assay suggested that αCT1 decreased GJIC in myocyte-fibroblast interactions and in fibroblast-fibroblast interactions. Our studies of recruited bone marrow cells to the cardiac infarct did not yield conclusive results and further testing is needed. Previous studies describe conduction slowing through the IBZ, though none have directly measured the delay in action potential propagation. Since this delay was induced by altered extracellular ion concentrations, these data suggest the possible influence of ephaptic coupling mechanisms in the IBZ. Studies from our lab demonstrate the presence of cardiac myocyte ephaptic coupling [120], though modeling studies suggest that ephaptic effects may be present in any intercellular space, indicating a possible role for fibroblasts in ephaptic coupling in the IBZ, though this requires further investigation.

Previous studies from our lab showed that αCT1 treatment of cryo-injured hearts resulted in an increase in phosphorylation at serine 368 of Cx43 (pS368) [104,105], which decreases unitary conductance of the GJ channel. Consistent with this, we show here that elevated Cx43 pS368 level correlates with reduction of intercellular communication between cultured myocytes and cardiac fibroblasts. Our studies also suggest that increased Cx43 pS368 corresponds to *increased* uniformity of action potential propagation through the IBZ [104]. This property may relate to the decreases in arrhythmic propensity observed in cryo-injured hearts [326]. This being said, the mechanism by which αCT1 improves the physiological metrics of injured hearts requires further investigation.

In chapter 4 we investigated how Cx43 heterocellular interactions changed when treated with αCT1. Cx43 and Cx43 pS368 are increased in myocyte-fibroblast interactions in our *in vitro* model. Super-resolution imaging techniques revealed a never-before-seen Cx43 GJ plaque sub-domain organization in which non-phosphorylated Cx43 and Cx43 pS368 are arranged in a mosaic pattern. Studies exist indicating the presence of myocyte-fibroblast coupling via Cx43 in both the normal and diseased heart, though presence of protein does not imply function. Cx43 pS368 is associated with decreased channel conductance. Our studies suggest that αCT1 increases myocyte-fibroblast interactions via Cx43, though it is possible that communication is reduced, since there is also a significant increase in Cx43 pS368 with αCT1 treatment.

Studies on the GJ plaque structure indicate that connexons waiting in the non-junctional perinexus zone are added to the GJ from the edge of the plaque. It is thought that Cx43 is inserted into the membrane mostly unphosphorylated and connexin incorporation into GJ plaques is associated with increasing phosphorylation. In light of the novel GJ plaque sub-domain organization reported herein, the data suggests that connexons are either differentially phosphorylated by PKC at S368 as they are inserted into the cell membrane, resulting in a mosaic pattern as they are incorporated into the GJ plaque, or they are differentially phosphorylated as sub-domains within the GJ plaque. Further trafficking, interaction, and biophysical studies are required to better understand how this phosphorylation sub-domain organization arises. An enhanced understanding of

functional coupling in the IBZ may enable development of improved therapies to reduce arrhythmias in post-MI patients.

In chapter 5 we explored proof-of-concept of reducing immune system recognition of cells through decreased MHC-I molecule surface presentation in BMSCs and H2K satellite cells for application in cell-based regeneration of skeletal muscle. We found that expression of MHC-I surface presentation could be reduced by ~30% on BMSCs and that H2K cells could be efficiently transduced with US proteins. Other studies have used US protein expressing BMSCs as a cell-based regenerative therapy and shown a 1.5- to 1.8-fold improvement in cell engraftment using these strategies [317]. Though further work in animal models needs to be undertaken to assess the utility of this strategy for regeneration of skeletal muscle, these studies provided proof-of-concept. While other skeletal muscle regeneration studies have utilized BMSCs for cell-based therapy, and BMSCs are known to contribute to skeletal muscle regeneration, none have used the approach of directly modulating the immune system for improved survival and engraftment of cells. These studies have the potential to advance the field by reducing cost and improving the effectiveness of cell-based therapies, leading to reduced scarring and improved patient outcomes.

6.2 Challenges and limitations

Cell source

In vitro models are limited by cell source. Our model uses neonatal rat ventricular myocytes and fibroblasts, which are easy to isolate, but do not necessarily have the same connexin distribution as adults heart. Post-natal cardiac development includes the progressive formation of brick-shaped myocytes with IDs and adhesion junctions at the short ends of the cell and lower amounts of connexin at lateral cell borders. Additionally, there are interspecies differences in cardiac electrophysiological properties, and these have been responsible for removal of FDA-approved drugs from the market due to previously unseen cardiotoxic effects. Isolated human cells provide an electrophysiologically germane model, but are difficult to obtain and maintain in culture. Large animal models like sheep and pig are more relevant in terms of size and physiology than are rodents, but these are expensive models. Human iPSCs have been increasingly used to model genetic mutations affecting cardiac function, and may be a good source for *in vitro* model development as well, though these cells are challenged by their limited ability to take on a mature cardiomyocyte phenotype.

The field of cell-based regenerative medicine has been challenged by cell source from the beginning. Ideally, cell-based therapies would use autologous cells to reduce the effect of the immune response, though this also requires development of serum-free culture technologies for cell expansion. Expansion of human stem

cells in culture is slow and requires Good Laboratory Practice (GLP) facilities, making these therapies costly. Use of non-autologous therapies requires immune modulation of the implanted cells or engineered tissues or requires patient immunosupression.

Disease-relevant animal models

Our *in vitro* model was developed using rat cells and validated against a mouse model of MI. While these models have been developed to closely represent human pathologies, they do not fully recapitulate human disease processes. Development of safe and effective pharmaceuticals would be improved by development of more disease-relevant and tissue-relevant models.

6.3 Future directions and recommendations

The *in vitro* IBZ model can be expanded and altered to meet the testing need, including examination of other cell types and different compounds. For genetic disease-relevant models, use of iPSCs from patients carrying a cardiac genetic mutation would allow development of therapeutics for those specific diseases. Perfusion bioreactor systems could be generated to fit the multi-well agarose micromolds currently used, especially if the candidate compound will be delivered systemically when used in the clinic. For local delivery, studies using cryo-injury

model in our lab used a methylcellulose patch to deliver αCT1, though this patch does not adhere tightly to the surface of the heart. If a candidate compound is targeting a specific time point in the healing process, developing a delivery system or a controlled release system would be pertinent.

Cell organization data in the cryo-IBZ model [231], as well as the work in our *in vitro* model (Chapter 2) suggested a difference in cell cohesion was evident at a 100 μM dose of αCT1. Though a dose curve was not tested in either the *in vitro* aggregate model or the cryo-injury model, the results of the *in vitro* model reflected those of the *in vivo* model, suggesting that this may be a good starting concentration for clinical testing of this drug. Previous work from the lab suggests that fibroblast migration in scratch-wound assays increases in a dose-dependent manner with αCT1 treatment, encompassing a range of 1 to 180 μM [327], though further testing will be required to determine a minimum effective dose.

Optical mapping of cryo-injured hearts showed that αCT1 altered conduction in the IBZ and this may be a result of changes in GJIC, as αCT1 reduced GJIC in heterocellular myocyte-fibroblast connections and in homocellular fibroblast cell-cell connections. This suggests that GJIC is likely altered in the IBZ, though the mechanism remains to be understood. Studies of functional myocyte-fibroblast coupling in the IBZ would be pertinent to determining how αCT1 affects heterocellular interactions in the IBZ. No functional coupling studies in the

diseased heart have been published to date. Only one study exists in normal heart, and it demonstrates presence of functional myocyte-fibroblast dye coupling [285].

Transfer of αCT1 to heart disease and myocardial infarction patients may initially involve the testing described above. Additionally, this peptide has completed Phase I and Phase II clinical trials for wound healing in chronic non-healing diabetic foot ulcers [180] and venous leg ulcers [181], where, among other results, this peptide was proven safe and effective on these skin wounds. The clinical progress attained in skin would speed up the time to clinic of this peptide for MI patients, though, efficacy dose testing would be critical before this peptide could be FDA approved. It would also be important to consider delivery methods. We use a patch for the cryoinjury procedure in mice, but it is rare that a patient's chest is opened when they present in the clinic with symptoms indicating MI. While systemic delivery is a simple option, this must be critically evaluated for the effect of the peptide on other tissues and organs in the body. Localized catheter delivery may be a possibility, and could be combined with endovascular procedures aimed at opening the coronary arteries.

Our study of bone marrow recruitment to the cardiac injury did not yield conclusive results, but did raise a number of questions about the model. Measuring the transduction efficiency of the injection of virus in the bone marrow cavity would enable assessment of whether recruitment is being challenged by low transduction efficiency or low cell homing to the cryo-injured heart. Additionally, bone marrow

chimeras may be a more robust approach to this question, as there is no transgenic BMSC mouse due to lack of a specific marker for these cells.

As discussed in Chapter 5, H2K satellite cell US protein transduction studies should be assessed for MHC-I surface presentation, and, pending results, taken into animal models of survival and engraftment, using the Y-chromosome to track these cells post-implantation. These studies may hold promise for translation to clinical therapies if MHC-I presentation can be sufficiently suppressed to allow better survival and engraftment of SCs for therapies in muscle loss or dystrophic disease.

REFERENCES

[1] World Health Organization - Cardiovascular diseases fact sheet, (2015).

[2] World Health Organization - The Atlas of Heart Disease and Stroke, (2015).

[3] D. Mozaffarian, E.J. Benjamin, a. S. Go, D.K. Arnett, M.J. Blaha, M. Cushman, et al., Heart Disease and Stroke Statistics--2015 Update: A Report From the American Heart Association, 2015.

[4] Urbanization and Cardiovascular Disease, World Hear. Fed. (2012).

[5] P. Puska, S.C. Smith, A. Matsumori, K.S. Reddy, K. Akinroye, E.M. Briceno, et al., State of the Heart - Cardiovascular Disease Report, World Hear. Fed. (2010).

[6] K. Thygesen, J.S. Alpert, A.S. Jaffe, M.L. Simoons, B.R. Chaitman, H.D. White, et al., Third universal definition of myocardial infarction, Eur. Heart J. 33 (2012) 2551–2567.

[7] R.G. McKay, M.A. Pfeffer, R.C. Pasternak, J.E. Markis, P.C. Come, S. Nakao, et al., Left ventricular remodeling after myocardial infarction: a corollary to infarct expansion, Circulation. 74 (1986) 693–702.

[8] J.M. Pfeffer, M. a Pfeffer, P.J. Fletcher, E. Braunwald, Progressive ventricular remodeling in rat with myocardial infarction, Am. J. Physiol. 260 (1991) H1406–14.

[9] P. Gaudron, I. Kugler, K. Hu, W. Bauer, C. Eilles, G. Ertl, Time course of cardiac structural, functional and electrical changes in asymptomatic patients after myocardial infarction: Their inter-relation and prognostic impact, J. Am. Coll. Cardiol. 38 (2001) 33–40.

[10] J.W. Holmes, H. Yamashita, L.K. Waldman, J.W. Covell, Scar remodeling and transmural deformation after infarction in the pig., Circulation. 90 (1994) 411–420.

[11] P.C. Ursell, P.I. Gardner, A. Albala, J.J. Fenoglio, A.L. Wit, Structural and electrophysiological changes in the epicardial border zone of canine myocardial infarcts during infarct healing, Circ. Res. 56 (1985) 436–51.

[12] R.B. Driesen, F.K. Verheyen, P. Dijkstra, F. Thoné, J.P. Cleutjens, M.-H. Lenders, et al., Structural remodelling of cardiomyocytes in the border zone of infarcted rabbit heart, Mol. Cell. Biochem. 302 (2007) 225–232.

[13] B.I. Jugdutt, Ventricular Remodeling After Infarction and the Extracellular Collagen Matrix: When Is Enough Enough?, Circulation. 108 (2003) 1395–1403.

[14] U.S. National Library of Medicine, NHLBI health topics: Heart attack, PubMed Heal. (2014).

[15] T.W. Englemann, Beiträge zur allgemeinen muskel- und nervenphysiologie, Pflugers Arch. Eur. J. Physiol. 3 (1870) 247–326.

[16] T.W. Englemann, Contractilität und doppelbrechung, Pflugers Arch. Eur. J. Physiol. 11 (1875) 432–464.

[17] J.A. McWilliam, Fibrillar contraction of the heart, J. Physiol. 8 (1887) 296–310. PMID: 16991467.

[18] J.P. Revel, M.J. Karnovsky, Hexagonal array of subunits in intercellular junctions of the mouse heart and liver, J. Cell Biol. 33 (1967) C7–C12. PMID: 6036535.

[19] M.M. Dewey, L. Barr, Intercellular connection between smooth muscle cells: The nexus, Science (80-.). 137 (1962) 670–672.

[20] M.M. Dewey, L. Barr, A study of the structure and distribution of the nexus, J. Cell Biol. 23 (1964) 553–85. PMID: 14245436.

[21] P. Kohl, A.G. Kamkin, I.S. Kiseleva, D. Noble, Mechanosensitive fibroblasts in the sino-atrial node region of rat heart: Interaction with cardiomyocytes and possible role, Exp. Physiol. 79 (1994) 943–956. PMID: 7873162.

[22] N.B. Gilula, O.R. Reeves, A. Steinbach, Metabolic coupling, ionic coupling and cell contacts., Nature. 235 (1972) 262–5. PMID: 4551177.

[23] W.H. Evans, P.E.M. Martin, Gap junctions: structure and function (Review), Mol. Membr. Biol. 19 (n.d.) 121–36.

[24] V. Cruciani, S.O. Mikalsen, The vertebrate connexin family, Cell. Mol. Life Sci. 63 (2006) 1125–1140.

[25] G.E. Sosinsky, B.J. Nicholson, Structural organization of gap junction channels., Biochim. Biophys. Acta. 1711 (2005) 99–125.

[26] P. Martin, W. Evans, Incorporation of connexins into plasma membranes and gap junctions, Cardiovasc. Res. 62 (2004) 378–387.

[27] K.I. Swenson, J.R. Jordan, E.C. Beyer, D.L. Paul, Formation of gap junctions by expression of connexins in Xenopus oocyte pairs., Cell. 57 (1989) 145–155.

[28] A.L. Harris, Emerging issues of connexin channels: biophysics fills the gap, Q. Rev. Biophys. 34 (2001) 325–472. PMID: 11838236.

[29] W.R. Loewenstein, Junctional intercellular communication: the cell-to-cell membrane channel, Physiol. Rev. 61 (1981) 829–913. PMID: 6270711.

[30] N.M. Kumar, N.B. Gilula, The gap junction communication channel, Cell. 84 (1996) 381–8.

[31] D.B. Alexander, G.S. Goldberg, Transfer of biologically important molecules between cells through gap junction channels., Curr. Med. Chem. 10 (2003) 2045–58. PMID: 12871102.

[32] G.S. Goldberg, V. Valiunas, P.R. Brink, Selective permeability of gap junction channels., Biochim. Biophys. Acta. 1662 (2004) 96–101.

[33] N.M. Kumar, Molecular biology of the interactions between connexins, Novartis Found. Symp. 219 (1999) 6–16; discussion 16–21, 38–43. PMID: 10207895.

[34] V.M. Unger, N.M. Kumar, N.B. Gilula, M. Yeager, Three-dimensional structure of a recombinant gap junction membrane channel., Science (80-.). 283 (1999) 1176–1180.

[35] J.L. Solan, P.D. Lampe, Connexin43 phosphorylation: structural changes and biological effects, Biochem. J. 419 (2009) 261–72.

[36] J.H.C. Lin, T. Takano, M.L. Cotrina, G. Arcuino, J. Kang, S. Liu, et al., Connexin 43 enhances the adhesivity and mediates the invasion of malignant glioma cells., J. Neurosci. 22 (2002) 4302–4311.

[37] L. a B. Elias, D.D. Wang, A.R. Kriegstein, Gap junction adhesion is necessary for radial migration in the neocortex., Nature. 448 (2007) 901–907.

[38] M.L. Cotrina, J.H.-C. Lin, M. Nedergaard, Adhesive properties of connexin hemichannels, Glia. 56 (2008) 1791–1798.

[39] M. Steinberg, Does differential adhesion govern self-assembly processes in histogenesis? Equilibrium configurations and the emergence of a hierarchy among populations of embryonic cells., J. Exp. Zool. 173 (1970) 395–433.

[40] R. a. Foty, M.S. Steinberg, The differential adhesion hypothesis: a direct evaluation, Dev. Biol. 278 (2005) 255–263.

[41] B. Bao, J. Jiang, T. Yanase, Y. Nishi, J.R. Morgan, Connexon-mediated cell adhesion drives microtissue self-assembly, FASEB J. 25 (2011) 255–264.

[42] J.E. Saffitz, J.G. Laing, K.A. Yamada, Connexin expression and turnover : implications for cardiac excitability, Circ. Res. 86 (2000) 723–8. PMID: 10764404.

[43] D.W. Laird, The life cycle of a connexin: gap junction formation, removal, and degradation., J. Bioenerg. Biomembr. 28 (1996) 311–8. PMID: 8844328.

[44] D.W. Laird, K.L. Puranam, J.P. Revel, Turnover and phosphorylation dynamics of connexin43 gap junction protein in cultured cardiac myocytes., Biochem. J. 273(Pt 1) (1991) 67–72. PMID: 1846532.

[45] B.J. Darrow, J.G. Laing, P.D. Lampe, J.E. Saffitz, E.C. Beyer, Expression of multiple connexins in cultured neonatal rat ventricular myocytes, Circ. Res. 76 (1995) 381–7. PMID: 7859384.

[46] M. a Beardslee, J.G. Laing, E.C. Beyer, J.E. Saffitz, Rapid turnover of connexin43 in the adult rat heart, Circ. Res. 83 (1998) 629–35.

[47] M.M. Falk, N.M. Kumar, N.B. Gilula, Membrane insertion of gap junction connexins: polytopic channel forming membrane proteins., J. Cell Biol. 127 (1994) 343–55. PMID: 7929580.

[48] M.M. Falk, N.B. Gilula, Connexin membrane protein biosynthesis is influenced by polypeptide positioning within the translocon and signal peptidase access, J. Biol. Chem. 273 (1998) 7856–7864.

[49] S.A. John, J.P. Revel, Connexon integrity is maintained by non-covalent bonds: intramolecular disulfide bonds link the extracellular domains in rat connexin-43, Biochem. Biophys. Res. Commun. 178 (1991) 1312–8.

[50] A. el Aoumari, E. Dupont, C. Fromaget, T. Jarry, J.P. Briand, B. Kreitman, et al., Immunolocalization of an extracellular domain of connexin43 in rat heart gap junctions., Eur. J. Cell Biol. 56 (1991) 391–400. PMID: 1724962.

[51] S. Rahman, G. Carlile, W.H. Evans, Assembly of hepatic gap junctions. Topography and distribution of connexin 32 in intracellular and plasma membranes determined using sequence-specific antibodies., J. Biol. Chem. 268 (1993) 1260–5. PMID: 8380409.

[52] D.W. Laird, Life cycle of connexins in health and disease., Biochem. J. 394 (2006) 527–543.

[53] M. Koval, J.E. Harley, E. Hick, T.H. Steinberg, Connexin46 is retained as monomers in a trans-Golgi compartment of osteoblastic cells., J. Cell Biol. 137 (1997) 847–57.

[54] L.S. Musil, D. a Goodenough, Multisubunit assembly of an integral plasma membrane channel protein, gap junction connexin43, occurs after exit from the ER., Cell. 74 (1993) 1065–1077.

[55] A.F. Paulson, P.D. Lampe, R.A. Meyer, E. TenBroek, M.M. Atkinson, T.F. Walseth, et al., Cyclic AMP and LDL trigger a rapid enhancement in gap junction assembly through a stimulation of connexin trafficking., J. Cell Sci. 113 (Pt 1 (2000) 3037–49. PMID: 10934042.

[56] T. Thomas, K. Jordan, J. Simek, Q. Shao, C. Jedeszko, P. Walton, et al., Mechanisms of Cx43 and Cx26 transport to the plasma membrane and gap junction regeneration., J. Cell Sci. 118 (2005) 4451–4462.

[57] J.M. Rhett, J. Jourdan, R.G. Gourdie, Connexin 43 connexon to gap junction transition is regulated by zonula occludens-1, Mol. Biol. Cell. 22 (2011) 1516–28.

[58] a P. Moreno, J.C. Sáez, G.I. Fishman, D.C. Spray, Human connexin43 gap junction channels. Regulation of unitary conductances by phosphorylation., Circ. Res. 74 (1994) 1050–1057.

[59] D.S. He, J.X. Jiang, S.M. Taffet, J.M. Burt, Formation of heteromeric gap junction channels by connexins 40 and 43 in vascular smooth muscle cells., Proc. Natl. Acad. Sci. U. S. A. 96 (1999) 6495–6500.

[60] G.T. Cottrell, J.M. Burt, Functional consequences of heterogeneous gap junction channel formation and its influence in health and disease., Biochim. Biophys. Acta. 1711 (2005) 126–141.

[61] M. Rackauskas, M.M. Kreuzberg, M. Pranevicius, K. Willecke, V.K. Verselis, F.F. Bukauskas, Gating properties of heterotypic gap junction channels formed of connexins 40, 43, and 45., Biophys. J. 92 (2007) 1952–1965.

[62] V. Valiunas, R. Weingart, Electrical properties of gap junction hemichannels identified in transfected HeLa cells., Pflugers Arch. 440 (2000) 366–79. PMID: 10954323.

[63] G.S. Goldberg, P.D. Lampe, B.J. Nicholson, Selective transfer of endogenous metabolites through gap junctions composed of different connexins., Nat. Cell Biol. 1 (1999) 457–459.

[64] T. Desplantez, E. Dupont, N.J. Severs, R. Weingart, Gap junction channels and cardiac impulse propagation, J. Membr. Biol. 218 (2007) 13–28.

[65] S. Elenes, a D. Martinez, M. Delmar, E.C. Beyer, a P. Moreno, Heterotypic docking of Cx43 and Cx45 connexons blocks fast voltage gating of Cx43., Biophys. J. 81 (2001) 1406–1418.

[66] D. a Goodenough, D.L. Paul, Gap junctions., Cold Spring Harb. Perspect. Biol. 1 (2009) a002576.

[67] G. Gaietta, T.J. Deerinck, S.R. Adams, J. Bouwer, O. Tour, D.W. Laird, et al., Multicolor and electron microscopic imaging of connexin trafficking., Science. 296 (2002) 503–7.

[68] M.M. Falk, S.M. Baker, A.M. Gumpert, D. Segretain, R.W. Buckheit, Gap junction turnover is achieved by the internalization of small endocytic double-membrane vesicles, Mol. Biol. Cell. 20 (2009) 3342–52.

[69] N.J. Severs, K.S. Shovel, A.M. Slade, T. Powell, V.W. Twist, C.R. Green, Fate of gap junctions in isolated adult mammalian cardiomyocytes., Circ. Res. 65 (1989) 22–42.

[70] T. Sasaki, P.R. Garant, Fate of annular gap junctions in the papillary cells of the enamel organ in the rat incisor., Cell Tissue Res. 246 (1986) 523–30. PMID: 3024840.

[71] B. Giepmans, Gap junctions and connexin-interacting proteins, Cardiovasc. Res. 62 (2004) 233–245.

[72] J.C. Hervé, N. Bourmeyster, D. Sarrouilhe, H.S. Duffy, Gap junctional complexes: From partners to functions, Prog. Biophys. Mol. Biol. 94 (2007) 29–65.

[73] T. Toyofuku, M. Yabuki, K. Otsu, T. Kuzuya, M. Hori, M. Tada, Direct association of the gap junction protein connexin-43 with ZO-1 in cardiac myocytes, J. Biol. Chem. 273 (1998) 12725–12731.

[74] B.N. Giepmans, W.H. Moolenaar, The gap junction protein connexin43 interacts with the second PDZ domain of the zona occludens-1 protein., Curr. Biol. 8 (1998) 931–4. PMID: 9707407.

[75] T. Toyofuku, Y. Akamatsu, H. Zhang, T. Kuzuya, M. Tada, M. Hori, c-Src regulates the interaction between connexin-43 and ZO-1 in cardiac myocytes, J. Biol. Chem. 276 (2001) 1780–1788.

[76] A.W. Hunter, J. Jourdan, R.G. Gourdie, Fusion of GFP to the carboxyl terminus of connexin43 increases gap junction size in HeLa cells., Cell Commun. Adhes. 10 (2003) 211–4.

[77] A.W. Hunter, R.J. Barker, C. Zhu, R.G. Gourdie, Zonula occludens-1 alters connexin43 gap junction size and organization by influencing channel accretion., Mol. Biol. Cell. 16 (2005) 5686–98.

[78] J.G. Laing, B.C. Chou, T.H. Steinberg, ZO-1 alters the plasma membrane localization and function of Cx43 in osteoblastic cells., J. Cell Sci. 118 (2005) 2167–76.

[79] J.G. Laing, J.E. Saffitz, T.H. Steinberg, K.A. Yamada, Diminished zonula occludens-1 expression in the failing human heart, Cardiovasc. Pathol. 16 (2007) 159–164.

[80] R.J. Barker, R.L. Price, R.G. Gourdie, Increased association of ZO-1 with connexin43 during remodeling of cardiac gap junctions., Circ. Res. 90 (2002) 317–24. PMID: 11861421.

[81] D. Segretain, C. Fiorini, X. Decrouy, N. Defamie, J.R. Prat, G. Pointis, A proposed role for ZO-1 in targeting connexin 43 gap junctions to the endocytic pathway., Biochimie. 86 (n.d.) 241–4.

[82] Y. Jinn, N. Inase, Connexin 43, E-cadherin, beta-catenin and ZO-1 expression, and aberrant methylation of the connexin 43 gene in NSCLC., Anticancer Res. 30 (2010) 2271–8. PMID: 20651379.

[83] A.F. Bruce, S. Rothery, E. Dupont, N.J. Severs, Gap junction remodelling in human heart failure is associated with increased interaction of connexin43 with ZO-1., Cardiovasc. Res. 77 (2008) 757–65.

[84] B.N. Giepmans, I. Verlaan, W.H. Moolenaar, Connexin-43 interactions with ZO-1 and alpha- and beta-tubulin., Cell Commun. Adhes. 8 (2001) 219–23. PMID: 12064592.

[85] A.W. Hunter, R.G. Gourdie, The Second PDZ Domain of Zonula Occludens-1 Is Dispensable for Targeting to Connexin43 Gap Junctions, Cell Commun. Adhes. 15 (2008) 55–63.

[86] C. Zhu, R.J. Barker, A.W. Hunter, Y. Zhang, J. Jourdan, R.G. Gourdie, Quantitative analysis of ZO-1 colocalization with Cx43 gap junction plaques in cultures of rat neonatal cardiomyocytes, Microsc. Microanal. 11 (2005) 244–248.

[87] U. Lauf, B.N.G. Giepmans, P. Lopez, S. Braconnot, S.-C. Chen, M.M. Falk, Dynamic trafficking and delivery of connexons to the plasma membrane and accretion to gap junctions in living cells., Proc. Natl. Acad. Sci. U. S. A. 99 (2002) 10446–51.

[88] D.W. Laird, Connexin phosphorylation as a regulatory event linked to gap junction internalization and degradation., Biochim. Biophys. Acta. 1711 (2005) 172–82.

[89] J.L. Solan, P.D. Lampe, Key connexin 43 phosphorylation events regulate the gap junction life cycle., J. Membr. Biol. 217 (2007) 35–41.

[90] L.S. Musil, D.A. Goodenough, Biochemical-Analysis of Connexin43 Intracellular-Transport, Phosphorylation, and Assembly Into Gap Junctional Plaques, J. Cell Biol. 115 (1991) 1357–1374.

[91] P.D. Lampe, A.F. Lau, The effects of connexin phosphorylation on gap junctional communication, Int. J. Biochem. Cell Biol. 36 (2004) 1171–1186.

[92] P.D. Lampe, E.M. TenBroek, J.M. Burt, W.E. Kurata, R.G. Johnson, a F. Lau, Phosphorylation of connexin43 on serine368 by protein kinase C regulates gap junctional communication, J. Cell Biol. 149 (2000) 1503–1512.

[93] T.J. King, P.D. Lampe, Temporal regulation of connexin phosphorylation in embryonic and adult tissues., Biochim. Biophys. Acta. 1719 (2005) 24–35.

[94] J.F. Ek-Vitorin, T.J. King, N.S. Heyman, P.D. Lampe, J.M. Burt, Selectivity of connexin 43 channels is regulated through protein kinase C-dependent phosphorylation., Circ. Res. 98 (2006) 1498–505.

[95] J.L. Solan, M.D. Fry, E.M. TenBroek, P.D. Lampe, Connexin43 phosphorylation at S368 is acute during S and G2/M and in response to protein kinase C activation., J. Cell Sci. 116 (2003) 2203–2211.

[96] D.S. Crow, E.C. Beyer, D.L. Paul, S.S. Kobe, a F. Lau, Phosphorylation of connexin43 gap junction protein in uninfected and Rous sarcoma virus-transformed mammalian fibroblasts., Mol. Cell. Biol. 10 (1990) 1754–1763.

[97] D.W. Laird, M. Castillo, L. Kasprzak, Gap junction turnover, intracellular trafficking, and phosphorylation of connexin43 in brefeldin A-treated rat mammary tumor cells, J. Cell Biol. 131 (1995) 1193–1203.

[98] V.M. Berthoud, M.L. Ledbetter, E.L. Hertzberg, J.C. Sáez, Connexin43 in MDCK cells: regulation by a tumor-promoting phorbol ester and Ca2+., Eur. J. Cell Biol. 57 (1992) 40–50. PMID: 1322299.

[99] J.L. Brissette, N.M. Kumar, N.B. Gilula, G.P. Dotto, The tumor promoter 12-O-tetradecanoylphorbol-13-acetate and the ras oncogene modulate expression and phosphorylation of gap junction proteins, Mol Cell Biol. 11 (1991) 5364–5371.

[100] P.D. Lampe, Analyzing phorbol ester effects on gap junctional communication: a dramatic inhibition of assembly, J. Cell Biol. 127 (1994) 1895–1905.

[101] J.K. Reynhout, P.D. Lampe, R.G. Johnson, An activator of protein kinase C inhibits gap junction communication between cultured bovine lens cells., Exp. Cell Res. 198 (1992) 337–42. PMID: 1309506.

[102] B.R. Kwak, T.A. van Veen, L.J. Analbers, H.J. Jongsma, TPA increases conductance but decreases permeability in neonatal rat cardiomyocyte gap junction channels., Exp. Cell Res. 220 (1995) 456–63.

[103] D.C. Spray, J.M. Burt, Structure-activity relations of the cardiac gap junction channel., Am. J. Physiol. 258 (1990) C195–205. PMID: 1689543.

[104] M.P. O'Quinn, J. a. Palatinus, B.S. Harris, K.W. Hewett, R.G. Gourdie, A peptide mimetic of the connexin43 carboxyl terminus reduces gap junction remodeling and induced arrhythmia following ventricular injury, Circ. Res. 108 (2011) 704–715.

[105] J. a. Palatinus, J.M. Rhett, R.G. Gourdie, Enhanced PKCε mediated phosphorylation of connexin43 at serine 368 by a carboxyl-terminal mimetic peptide is dependent on injury, Channels. 5 (2011) 236–240.

[106] A. Nag, Study of non-muscle cells of the adult mammalian heart: a fine structural analysis and distribution, Cytobios. 28 (1980) 41–61. PMID: 7428441.

[107] H.W. Vliegen, a van der Laarse, C.J. Cornelisse, F. Eulderink, Myocardial changes in pressure overload-induced left ventricular hypertrophy. A study on tissue composition, polyploidization and multinucleation., Eur. Heart J. 12 (1991) 488–494. PMID: 1829680.

[108] C. Adler, W. Ringlage, N. Böhm, DNA content and cell number in heart and liver of children. Comparable biochemical, cytophotometric and histological investigations (author's transl), Pathol Res Pr. 172 (1981) 25–41.

[109] I. Banerjee, J.W. Fuseler, R.L. Price, T.K. Borg, T.A. Baudino, Determination of cell types and numbers during cardiac development in the neonatal and adult rat and mouse, Am. J. Physiol. - Hear. Circ. Physiol. 293 (2007) 1883–1891.

[110] I. LeGrice, A. Pope, B. Smaill, The architecture of the heart: myocyte organization and the cardiac extracellular matrix, in: F.J. Villarreal (Ed.), Interstitial Fibros. Hear. Fail. V 253 Dev. Cardiovasc. Med., Springer New York, 2005: pp. 3–21.

[111] P.W. Hales, J.E. Schneider, R. a B. Burton, B.J. Wright, C. Bollensdorff, P. Kohl, Histo-anatomical structure of the living isolated rat heart in two contraction states assessed by diffusion tensor MRI, Prog. Biophys. Mol. Biol. 110 (2012) 319–330.

[112] N.J. Severs, E. Dupont, S.R. Coppen, D. Halliday, E. Inett, D. Baylis, et al., Remodelling of gap junctions and connexin expression in heart disease, Biochim. Biophys. Acta - Biomembr. 1662 (2004) 138–148.

[113] D.B. Gros, H.J. Jongsma, Connexins in mammalian heart function, Bioessays. 18 (1996) 719–730.

[114] C. Vozzi, E. Dupont, S.R. Coppen, H.I. Yeh, N.J. Severs, Chamber-related differences in connexin expression in the human heart., J. Mol. Cell. Cardiol. 31 (1999) 991–1003.

[115] R.G. Gourdie, C.R. Green, N.J. Severs, R.P. Thompson, Immunolabelling patterns of gap junction connexins in the developing and mature rat heart., Anat. Embryol. 185 (1992) 363–78. PMID: 1319120.

[116] R.G. Gourdie, N.J. Severs, C.R. Green, S. Rothery, P. Germroth, R.P. Thompson, The spatial distribution and relative abundance of gap-junctional connexin40 and connexin43 correlate to functional properties of components of the cardiac atrioventricular conduction system, J. Cell Sci. 105 (1993) 985–991. PMID: 8227219.

[117] P. Kohl, P. Camelliti, Fibroblast-myocyte connections in the heart, Hear. Rhythm. 9 (2012) 461–464.

[118] N. Sperelakis, An electric field mechanism for transmission of excitation between myocardial cells., Circ. Res. 91 (2002) 985–7. PMID: 12456483.

[119] J.M. Rhett, E.L. Ongstad, J. Jourdan, R.G. Gourdie, Cx43 associates with Na(v)1.5 in the cardiomyocyte perinexus., J. Membr. Biol. 245 (2012) 411–22.

[120] R. Veeraraghavan, J. Lin, G.S. Hoeker, J.P. Keener, R.G. Gourdie, S. Poelzing, Sodium channels in the Cx43 gap junction perinexus may constitute a cardiac ephapse: an experimental and modeling study, Pflügers Arch. - Eur. J. Physiol. (2015) 2093–2105.

[121] J. Lin, J.P. Keener, Ephaptic coupling in cardiac myocytes, IEEE Trans. Biomed. Eng. 60 (2013) 576–582.

[122] A. De Maziere, A. Vanginneken, R. Wilders, H. Jongsma, L. Bouman, Spatial and functional-relationship between myocytes and fibroblasts in the rabbit sinoatrial node, J. Mol. Cell. Cardiol. 24 (1992) 567–578.

[123] T. Mikawa, R.G. Gourdie, Pericardial mesoderm generates a population of coronary smooth muscle cells migrating into the heart along with ingrowth of the epicardial organ, Dev. Biol. 174 (1996) 221–232.

[124] L.M. Eisenberg, R.R. Markwald, Molecular regulation of atrioventricular valvuloseptal morphogenesis, Circ. Res. 77 (1995) 1–6.

[125] A.C. Gittenberger-de Groot, M.P.F.M. Vrancken Peeters, M.M.T. Mentink, R.G. Gourdie, R.E. Poelmann, Epicardium-derived cells contribute a novel population to the myocardial wall and the atrioventricular cushions., Circ. Res. 82 (1998) 1043–1052.

[126] F.J. De Lange, A.F.M. Moorman, R.H. Anderson, J. Männer, A.T. Soufan, C. De Gier-De Vries, et al., Lineage and morphogenetic analysis of the cardiac valves, Circ. Res. 95 (2004) 645–654.

[127] E.J. Armstrong, J. Bischoff, Heart valve development: endothelial cell signaling and differentiation, Circ. Res. 95 (2004) 459–470.

[128] A.K. Ghosh, V. Nagpal, J.W. Covington, M.A. Michaels, D.E. Vaughan, Molecular basis of cardiac endothelial-to-mesenchymal transition (EndMT): Differential expression of microRNAs during EndMT, Cell. Signal. 24 (2012) 1031–1036.

[129] E.C. Goldsmith, A. Hoffman, M.O. Morales, J.D. Potts, R.L. Price, A. McFadden, et al., Organization of fibroblasts in the heart, Dev. Dyn. 230 (2004) 787–794.

[130] M.O. Morales, R.L. Price, E.C. Goldsmith, Expression of Discoidin Domain Receptor 2 (DDR2) in the developing heart, Microsc. Microanal. 11 (2005) 260–267.

[131] J. Endo, M. Sano, J. Fujita, K. Hayashida, S. Yuasa, N. Aoyama, et al., Bone marrow derived cells are involved in the pathogenesis of cardiac hypertrophy in response to pressure overload, Circulation. 116 (2007) 1176–1184.

[132] A. Grigore, D. Arsene, F. Filipoiu, F. Cionca, S. Enache, M. Ceauşu, et al., Cellular immunophenotypes in human embryonic, fetal and adult heart, Rom. J. Morphol. Embryol. 53 (2012) 299–311. PMID: 22732799.

[133] R.M. Evans, Vimentin: The conundrum of the intermediate filament gene family, BioEssays. 20 (1998) 79–86.

[134] A. Acharya, S.T. Baek, G. Huang, B. Eskiocak, S. Goetsch, C.Y. Sung, et al., The bHLH transcription factor Tcf21 is required for lineage-specific EMT of cardiac fibroblast progenitors, Development. 139 (2012) 2139–2149.

[135] P. Tandon, Y. V Miteva, L.M. Kuchenbrod, I.M. Cristea, F.L. Conlon, Tcf21 regulates the specification and maturation of proepicardial cells, Development. 140 (2013) 2409–21.

[136] P. Kong, P. Christia, A. Saxena, Y. Su, N.G. Frangogiannis, Lack of specificity of fibroblast-specific protein 1 in cardiac remodeling and fibrosis., Am. J. Physiol. Heart Circ. Physiol. 305 (2013) H1363–72.

[137] P. Garin-Chesa, L.J. Old, W.J. Rettig, Cell surface glycoprotein of reactive stromal fibroblasts as a potential antibody target in human epithelial cancers, Proc. Natl. Acad. Sci. U. S. A. 87 (1990) 7235–7239.

[138] J.E. Park, M.C. Lenter, R.N. Zimmerman, P. Garin-Chesa, L.J. Old, W.J. Rettig, Fibroblast Activation Protein, a dual specificity serine protease expressed in reactive human tumor stromal fibroblasts, 274 (1999) 36505–36512.

[139] P.S. Acharya, A. Zukas, V. Chandan, A. Katzenstein, E. Puré, Fibroblast activation protein: a serine protease expressed at the remodeling interface in idiopathic pulmonary fibrosis, Hum. Pathol. 37 (2006) 352–360.

[140] E.C. Goldsmith, A.D. Bradshaw, M.R. Zile, F.G. Spinale, Myocardial fibroblast-matrix interactions and potential therapeutic targets, J. Mol. Cell. Cardiol. 29 (2014) 92–99.

[141] T. Moore-Morris, N. Guimarães-Camboa, I. Banerjee, A.C. Zambon, T. Kisseleva, A. Velayoudon, et al., Resident fibroblast lineages mediate pressure overload-induced cardiac fibrosis, J. Clin. Invest. 124 (2014) 2921–34.

[142] R. Kakkar, R.T. Lee, Intramyocardial fibroblast-myocyte communication, Circ. Res. 106 (2010) 47–57.

[143] F.G. Ottaviano, K.O. Yee, Communication signals between cardiac fibroblasts and cardiac myocytes, J. Cardiovasc. Pharmacol. 57 (2011) 513–521.

[144] Y. Tian, E.E. Morrisey, Importance of myocyte-nonmyocyte interactions in cardiac development and disease, Circ. Res. 110 (2012) 1023–1034.

[145] A. Kamkin, I. Kiseleva, G. Isenberg, Activation and inactivation of a non-selective cation conductance by local mechanical deformation of acutely isolated cardiac fibroblasts, Cardiovasc. Res. 57 (2003) 793–803.

[146] I. Kiseleva, A. Kamkin, P. Kohl, M.J. Lab, Calcium and mechanically induced potentials in fibroblasts of rat atrium, Cardiovasc. Res. 32 (1996) 98–111.

[147] M. Miragoli, G. Gaudesius, S. Rohr, Electrotonic modulation of cardiac impulse conduction by myofibroblasts, Circ. Res. 98 (2006) 801–810.

[148] M.M. Maleckar, J.L. Greenstein, W.R. Giles, N. a. Trayanova, Electrotonic coupling between human atrial myocytes and fibroblasts alters myocyte excitability and repolarization, Biophys. J. 97 (2009) 2179–2190.

[149] G. Gaudesius, M. Miragoli, S.P. Thomas, S. Rohr, Coupling of cardiac electrical activity over extended distances by fibroblasts of cardiac origin, Circ. Res. 93 (2003) 421–428.

[150] Y. Zhang, E.M. Kanter, J.G. Laing, C. Aprhys, D.C. Johns, E. Kardami, et al., Connexin43 expression levels influence intercellular coupling and cell proliferation of native murine cardiac fibroblasts, Cell Commun. Adhes. 15 (2008) 289–303.

[151] C. Louault, N. Benamer, J.F. Faivre, D. Potreau, J. Bescond, Implication of connexins 40 and 43 in functional coupling between mouse cardiac fibroblasts in primary culture, Biochim. Biophys. Acta - Biomembr. 1778 (2008) 2097–2104.

[152] K. Goshima, Formation of nexuses and electrotonic transmission between myocardial and FL cells in monolayer culture, Exp. Cell Res. 63 (1970) 124–130.

[153] N.G. Frangogiannis, C.W. Smith, M.L. Entman, The inflammatory response in myocardial infarction, Cardiovasc. Res. 53 (2002) 31–47.

[154] G. Ertl, S. Frantz, Healing after myocardial infarction., Cardiovasc. Res. 66 (2005) 22–32.

[155] Y. Asazuma-Nakamura, P. Dai, Y. Harada, Y. Jiang, K. Hamaoka, T. Takamatsu, Cx43 contributes to TGF-β signaling to regulate differentiation of cardiac fibroblasts into myofibroblasts, Exp. Cell Res. 315 (2009) 1190–1199.

[156] A. Desmoulière, A. Geinoz, F. Gabbiani, G. Gabbiani, Transforming growth factor-beta 1 induces alpha-smooth muscle actin expression in granulation tissue myofibroblasts and in quiescent and growing cultured fibroblasts., J. Cell Biol. 122 (1993) 103–11.

[157] S. Rosenkranz, TGF-beta1 and angiotensin networking in cardiac remodeling., Cardiovasc. Res. 63 (2004) 423–32.

[158] J.J. Tomasek, J. McRae, G.K. Owens, C.J. Haaksma, Regulation of alpha-smooth muscle actin expression in granulation tissue myofibroblasts is dependent on the intronic CArG element and the transforming growth factor-beta1 control element., Am. J. Pathol. 166 (2005) 1343–51.

[159] W. Chen, N.G. Frangogiannis, Fibroblasts in post-infarction inflammation and cardiac repair, Biochim. Biophys. Acta - Mol. Cell Res. 1833 (2013) 945–953.

[160] S. Saba, M. a. Mathier, H. Mehdi, T. Liu, B.R. Choi, B. London, et al., Dual-dye optical mapping after myocardial infarction: does the site of ventricular stimulation alter the properties of electrical propagation?, J. Cardiovasc. Electrophysiol. 19 (2008) 197–202.

[161] S.R. Ali, S. Ranjbarvaziri, M. Talkhabi, P. Zhao, a. Subat, a. Hojjat, et al., Developmental Heterogeneity of Cardiac Fibroblasts Does Not Predict Pathological Proliferation and Activation, Circ. Res. 115 (2014) 625–635.

[162] A. Ruiz-Villalba, A.M. Simón, C. Pogontke, M.I. Castillo, G. Abizanda, B. Pelacho, et al., Interacting resident epicardium-derived fibroblasts and recruited bone marrow cells form myocardial infarction scar, J. Am. Coll. Cardiol. 65 (2015) 2057–2066.

[163] H. Möllmann, H.M. Nef, S. Kostin, C. von Kalle, I. Pilz, M. Weber, et al., Bone marrow-derived cells contribute to infarct remodelling, Cardiovasc. Res. 71 (2006) 661–671.

[164] R.P. Visconti, R.R. Markwald, Recruitment of new cells into the postnatal heart: potential modification of phenotype by periostin, Ann. N. Y. Acad. Sci. 1080 (2006) 19–33.

[165] M. van Amerongen, G. Bou-Gharis, E. Popa, J. van Ark, A. Petersen, G. van Dam, et al., Bone marrow-derived myofibroblasts contribute functionally to scar formation after myocardial infarction, J. Pathol. 214 (2008) 377–386.

[166] C. Vasquez, P. Mohandas, K.L. Louie, N. Benamer, A.C. Bapat, G.E. Morley, 12 , 100, (n.d.) 1–5.

[167] Y. Zhang, E.M. Kanter, K.A. Yamada, Remodeling of cardiac fibroblasts following myocardial infarction results in increased gap junction intercellular communication, Cardiovasc. Pathol. 19 (2010) e233–e240.

[168] N. El-Sherif, R. Mehra, W.B. Gough, R.H. Zeiler, Ventricular activation patterns of spontaneous and induced ventricular rhythms in canine one-day-old myocardial infarction. Evidence for focal and reentrant mechanisms, Circ. Res. 51 (1982) 152–166.

[169] C.R. Green, N.J. Severs, Robert Feulgen Prize Lecture. Distribution and role of gap junctions in normal myocardium and human ischaemic heart disease., Histochemistry. 99 (1993) 105–20. PMID: 8478212.

[170] J.H. Smith, C.R. Green, N.S. Peters, S. Rothery, N.J. Severs, Altered patterns of gap junction distribution in ischemic heart disease. An immunohistochemical study of human myocardium using laser scanning confocal microscopy., Am. J. Pathol. 139 (1991) 801–821. PMID: 1656760.

[171] O. Bernus, C.W. Zemlin, R.M. Zaritsky, S.F. Mironov, A.M. Pertsov, Alternating conduction in the ischaemic border zone as precursor of reentrant arrhythmias: A simulation study, Europace. 7 (2005).

[172] C. Vasquez, N. Benamer, G.E. Morley, The cardiac fibroblast: functional and electrophysiological considerations in healthy and diseased hearts, J Cardiovasc Pharmacol. 57 (2011) 380–388.

[173] P. Camelliti, G.P. Devlin, K.G. Matthews, P. Kohl, C.R. Green, Spatially and temporally distinct expression of fibroblast connexins after sheep ventricular infarction, Cardiovasc. Res. 62 (2004) 415–425.

[174] Y. Xie, A. Garfinkel, P. Camelliti, P. Kohl, J.N. Weiss, Z. Qu, Effects of fibroblast-myocyte coupling on cardiac conduction and vulnerability to reentry: A computational study, Hear. Rhythm. 6 (2009) 1641–1649.

[175] J.H.-C. Lin, H. Weigel, M.L. Cotrina, S. Liu, E. Bueno, A.J. Hansen, et al., Gap-junction-mediated propagation and amplification of cell injury, Nat. Neurosci. 1 (1998) 494–500.

[176] M. Chanson, J.-P. Derouette, I. Roth, B. Foglia, I. Scerri, T. Dudez, et al., Gap junctional communication in tissue inflammation and repair., Biochim. Biophys. Acta. 1711 (2005) 197–207.

[177] A. De Maio, V.L. Vega, J.E. Contreras, Gap junctions, homeostasis, and injury, J. Cell. Physiol. 191 (2002) 269–282.

[178] R. Mori, K.T. Power, C.M. Wang, P. Martin, D.L. Becker, Acute downregulation of connexin43 at wound sites leads to a reduced inflammatory response, enhanced keratinocyte proliferation and wound fibroblast migration, J. Cell Sci. 119 (2006) 5193–5203.

[179] G.S. Ghatnekar, M.P. O'Quinn, L.J. Jourdan, A.A. Gurjarpadhye, R.L. Draughn, R.G. Gourdie, Connexin43 carboxyl-terminal peptides reduce scar progenitor and promote regenerative healing following skin wounding, Regen. Med. 4 (2009) 205–223.

[180] C.L. Grek, G.M. Prasad, V. Viswanathan, D.G. Armstrong, R.G. Gourdie, G.S. Ghatnekar, Topical administration of a connexin43-based peptide augments healing of chronic neuropathic diabetic foot ulcers: A multicenter, randomized trial., Wound Repair Regen. 23 (2015) 203–12.

[181] G. Ghatnekar, C. Grek, D.G. Armstrong, S.C. Desai, R. Gourdie, The Effect of a Connexin43-based peptide on the Healing of Chronic Venous Leg Ulcers: A Multicenter, Randomized Trial., J. Invest. Dermatol. 135 (2014) 289–298.

[182] J.A. Palatinus, R.G. Gourdie, Diabetes Increases Cryoinjury Size with Associated Effects on Cx43 Gap Junction Function and Phosphorylation in the Mouse Heart, J. Diabetes Res. (2015).

[183] R.S. Kieval, J.F. Spear, E.N. Moore, Gap junctional conductance in ventricular myocyte pairs isolated from postischemic rabbit myocardium., Circ. Res. 71 (1992) 127–36. PMID: 1606660.

[184] N.S. Peters, C.R. Green, P.A. Poole-Wilson, N.J. Severs, Reduced content of connexin43 gap junctions in ventricular myocardium from hypertrophied and ischemic human hearts., Circulation. 88 (1993) 864–75. PMID: 8394786.

[185] R.A. Luke, J.E. Saffitz, Remodeling of ventricular conduction pathways in healed canine infarct border zones., J. Clin. Invest. 87 (1991) 1594–602.

[186] M.A. Beardslee, D.L. Lerner, P.N. Tadros, J.G. Laing, E.C. Beyer, K.A. Yamada, et al., Dephosphorylation and intracellular redistribution of ventricular connexin43 during electrical uncoupling induced by ischemia., Circ. Res. 87 (2000) 656–62. PMID: 11029400.

[187] D.L. Lerner, K.A. Yamada, R.B. Schuessler, J.E. Saffitz, Accelerated onset and increased incidence of ventricular arrhythmias induced by ischemia in Cx43-deficient mice., Circulation. 101 (2000) 547–52. PMID: 10662753.

[188] W. Srisakuldee, M.M. Jeyaraman, B.E. Nickel, S. Tanguy, Z.-S. Jiang, E. Kardami, Phosphorylation of connexin-43 at serine 262 promotes a cardiac injury-resistant state, Cardiovasc. Res. 83 (2009) 672–681.

[189] M. Salto-Tellez, S. Yung Lim, R.M. El Oakley, T.P.L. Tang, Z.A.M. ALmsherqi, S.-K. Lim, Myocardial infarction in the C57BL/6J mouse, Cardiovasc. Pathol. 13 (2004) 91–97.

[190] E.J. van den Bos, B.M.E. Mees, M.C. de Waard, R. de Crom, D.J. Duncker, A novel model of cryoinjury-induced myocardial infarction in the mouse: A comparison with coronary artery ligation, Am. J. Physiol. - Hear. Circ. Physiol. 289 (2005) H1291–300.

[191] J.A. Jensen, J.C. Kosek, T.K. Hunt, W.H. Goodson, D.C. Miller, Cardiac cryolesions as an experimental model of myocardial wound healing., Ann. Surg. 206 (1987) 798–803. PMID: 3689016.

[192] M.B. Myers, G. Cherry, Ventricular fibrillation area thresholds in the dog and pig. Determined by a new experimental model for the production of myocardial infarction, J. Thorac. Cardiovasc. Surg. 59 (1970) 401–12. PMID: 5415085.

[193] M.M. Swindle, A. Makin, A.J. Herron, F.J. Clubb, K.S. Frazier, Swine as Models in Biomedical Research and Toxicology Testing, Vet. Pathol. 49 (2012) 344–356.

[194] R.L. Korn, J. V Pollock, J.A. Spath, Effects of intracoronary verapamil administration in a sheep model of acute myocardial ischemia and reperfusion, Circ. Res. 62 (1988) 1138–46. PMID: 3383362.

[195] E. Tzatzalos, O.J. Abilez, P. Shukla, J.C. Wu, Engineered heart tissues and induced pluripotent stem cells: Macro- and microstructures for disease modeling, drug screening, and translational studies, Adv. Drug Deliv. Rev. (2015).

[196] A. Mathur, Z. Ma, P. Loskill, S. Jeeawoody, K.E. Healy, In vitro cardiac tissue models: Current status and future prospects, Adv. Drug Deliv. Rev. (2015).

[197] N. Sun, M. Yazawa, J. Liu, L. Han, V. Sanchez-Freire, O.J. Abilez, et al., Patient-specific induced pluripotent stem cells as a model for familial dilated cardiomyopathy, Sci. Transl. Med. 4 (2012) 130ra47.

[198] F. Lan, A.S. Lee, P. Liang, V. Sanchez-Freire, P.K. Nguyen, L. Wang, et al., Abnormal Calcium Handling Properties Underlie Familial Hypertrophic Cardiomyopathy Pathology in Patient-Specific Induced Pluripotent Stem Cells, Cell Stem Cell. 12 (2013) 101–113.

[199] I.C. Turnbull, I. Karakikes, G.W. Serrao, P. Backeris, J.-J. Lee, C. Xie, et al., Advancing functional engineered cardiac tissues toward a preclinical model of human myocardium, FASEB J. 28 (2014) 644–654.

[200] A. Mathur, P. Loskill, K. Shao, N. Huebsch, S. Hong, S.G. Marcus, et al., Human iPSC-based Cardiac Microphysiological System For Drug Screening Applications, Sci. Rep. 5 (2015) 8883.

[201] T. Eschenhagen, C. Fink, U. Remmers, H. Scholz, J. Wattchow, J. Weil, et al., Three-dimensional reconstitution of embryonic cardiomyocytes in a collagen matrix: a new heart muscle model system., FASEB J. 11 (1997) 683–694. PMID: 9240969.

[202] Y. Sawa, S. Miyagawa, T. Sakaguchi, T. Fujita, A. Matsuyama, A. Saito, et al., Tissue engineered myoblast sheets improved cardiac function sufficiently to discontinue LVAS in a patient with DCM: Report of a case, Surg. Today. 42 (2012) 181–184.

[203] T. Eschenhagen, Engineering Myocardial Tissue, Circ. Res. 97 (2005) 1220–1231.

[204] M.N. Hirt, A. Hansen, T. Eschenhagen, Cardiac Tissue Engineering: State of the Art, Circ. Res. 114 (2014) 354–367.

[205] A.A. Moscona, Tissues from dissociated cells, Sci. Am. 200 (1959) 132–4 passim. PMID: 13646649.

[206] L. Terracio, B. Miller, T.K. Borg, Effects of cyclic mechanical stimulation of the cellular components of the heart: in vitro, In Vitro Cell. Dev. Biol. 24 (1988) 53–8. PMID: 3276657.

[207] M. Radisic, H. Park, H. Shing, T. Consi, F.J. Schoen, R. Langer, et al., Functional assembly of engineered myocardium by electrical stimulation of cardiac myocytes cultured on scaffolds., Proc. Natl. Acad. Sci. U. S. A. 101 (2004) 18129–18134.

[208] J. Leor, S. Aboulafia-Etzion, A. Dar, L. Shapiro, I.M. Barbash, A. Battler, et al., Bioengineered cardiac grafts: A new approach to repair the infarcted myocardium?, Circulation. 102 (2000) III56–61. PMID: 11082363.

[209] R.L. Carrier, M. Papadaki, M. Rupnick, F.J. Schoen, N. Bursac, R. Langer, et al., Cardiac tissue engineering: cell seeding, cultivation parameters, and tissue construct characterization, Biotechnol. Bioeng. 64 (1999) 580–9. PMID: 10404238.

[210] A. Lesman, M. Habib, O. Caspi, A. Gepstein, G. Arbel, S. Levenberg, et al., Transplantation of a tissue-engineered human vascularized cardiac muscle., Tissue Eng. Part A. 16 (2010) 115–25.

[211] H.C. Ott, T.S. Matthiesen, S.-K. Goh, L.D. Black, S.M. Kren, T.I. Netoff, et al., Perfusion-decellularized matrix: using nature's platform to engineer a bioartificial heart, Nat. Med. 14 (2008) 213–221.

[212] T. Shimizu, M. Yamato, Y. Isoi, T. Akutsu, T. Setomaru, K. Abe, et al., Fabrication of Pulsatile Cardiac Tissue Grafts Using a Novel 3-Dimensional Cell Sheet Manipulation Technique and Temperature-Responsive Cell Culture Surfaces, Circ. Res. 90 (2002) 40e–48.

[213] J.S. WENDEL, L. YE, R. TAO, J. ZHANG, J. ZHANG, T.J. KAMP, et al., Functional Effects of a Tissue-Engineered Cardiac Patch From Human Induced Pluripotent Stem Cell-Derived Cardiomyocytes in a Rat Infarct Model, (2014) 1–10.

[214] H. Kubo, T. Shioyama, M. Oura, a. Suzuki, T. Ogawa, H. Makino, et al., Development of automated 3-dimensional tissue fabrication system Tissue factory - Automated cell isolation from tissue for regenerative medicine, Proc. Annu. Int. Conf. IEEE Eng. Med. Biol. Soc. EMBS. (2013) 358–361.

[215] H. Naito, I. Melnychenko, M. Didié, K. Schneiderbanger, P. Schubert, S. Rosenkranz, et al., Optimizing engineered heart tissue for therapeutic applications as surrogate heart muscle, Circulation. 114 (2006) 72–79.

[216] M. Radisic, A. Marsano, R. Maidhof, Y. Wang, G. Vunjak-Novakovic, Cardiac tissue engineering using perfusion bioreactor systems., Nat. Protoc. 3 (2008) 719–738.

[217] T. Kofidis, J.L. de Bruin, G. Hoyt, D.R. Lebl, M. Tanaka, T. Yamane, et al., Injectable bioartificial myocardial tissue for large-scale intramural cell transfer and functional recovery of injured heart muscle., J. Thorac. Cardiovasc. Surg. 128 (2004) 571–8.

[218] L. Cohen, L. Deckelbaum, J. Isaacsohn, F.A. Lee, C.A. McPherson, M. Moser, et al., Cardiovascular Drugs, in: n.d.: pp. 293–304.

[219] The cardiovascular market outlook to 2016: Competitive landscape, global market analysis, key trends, and pipeline analysis, 2011.

[220] B.H. Munos, W.W. Chin, A Call for Sharing : Adapting Pharmaceutical Research to New Realities, Sciencemag. 1 (2009) 1–4.

[221] S.M. Paul, D.S. Mytelka, C.T. Dunwiddie, C.C. Persinger, B.H. Munos, S.R. Lindborg, et al., How to improve R&D productivity: the pharmaceutical industry's grand challenge., Nat. Rev. Drug Discov. 9 (2010) 203–214.

[222] M. Herper, The cost of creating a new drug now $5 billion, pushing big pharma to change, Forbes.com. (2013).

[223] S. Kaese, S. Verheule, Cardiac electrophysiology in mice: a matter of size., Front. Physiol. 3 (2012) 345.

[224] C.L. Lawrence, C.E. Pollard, T.G. Hammond, J.-P. Valentin, *In vitro* models of proarrhythmia, Br. J. Pharmacol. 154 (2008) 1516–1522.

[225] L. Hutchinson, R. Kirk, High drug attrition rates--where are we going wrong?, Nat. Rev. Clin. Oncol. 8 (2011) 189–190.

[226] N. Ferri, P. Siegl, A. Corsini, J. Herrmann, A. Lerman, R. Benghozi, Drug attrition during pre-clinical and clinical development: Understanding and managing drug-induced cardiotoxicity, Pharmacol. Ther. 138 (2013) 470–484.

[227] M. Brandenburger, J. Wenzel, R. Bogdan, D. Richardt, F. Nguemo, M. Reppel, et al., Organotypic slice culture from human adult ventricular myocardium, Cardiovasc. Res. 93 (2012) 50–59.

[228] FDA, Drugs@FDA: FDA Approved Drug Products, (2015).

[229] K. Rodgers, A. Papinska, N. Mordwinkin, Regulatory aspects of small molecule drugs for heart regeneration, Adv. Drug Deliv. Rev. (2015) 1–8.

[230] E.L. Ongstad, M.P. O'Quinn, G.S. Ghatnekar, M.J. Yost, R.G. Gourdie, A connexin43 mimetic peptide promotes regenerative healing and improves mechanical properties in skin and heart, Adv. Wound Care. 2 (2013) 55–62.

[231] M.P. O'Quinn, The Effects of a Cx43 Carboxyl Terminal Peptide on Cardiac Wound Healing and Arrhythmogenesis, Medical University of South Carolina, 2009.

[232] C.S. Stern, J. Lebowitz, Latest drug developments in the field of cardiovascular disease., Int. J. Angiol. 19 (2010) e100–5. PMID: 22477616.

[233] C. Cabo, J. Yao, P. a. Boyden, S. Chen, W. Hussain, H.S. Duffy, et al., Heterogeneous gap junction remodeling in reentrant circuits in the epicardial border zone of the healing canine infarct, Cardiovasc. Res. 72 (2006) 241–249.

[234] A. Schmidt, C.F. Azevedo, A. Cheng, S.N. Gupta, D.A. Bluemke, T.K. Foo, et al., Infarct Tissue Heterogeneity by Magnetic Resonance Imaging Identifies Enhanced Cardiac Arrhythmia Susceptibility in Patients With Left Ventricular Dysfunction, Circulation. 115 (2007) 2006–2014.

[235] J. DiMasi, L. Feldman, A. Seckler, A. Wilson, Trends in Risks Associated With New Drug Development: Success Rates for Investigational Drugs, Clin. Pharmacol. Ther. 87 (2010) 272–277.

[236] N. Mohd, R. Universiti, T. Mara, B. Wah, Y. Universiti, T. Mara, Power comparisons of Shapiro-Wilk, Kolmogorov-Smirnov, Lilliefors and Anderson-Darling tests, J. Stat. Model. Anal. 2 (2011) 21–33.

[237] S.S. Shapiro, M.B. Wilk, An analysis of variance test for normality (complete samples), Biometrika. 52 (1965) 591–611.

[238] D. Cramer, Fundamental statistics for social research, Routledge, London, 1998.

[239] D. Cramer, D. Howitt, The SAGE Dictionary of Statistics, Statistics (Ber). (2004) 188.

[240] D.P. Doane, L.E. Seward, Measuring Skewness : A Forgotten Statistic?, J. Stat. Educ. 19 (2011) 1–18.

[241] a W. Hunter, J. Jourdan, R.G. Gourdie, Fusion of GFP to the carboxyl terminus of connexin43 increases gap junction size in HeLa cells, Cell Commun Adhes. 10 (2003) 211–214.

[242] M.B. Rook, A.C.G. van Ginneken, B. de Jonge, A. el Aoumari, D. Gros, H.J. Jongsma, Differences in gap junction channels between cardiac myocytes, fibroblasts, and heterologous pairs, Am. J. Physiol. - Cell Physiol. 263 (1992) C959–C977. PMID: 1279981.

[243] C.K. Manjunath, E. Page, Cell biology and protein composition of cardiac gap junctions., Am. J. Physiol. 248 (1985) H783–91. PMID: 2408491.

[244] C.R. Green, N.S. Peters, R.G. Gourdie, S. Rothery, N.J. Severs, Validation of immunohistochemical quantification in confocal scanning laser microscopy: a comparative assessment of gap junction size with confocal and ultrastructural techniques., J. Histochem. Cytochem. 41 (1993) 1339–1349.

[245] A. Napolitano, D. Dean, A. Man, J. Youssef, D. Ho, A. Rago, et al., Scaffold-free three-dimensional cell culture utilizing micromolded nonadhesive hydrogels, Biotechniques. 43 (2007) 494–500.

[246] A.P. Napolitano, P. Chai, D.M. Dean, J.R. Morgan, Dynamics of the Self-Assembly of Complex Cellular Aggregates on Micromolded Nonadhesive Hydrogels, Tissue Eng. 13 (2007) 2087–2094.

[247] C.C. Review, Engineering Principles of Clinical Cell-Based Tissue Engineering, (2004) 1541–1558.

[248] T.I. Croll, S. Gentz, K. Mueller, M. Davidson, A.J. O'Connor, G.W. Stevens, et al., Modelling oxygen diffusion and cell growth in a porous, vascularising scaffold for soft tissue engineering applications, Chem. Eng. Sci. 60 (2005) 4924–4934.

[249] J.M. Kelm, E. Ehler, L.K. Nielsen, S. Schlatter, J.-C. Perriard, M. Fussenegger, Design of artificial myocardial microtissues., Tissue Eng. 10 (2004) 201–214.

[250] A.P. Napolitano, D.M. Dean, A.J. Man, J. Youssef, D.N. Ho, A.P. Rago, et al., Scaffold-free three-dimensional cell culture utilizing micromolded nonadhesive hydrogels, Biotechniques. 43 (2007) 494–500.

[251] F. Kieken, N. Mutsaers, E. Dolmatova, K. Virgil, A.L. Wit, A. Kellezi, et al., Structural and molecular mechanisms of gap junction remodeling in epicardial border zone myocytes following myocardial infarction, Circ. Res. 104 (2009) 1103–1112.

[252] R.M. Sutherland, Cell and environment interactions in tumor microregions: the multicell spheroid model., Science. 240 (1988) 177–184.

[253] J. Friedrich, R. Ebner, L. a. Kunz-Schughart, Experimental anti-tumor therapy in 3-D: Spheroids – old hat or new challenge?, Int. J. Radiat. Biol. 83 (2007) 849–871.

[254] L. a. Kunz-Schughart, The Use of 3-D Cultures for High-Throughput Screening: The Multicellular Spheroid Model, J. Biomol. Screen. 9 (2004) 273–285.

[255] B.R. Desroches, P. Zhang, B.-R. Choi, M.E. King, a. E. Maldonado, W. Li, et al., Functional scaffold-free 3-D cardiac microtissues: a novel model for the investigation of heart cells, AJP Hear. Circ. Physiol. 302 (2012) H2031–H2042.

[256] N.G. Frangogiannis, Inflammation in cardiac injury, repair and regeneration, Curr. Opin. Cardiol. 30 (2015) 240–245.

[257] H. Mollmann, H. Nef, S. Kostin, C. Vonkalle, I. Pilz, M. Weber, et al., Bone marrow-derived cells contribute to infarct remodelling, Cardiovasc. Res. 71 (2006) 661–671.

[258] S.B. Haudek, Y. Xia, P. Huebener, J.M. Lee, S. Carlson, J.R. Crawford, et al., Bone marrow-derived fibroblast precursors mediate ischemic cardiomyopathy in mice, Proc. Natl. Acad. Sci. U. S. A. 103 (2006) 18284–18289.

[259] S.R. Ali, S. Ranjbarvaziri, M. Talkhabi, P. Zhao, A. Subat, A. Hojjat, et al., Developmental heterogeneity of cardiac fibroblasts does not predict pathological proliferation and activation, Circ. Res. 115 (2014) 625–635.

[260] K.S. McDowell, H.J. Arevalo, M.M. Maleckar, N. a. Trayanova, Susceptibility to arrhythmia in the infarcted heart depends on myofibroblast density, Biophys. J. 101 (2011) 1307–1315.

[261] C. Vasquez, P. Mohandas, K.L. Louie, N. Benamer, A.C. Bapat, G.E. Morley, Enhanced fibroblast-myocyte interactions in response to cardiac injury, Circ. Res. 107 (2010) 1011–1020.

[262] T. Mayama, K. Matsumura, H. Lin, K. Ogawa, I. Imanaga, Remodelling of cardiac gap junction connexin 43 and arrhythmogenesis, Exp Clin Cardiol. 12 (2007) 67–76. PMID: 18650985.

[263] C.W. Lo, Role of gap junctions in cardiac conduction and development: insights from the connexin knockout mice., Circ. Res. 87 (2000) 346–348.

[264] D.B. Gros, H.J. Jongsma, Connexins in mammalian heart function, BioEssays. 18 (1996) 719–730.

[265] G.E. Mark, F.F. Strasser, Pacemaker activity and mitosis in cultures of newborn rat heart ventricle cells, Exp. Cell Res. 44 (1966) 217–233.

[266] A. Hyde, B. Blondel, A. Matter, J.P. Cheneval, B. Filloux, L. Girardier, Homo- and heterocellular junctions in cell cultures: An electrophysiological and morphological study, Prog. Brain Res. 31 (1969) 283–311.

[267] J.J. Santiago, A.L. Dangerfield, S.G. Rattan, K.L. Bathe, R.H. Cunnington, J.E. Raizman, et al., Cardiac fibroblast to myofibroblast differentiation in vivo and in vitro: Expression of focal adhesion components in neonatal and adult rat ventricular myofibroblasts, Dev. Dyn. 239 (2010) 1573–1584.

[268] S. Rohr, Myofibroblasts in diseased hearts: New players in cardiac arrhythmias?, Hear. Rhythm. 6 (2009) 848–856.

[269] S.K. Masur, H.S. Dewal, T.T. Dinh, I. Erenburg, S. Petridou, Myofibroblasts differentiate from fibroblasts when plated at low density, Proc. Natl. Acad. Sci. U. S. A. 93 (1996) 4219–4223.

[270] M.M. Jeyaraman, W. Srisakuldee, B.E. Nickel, E. Kardami, Connexin43 phosphorylation and cytoprotection in the heart, Biochim. Biophys. Acta - Biomembr. 1818 (2012) 2009–2013.

[271] D. Orlic, J. Kajstura, S. Chimenti, I. Jakoniuk, S.M. Anderson, B. Li, et al., Bone marrow cells regenerate infarcted myocardium., Nature. 410 (2001) 701–5.

[272] A. Abdel-Latif, R. Bolli, I.M. Tleyjeh, V.M. Montori, E.C. Perin, C.A. Hornung, et al., Adult bone marrow-derived cells for cardiac repair: a systematic review and meta-analysis, Arch. Intern. Med. 167 (2007) 989–97.

[273] R.C. Lai, F. Arslan, M.M. Lee, N.S.K. Sze, A. Choo, T.S. Chen, et al., Exosome secreted by MSC reduces myocardial ischemia/reperfusion injury, Stem Cell Res. 4 (2010) 214–222.

[274] A.G.-E. Ibrahim, K. Cheng, E. Marbán, Exosomes as critical agents of cardiac regeneration triggered by cell therapy, Stem Cell Reports. 2 (2014) 606–19.

[275] Y. Watanabe, Fine structure of bone marrow stroma., Nihon Ketsueki Gakkai Zasshi. 48 (1985) 1688–700. PMID: 3836546.

[276] R. Veeraraghavan, M.E. Salama, S. Poelzing, Interstitial volume modulates the conduction velocity-gap junction relationship., Am. J. Physiol. Heart Circ. Physiol. 302 (2012) H278–86.

[277] P. V Bayly, B.H. KenKnight, J.M. Rogers, R.E. Hillsley, R.E. Ideker, W.M. Smith, Estimation of conduction velocity vector fields from epicardial mapping data., IEEE Trans. Biomed. Eng. 45 (1998) 563–71.

[278] M. Miragoli, N. Salvarani, S. Rohr, Myofibroblasts Induce Ectopic Activity in Cardiac Tissue, Circ. Res. (2007) 755–758.

[279] A. Kamkin, I. Kiseleva, K.-D. Wagner, A. Pylaev, K.P. Leiterer, H. Theres, et al., A possible role for atrial fibroblasts in postinfarction bradycardia, Am. J. Physiol. Heart Circ. Physiol. 282 (2002) H842–H849.

[280] I. Kiseleva, A. Kamkin, A. Pylaev, D. Kondratjev, K.P. Leiterer, H. Theres, et al., Electrophysiological properties of mechanosensitive atrial fibroblasts from chronic infarcted rat heart, J. Mol. Cell. Cardiol. 30 (1998) 1083–1093.

[281] K. Dawson, C.T. Wu, X.Y. Qi, S. Nattel, Congestive heart failure effects on atrial fibroblast phenotype: differences between freshly-isolated and cultured cells, PLoS One. 7 (2012) e52032.

[282] L. Chilton, S. Ohya, D. Freed, E. George, V. Drobic, Y. Shibukawa, et al., K+ currents regulate the resting membrane potential, proliferation, and contractile responses in ventricular fibroblasts and myofibroblasts, Am. J. Physiol. Heart Circ. Physiol. 288 (2005) H2931–H2939.

[283] V. Jacquemet, Pacemaker activity resulting from the coupling with nonexcitable cells, Phys. Rev. E, Stat. Nonlinear, Soft Matter Physics. 74 (2006).

[284] T.P. Nguyen, Y. Xie, A. Garfinkel, Z. Qu, J.N. Weiss, Arrhythmogenic consequences of myofibroblast-myocyte coupling, Cardiovasc. Res. 93 (2012) 242–251.

[285] P. Camelliti, C.R. Green, I. LeGrice, P. Kohl, Fibroblast network in rabbit sinoatrial node: Structural and functional identification of homogeneous and heterogeneous cell coupling, Circ. Res. 94 (2004) 828–835.

[286] M. Malecki, E. Putzer, C. Sabo, A. Foorohar, C. Quach, C. Stampe, et al., Directed cardiomyogenesis of autologous human induced pluripotent stem cells recruited to infarcted myocardium with bioengineered antibodies, Mol. Cell. Ther. 2 (2014) 13.

[287] C.E. Murry, M.H. Soonpaa, H. Reinecke, H. Nakajima, H.O. Nakajima, M. Rubart, et al., Haematopoietic stem cells do not transdifferentiate into cardiac myocytes in myocardial infarcts., Nature. 428 (2004) 664–8.

[288] L.B. Balsam, A.J. Wagers, J.L. Christensen, T. Kofidis, I.L. Weissman, R.C. Robbins, Haematopoietic stem cells adopt mature haematopoietic fates in ischaemic myocardium., Nature. 428 (2004) 668–673.

[289] R. Driesen, G. Dispersyn, F. Verheyen, S. Vandeneijnde, L. Hofstra, F. Thone, et al., Partial cell fusion: A newly recognized type of communication between dedifferentiating cardiomyocytes and fibroblasts, Cardiovasc. Res. 68 (2005) 37–46.

[290] Z. Hajdu, S.J. Romeo, P.A. Fleming, R.R. Markwald, R.P. Visconti, C.J. Drake, Recruitment of bone marrow-derived valve interstitial cells is a normal homeostatic process, J. Mol. Cell. Cardiol. 51 (2011) 955–965.

[291] M. Evrard, S.Z. Chong, S. Devi, W.K. Chew, B. Lee, M. Poidinger, et al., Visualization of bone marrow monocyte mobilization using Cx3cr1gfp/+Flt3L-/- reporter mouse by multiphoton intravital microscopy, J. Leukoc. Biol. 97 (2015) 611–9.

[292] R. Gazit, P.K. Mandal, W. Ebina, A. Ben-Zvi, C. Nombela-Arrieta, L.E. Silberstein, et al., Fgd5 identifies hematopoietic stem cells in the murine bone marrow, J. Exp. Med. 211 (2014) 1315–1331.

[293] Y. Chen, L.-X. Xiang, J.-Z. Shao, R.-L. Pan, Y.-X. Wang, X.-J. Dong, et al., Recruitment of endogenous bone marrow mesenchymal stem cells towards injured liver, J. Cell. Mol. Med. 14 (2009) 1494–1508.

[294] J.R. Baum, B. Long, C. Cabo, H.S. Duffy, Myofibroblasts cause heterogeneous Cx43 reduction and are unlikely to be coupled to myocytes in the healing canine infarct, AJP Hear. Circ. Physiol. 302 (2012) H790–H800.

[295] J.F. Ek-Vitorin, T.J. King, N.S. Heyman, P.D. Lampe, J.M. Burt, Selectivity of connexin 43 channels is regulated through protein kinase C-dependent phosphorylation, Circ. Res. 98 (2006) 1498–1505.

[296] A.S. Brack, T.A. Rando, Tissue-specific stem cells: lessons from the skeletal muscle satellite cell., Cell Stem Cell. 10 (2012) 504–14.

[297] X. Fu, H. Wang, P. Hu, Stem cell activation in skeletal muscle regeneration, Cell. Mol. Life Sci. 72 (2015) 1663–1677.

[298] J.H. Kim, P. Jin, R. Duan, E.H. Chen, Mechanisms of myoblast fusion during muscle development., Curr. Opin. Genet. Dev. 32 (2015) 162–70.

[299] B.F. Grogan, J.R. Hsu, Skeletal Trauma Research Consortium, Volumetric muscle loss., J. Am. Acad. Orthop. Surg. 19 Suppl 1 (2011) S35–7. PMID: 21304045.

[300] A. Yoshida, K. Kobayashi, H. Manya, K. Taniguchi, H. Kano, M. Mizuno, et al., Muscular Dystrophy and Neuronal Migration Disorder Caused by Mutations in a Glycosyltransferase, POMGnT1, Dev. Cell. 1 (2001) 717–724.

[301] M.T. Wolf, C.L. Dearth, S.B. Sonnenberg, E.G. Loboa, S.F. Badylak, Naturally derived and synthetic scaffolds for skeletal muscle reconstruction, Adv. Drug Deliv. Rev. 84 (2015) 208–221.

[302] C.A. Cezar, D.J. Mooney, Biomaterial-based delivery for skeletal muscle repair, Adv. Drug Deliv. Rev. 84 (2015) 188–197.

[303] F. Rinaldi, R.C.R. Perlingeiro, Stem cells for skeletal muscle regeneration: therapeutic potential and roadblocks, Transl. Res. 163 (2014) 409–417.

[304] K.J.A. McCullagh, R.C.R. Perlingeiro, Coaxing stem cells for skeletal muscle repair, Adv. Drug Deliv. Rev. 84 (2015) 198–207.

[305] M. Juhas, N. Bursac, Engineering skeletal muscle repair, Curr. Opin. Biotechnol. 24 (2013) 880–886.

[306] M. Raghavan, N. Del Cid, S.M. Rizvi, L.R. Peters, MHC class I assembly: out and about., Trends Immunol. 29 (2008) 436–43.

[307] K. Sato, K. Ozaki, M. Mori, K. Muroi, K. Ozawa, Mesenchymal stromal cells for graft-versus-host disease : basic aspects and clinical outcomes., J. Clin. Exp. Hematop. 50 (2010) 79–89.

[308] K. Le Blanc, C. Tammik, K. Rosendahl, E. Zetterberg, O. Ringdén, HLA expression and immunologic properties of differentiated and undifferentiated mesenchymal stem cells., Exp. Hematol. 31 (2003) 890–6. PMID: 14550804.

[309] J. Chamberlain, T. Yamagami, E. Colletti, N.D. Theise, J. Desai, A. Frias, et al., Efficient generation of human hepatocytes by the intrahepatic delivery of clonal human mesenchymal stem cells in fetal sheep., Hepatology. 46 (2007) 1935–45.

[310] A.I. Caplan, Why are MSCs therapeutic? New data: new insight., J. Pathol. 217 (2009) 318–24.

[311] K. Le Blanc, Mesenchymal stromal cells: Tissue repair and immune modulation., Cytotherapy. 8 (2006) 559–61.

[312] E.J. Colletti, J.A. Airey, W. Liu, P.J. Simmons, E.D. Zanjani, C.D. Porada, et al., Generation of tissue-specific cells from MSC does not require fusion or donor-to-host mitochondrial/membrane transfer., Stem Cell Res. 2 (2009) 125–38.

[313] A.J. Nauta, G. Westerhuis, A.B. Kruisselbrink, E.G.A. Lurvink, R. Willemze, W.E. Fibbe, Donor-derived mesenchymal stem cells are immunogenic in an allogeneic host and stimulate donor graft rejection in a nonmyeloablative setting., Blood. 108 (2006) 2114–20.

[314] E.W. Petersdorf, G.M. Longton, C. Anasetti, E.M. Mickelson, S.K. McKinney, A.G. Smith, et al., Association of HLA-C disparity with graft failure after marrow transplantation from unrelated donors., Blood. 89 (1997) 1818–23. PMID: 9057668.

[315] H.L. Ploegh, Viral strategies of immune evasion., Science. 280 (1998) 248–53. PMID: 9535648.

[316] A. Lin, H. Xu, W. Yan, Modulation of HLA expression in human cytomegalovirus immune evasion., Cell. Mol. Immunol. 4 (2007) 91–8. PMID: 17484802.

[317] M. a. Soland, M.G. Bego, E. Colletti, C.D. Porada, E.D. Zanjani, S. St. Jeor, et al., Modulation of Human Mesenchymal Stem Cell Immunogenicity through Forced Expression of Human Cytomegalovirus US Proteins, PLoS One. 7 (2012) e36163.

[318] P.S. Jat, M.D. Noble, P. Ataliotis, Y. Tanaka, N. Yannoutsos, L. Larsen, et al., Direct derivation of conditionally immortal cell lines from an H-2Kb-tsA58 transgenic mouse., Proc. Natl. Acad. Sci. U. S. A. 88 (1991) 5096–100. PMID: 1711218.

[319] J.E. Morgan, J.R. Beauchamp, C.N. Pagel, M. Peckham, P. Ataliotis, P.S. Jat, et al., Myogenic cell lines derived from transgenic mice carrying a thermolabile T antigen: a model system for the derivation of tissue-specific and mutation-specific cell lines., Dev. Biol. 162 (1994) 486–498.

[320] S. Muses, J.E. Morgan, D.J. Wells, A New Extensively Characterised Conditionally Immortal Muscle Cell-Line for Investigating Therapeutic Strategies in Muscular Dystrophies, PLoS One. 6 (2011) e24826.

[321] K. Suzuki, N.J. Brand, S. Allen, M. a. Khan, A.O. Farrell, B. Murtuza, et al., Overexpression of connexin 43 in skeletal myoblasts: Relevance to cell transplantation to the heart, J. Thorac. Cardiovasc. Surg. 122 (2001) 759–766.

[322] B. Murtuza, K. Suzuki, G. Bou-Gharios, J.R. Beauchamp, R.T. Smolenski, T.A. Partridge, et al., Transplantation of skeletal myoblasts secreting an IL-1 inhibitor modulates adverse remodeling in infarcted murine myocardium., Proc. Natl. Acad. Sci. U. S. A. 101 (2004) 4216–21.

[323] S. Durrani, M. Konoplyannikov, M. Ashraf, K.H. Haider, Skeletal myoblasts for cardiac repair., Regen. Med. 5 (2010) 919–32.

[324] P. Menasché, Skeletal myoblasts as a therapeutic agent., Prog. Cardiovasc. Dis. 50 (n.d.) 7–17.

[325] H.K. Haider, A.C.K. Tan, S. Aziz, J.C. Chachques, E.K.W. Sim, Myoblast transplantation for cardiac repair: a clinical perspective., Mol. Ther. 9 (2004) 14–23. PMID: 14741773.

[326] M.P. O'Quinn, J.A. Palatinus, B.S. Harris, K.W. Hewett, R.G. Gourdie, A peptide mimetic of the connexin43 carboxyl terminus reduces gap junction remodeling and induced arrhythmia following ventricular injury, Circ. Res. 108 (2011) 704–715.

[327] J.M. Rhett, The Connexon Switch: Zonula Occludens-1 Regulates Connexin43 Hemichannel to Gap Junction Transition, Medical University of South Carolina, 2010.

[328] A.M. Zafari, S.M. Garas, A.M. Jeroudi, S. V Reddy, Myocardial Infarction, MedScape Drugs Dis. (2015).

[329] J.M. Rhett, G.S. Ghatnekar, J. a. Palatinus, M. O'Quinn, M.J. Yost, R.G. Gourdie, Novel therapies for scar reduction and regenerative healing of skin wounds, Trends Biotechnol. 26 (2008) 173–180.

[330] N.J. Severs, A.F. Bruce, E. Dupont, S. Rothery, Remodelling of gap junctions and connexin expression in diseased myocardium, Cardiovasc. Res. 80 (2008) 9–19.

[331] P. Kohl, P. Camelliti, Fibroblast–myocyte connections in the heart, Hear. Rhythm. 9 (2012) 461–464.